Modélisation et commande des convertisseurs MMC en vue de leur intégration dans le réseau électrique

Shabab Samimi

N° d'ordre : 301

CENTRALE LILLE

THESE

Présentée en vue
d'obtenir le grade de

DOCTEUR

En

Spécialité : Génie Électrique

Par

SAMIMI Shabab

DOCTORAT DELIVRE PAR CENTRALE LILLE

Titre de la thèse :

Modélisation et Commande des Convertisseurs MMC en vue de leur Intégration dans le Réseau Electrique

Soutenue le 9 Novembre devant le jury d'examen :

Président	*Philippe LADOUX, Professeur, Université de Toulouse*
Rapporteur	*Stephen FINNEY, Professeur, University of Strathclyde*
Rapporteur	*Abdelkrim BENCHAIB, Ingénieur R&D, HDR, GE/SGI*
Examinateur	*Oriol GOMIS, Professor Titular d'Universitat, Université de Politècnica de Catalunya*
Examinateur	*Stybille DIECKERHOFF, Professeur, T.University of Berlin*
Directeur de thèse	*Xavier GUILLAUD, Professeur, École Centrale Lille*
Encadrant	*Philippe DELARUE, Maître de conférences, Université de Lille1*
Encadrant	*François GRUSON, Maître de conférences, A&M Paris Tech*

Thèse préparée dans le Laboratoire L2EP

Ecole Doctorale SPI 072 (Lille I, Lille III, Artois, ULCO, UVHC, EC Lille)

A mes enfants:
Lili et Anna

ABSTRACT

In future, the capability of the electric power transmission continues to grow due to renewable energy production and the needs of electrical market. Consequently many HVDC transmission systems are developed. Definitely the power electronic interfaces will play a key role to provide high reliability, good efficiency and cost effectiveness for this AC/DC conversion.

Recently, the Modular Multilevel Converter (MMC) has taken the advantage over the more classical converter as three-level VSC. Since MMC topology is complex, two different control levels may be distinguished: the control of the switches mainly orientated on the balance of hundreds of voltage on the elementary submodules, the higher level control whose aim is to control the currents, power and energy in the system.

This thesis is oriented mainly on the latter. It discusses a hierarchical and formal approach for the MMC to control the energy in all the storage elements. At first it is shown that an energy control is required mandatory. Secondly, it supposes to develop an energetic model which is inverted to design the energy control. Then different solutions of control have been developed and discussed.

In the majority of applications, MMC is integrated in an HVDC point to point link where the two AC/DC substations have different roles. A specific attention has to be paid on the station which controls the voltage since the way to manage the energy in the MMC has a critical role in the DC voltage stability.

Finally, all these types of control have been tested and discussed on an HVDC. It is shown that the exchange between the DC bus and the MMC placed on both sides play a key role in the DC bus voltage regulation.

KEYWORDS

Modular Multilevel Converters, energy and Power Control, Modeling, High Voltage Direct Current (HVDC),

REMERCIMENTS

Je tiens en premier lieu à remercier les membres du Jury, M. Stephen FINNEY, M. Abdelkrim BENCHAIB, M. Philippe LADOUX, M. Oriol GOMIS et Mme. Stybille DIECKERHOFF, pour avoir accepté d'expertiser ma thèse. J'ai apprécié vos remarques et je suis très honorée de vous avoir eus comme jury.

Je remercie mes trois encadrants, M. Xavier GUILLAUD, M. Philippe DELARUE et M. François GRUSON pour leurs conseils avisés, leur patience et l'énergie qu'ils ont apportée à ce projet, grâce à vous cette thèse a été appréciée par le jury et a été à la hauteur de mes espérances.

Je remercie aussi M. Frédéric Colas de l'Université de Art et Métier Paris Tech pour ses conseils.

Et je finis par adresse ma gratitude à mes collègues, mes parents et mon époux pour avoir fait oublier les moments difficiles.

RESUME ETENDU

1- Contexte de l'étude

Les réseaux AC fonctionnants au plus près de leurs limites et l'intégration de plus en plus importante en termes de proportion dans le mix énergétique rendent le transport et la distribution d'électricité de plus en plus vulnérables devant les perturbations et incertitudes. EN effet, le système de transport d'électricité doit évoluer pour satisfaire aux besoins du marché de l'électricité et de l'insertion de la production renouvelable. En modifiant le paysage de la production d'électricité, cela va changer fondamentalement le comportement du réseau électrique que nous connaissions jusque-là, ce qui pourrait constituer un défi majeur du 21eme siècle. Dans ce contexte, les instances européennes ont convenu de faire évoluer le réseau européen et ont défini une cible de 20% d'énergies renouvelables dans la consommation énergétique de l'UE d'ici à 2020.Par conséquent, et sur la base de la conception du marché d'électricité et afin de ramener plus flexibilité et augmenter la sécurité d'approvisionnement, de nouvelles technologies, philosophies de contrôle et d'exploitation doivent être mis en place afin de satisfaire aux nouvelles exigences.

Pour atteindre cet objectif, le transport d'énergie en courant continu et à haute tension (HVDC) est actuellement en pleine expansion. La Figure 1 montre le développement des systèmes de transport HVDC en Europe. Les nouveaux actionneurs à base d'électronique de puissance vont jouer un rôle clé dans la maitrise du réseau électrique du futur en aidant le système à augmenter sa marge de stabilité et ainsi augmenter la part des énergies renouvelables dans le mix énergétique. Ces actionneurs à base d'électronique de puissance vont permettre plus de flexibilité en interconnectant les liens HVDC et systèmes de stockage tout en fournissant des services systèmes nécessaires au bon fonctionnement du réseau électrique

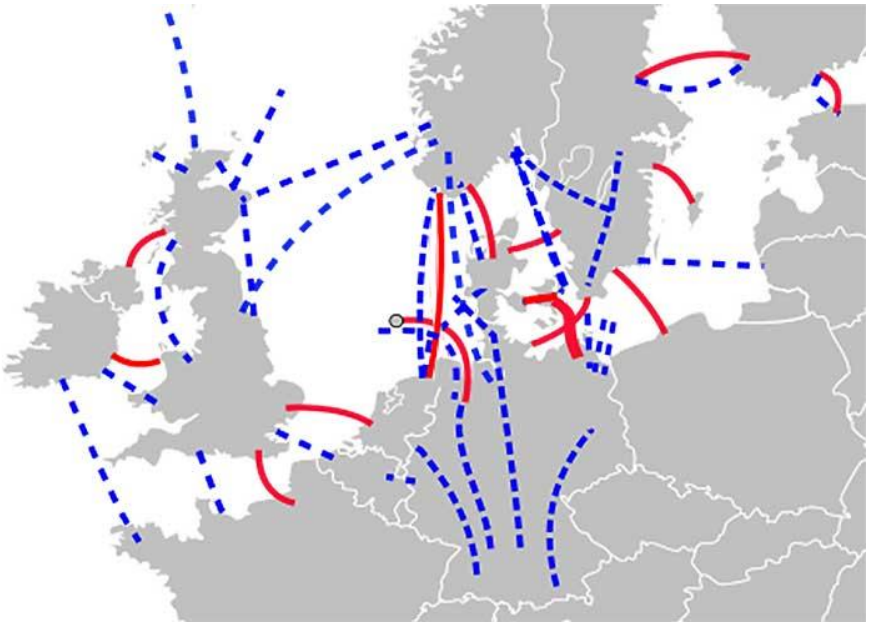

Figure 1: Plan de développement du réseau HVDC en Europe

En ce qui concerne les lignes de transmission à courant continu (HVDC), une structure MTDC (multi-terminaux DC) peut être vue comme une solution rentable qui améliorerait la fiabilité et la flexibilité. Par conséquent, les interfaces d'électroniques de puissance vont jouer un rôle majeur. Ces interfaces doivent notamment faire preuve d'une extrême fiabilité, d'une bonne efficacité tout en assurant une conversion AC/DC qui soit économiquement abordable.

Ces dernières années, la technologie MMC (convertisseur modulaire multi-niveaux) connaît un essor par rapport à des technologies de convertisseurs classiques, comme le convertisseur trois-niveaux (VSC). La technologie MMC a permis de surmonter les limites des autres topologies multi-niveaux pour les applications HVDC. Cette topologie est constituée de plusieurs sous-modules (SMs) connectés en séries. Chaque sous-module contient deux IGBTs avec leurs diodes antiparallèles et un condensateur qui sert d'accumulateur d'énergie. En fonction de l'application et de la capacité de puissance requise, les niveaux du MMC peut varier de quelques dizaines à des centaines de sous-modules par demi-bras. Pour les systèmes HVDC, un MMC peut comprendre des milliers de commutateurs de puissance.

Compte tenu du nombre très élevé de composants semi-conducteurs dans la topologie du MMC, il est très difficile de modéliser, contrôler et simuler l'ensemble de ces composants dans un même environnement de simulation. En conséquence, le contrôle/commande de ce type de convertisseur a été scindée en deux niveaux distincts dont le premier niveau porte sur le contrôle des interrupteurs et vise à l'équilibrage d'une centaine de tensions des sous-modules. Le second niveau a pour objectif le contrôle des courants, de la puissance et de l'énergie dans le système [14,15]. Cette thèse est axée sur ce deuxième niveau de contrôle. Le sujet de la thèse est tout à fait dans la préoccupation du moment et s'attaque à la l'identification des degrés de liberté d'un convertisseur MMC permanant son contrôle ainsi que son intégration dans système HVDC tout en mettant en lumières l'influence des choix de réglage sur les comportements dynamiques.

2- Plan de la thèse

Le but de ce travail est d'évaluer les stratégies de contrôle global du MMC axées sur le contrôle des courants, de la puissance et de l'énergie dans le système. Plus spécifiquement, une approche hiérarchisée et formelle basée sur l'inversion du modèle pour le contrôle de l'énergie de l'ensemble des éléments de stockage du MMC en vue de l'intégration du MMC dans une liaison HVDC est proposée.

La thèse est organisée comme suit :

Le chapitre 1 est dédié à la présentation de la topologie du MMC. Les différentes configurations sont notamment exposées. Puisque la topologie est relativement complexe, deux niveaux de contrôle distincts peuvent être définis : le contrôle des interrupteurs pour l'équilibrage des centaines de tension des sous-modules, et le contrôle haut niveau pour la gestion des courants, des puissances et de l'énergie du système.

Le chapitre 2 se focalise sur le contrôle des courants du MMC, à savoir le courant différentiel et le courant du réseau. Différentes méthodes de contrôle sont étudiées. Le contrôle

proposé est comparées avec le contrôle classique CCSC. Enfin, ce chapitre se termine par un état de l'art détaillé sur les différentes méthodes de linéarisation.

Le chapitre 3 s'intéresse aux différents types de contrôle de l'énergie du MMC. Tout d'abord, les différentes topologies pour le modèle énergétique du MMC sont exposées. Ensuite, les bases des stratégies de contrôle de l'énergie stockée dans un MCC sont présentées. Finalement, la méthode développée dans ces travaux est comparée à la méthode classique CCSC via des simulations.

Le chapitre 4 traite de la connexion de deux stations MMC par une liaison HVDC. Ce chapitre est divisé en deux grandes sections. La première considère une seule station MMC connectée à un bus DC variable. L'objectif est le contrôle de la tension de bus DC. Dans la deuxième section, les interactions causées par la connexion du MMC contrôlant le flux de puissance sont analysées. Par ailleurs, une stratégie de contrôle d'énergie du MMC est proposée pour obtenir les dynamiques souhaitées du bus DC et de la liaison HVDC. La solution retenue pour la gestion de l'énergie joue un rôle crucial sur la stabilité de la liaison HVDC.

Le chapitre de conclusion dresse un bilan des travaux et ouvre sur des perspectives de recherche.

3- Les conclusions de la thèse

Ces travaux ont pour objectifs d'évaluer les stratégies de contrôle haut niveau pour le MMC afin d'obtenir les dynamiques souhaitées dans une liaison HVDC. Dans cette étude, le contrôle bas niveau est supposé idéal. C'est pourquoi, un modèle équivalent du MMC basé sur l'énergie stockée dans un bras peut être développé. Les stratégies présentées se concentrent sur le contrôle de la puissance du MMC et de la tension du bus DC. Les boucles de contrôle associées sont développées et validées pour le point de fonctionnement nominal. Les simulations sont réalisées dans l'environnement EMPT-RV.

Le chapitre 1 rappelle les principes généraux du MMC, à savoir, les différentes topologies, les structures de sous-modules et les méthodes d'équilibrages des tensions des sous-modules. Un modèle équivalent du MMC considérant les modèles moyens de chaque bras est présenté préalablement à l'élaboration d'une méthode de contrôle haut-niveau. La dernière partie de ce chapitre est un état de l'art des stratégies de contrôle haut niveau.

Les contrôles du MMC sont basés sur une boucle interne rapide de contrôle de courant, et une boucle externe, plus lente, de contrôle de tension ou de puissance. Le chapitre 2 est dédié au contrôle des courants. On distingue les courants de réseau et les courants différentiels. La méthode basique de contrôle, qui comprend un contrôle des courants de réseau dans la base dq, présente de bonnes performances dynamiques uniquement pour les courants de réseau et les oscillations sur les autres variables. Ensuite, le contrôle classique CCSC possède de meilleurs performances en régime établi, mais les oscillations du courant différentiel en transitoire montrent le besoin d'un contrôle de ces courants. De manière générale, afin d'avoir un contrôle complet du système, il est nécessaire que le nombre de contrôleurs soit égal aux nombres de

variables d'état indépendantes de ce même système. C'est pourquoi, d'autres boucles de contrôles doivent être ajoutées à cette première proposition. Un contrôle actif des courants différentiels est proposé. Ses performances sont satisfaisantes par rapport aux différents courants du MMC. Par ailleurs, the influence of the MMC insert index calculating on the differential currents oscillations is investigated.

Dans le chapitre 3, les principes du contrôle d'énergie du MMC sont exposés. Dans une première partie, les différentes topologies de modèles énergétiques sont développées. Pour faciliter ce contrôle, deux variables d'énergies sont introduites : la somme et la différence d'énergie par phase (W^{Σ}, W^{Δ}) suivi d'une analyse montrant l'indépendance des valeurs moyennes de des deux variables ainsi que leur contrôlabilité. L'analyse proposée inclue les boucles de contrôle de la somme et différence de l'énergie du MMC connecté au bus DC de tension constante.

Utilisant toujours les méthodes d'obtention de structures de contrôle basées sur le model inverse, deux possibilités de modélisation sont suggérées dans ce chapitre: model instantané et model moyen. La comparaison des résultats de simulation obtenus avec chacune des méthodes montrent des différences significatives en termes de pertes.

A partir des résultats obtenus de la modélisation de l'énergie, il apparait clairement que la somme peut être commandée soit par la puissance AC soit par la puissance DC. La comparaison de ces méthodes de contrôle montre bien que cette manière de gérer l'énergie change fondamentalement les dynamiques.

Dans le chapitre 4, le contrôle d'une liaison MMC-HVDC point à point est étudié. Un modèle simplifié du câble DC est considéré. Dans cette topologie, contrairement aux liaisons classiques VSC-HVDC à deux ou trois niveaux, aucune capacité n'est connectée directement sur le bus DC. C'est pourquoi, dans un tel lien HVDC, la tension de bus DC est plus volatile que celle d'une structure VSC-HVDC. Une solution d'échange d'énergie entre l'énergie stockée et le bus DC a été proposée pour améliorer la stabilité de la tension du bus DC.

Les perspectives de travail sont les suivantes :

- Etudes d'un système MTDC (dynamiques des tensions et des échanges de puissances) avec les stratégies de contrôle développées.
- Evaluation de la robustesse des méthodes de contrôle proposées suite à des défauts AC équilibrés ou non.
- Amélioration des contrôleurs PI classiques et étude des performances des stratégies de contrôle du MMC avec des contrôleurs plus élaborées.
- Mise en œuvre de la méthodologie proposée pour le développement du contrôle du MMC avec une topologie de sous-modules « full bridge ».

Pour satisfaire aux besoins du marché de l'électricité et de l'insertion de la production renouvelable, le système de transport d'électricité doit évoluer. En particulier, les systèmes de transport dits « HVDC » (courant continu très haute tension) se développent. Les interfaces d'électroniques de puissance vont donc jouer un rôle majeur. Ces interfaces doivent faire preuve d'une extrême fiabilité, d'une bonne efficacité et rester économiquement abordables.

Récemment, la technologie MMC (convertisseur modulaire multi-niveaux) connaît un essor par rapport à des technologies classiques, comme le convertisseur trois-niveaux (VSC). Sa topologie étant relativement complexe, deux niveaux principaux de contrôle peuvent être définis. Le premier niveau, porte sur le contrôle des interrupteurs pour l'équilibre des tensions des entaines de sous-modules. Le second niveau contrôle les courants, la puissance et l'énergie dans le système.

Cette thèse est axée sur ce deuxième niveau de contrôle. Une approche hiérarchisée et formelle, basée sur l'inversion du modèle pour le contrôle de l'énergie du MMC est présentée. Pour ce contrôle, différentes méthodes ont été proposées et comparées. Cela implique de développer de nouveaux types de modélisation, à inverser pour la mise en place du contrôle. A nouveau, différentes solutions ont été développées.

Le MMC est généralement intégré dans une liaison HVDC où les deux stations AC/DC ont des rôles différents. Un soin particulier doit être apporté à la station dédiée au contrôle de la tension. En effet, la gestion de l'énergie dans le MCC a un rôle critique pour la stabilité de la tension.

En conclusion, les différents types de contrôle évoqués ont été étudiés dans le cas d'une liaison HVDC. Il a été montré que les échanges entre le bus DC et les MMC jouent un rôle important pour la régulation de la tension du bus DC.

MOTS CLES :

Convertisseur modulaire multiniveau, Contôle de l'enérgie et la puissance, Modélisation, Haute Tension Courant Continu (HVDC)

SYMBOLS & ABBREVIATIONS

Symbols

C	SM capacitance
C_{tot}	Equivalent Arm capacitance of Phase i
C_{DC}	Cable capacitance
v_{ci}	SM capacitor voltage
m_{uli}	Upper or Lower Arm Insertion Index
n_i	Number of the SM in an arm
v_{muli}	Upper or Lower arm modulated voltage
i_{muli}	Equivalent Upper or Lower arm capacitor current
i_{uli}	Upper or Lower arm current
$v_{culitot}$	Equivalent Upper or Lower arm capacitor voltage
i_{gi}	AC grid current
v_{gi}	AC grid Voltage
I_{dc}	DC current
v_{diffi}	Internal voltage (driving i_{diffi}).
v_{vi}	Internal voltage (driving i_{gi}).
v_{diff}	High Voltage Direct Current
W_i^{Σ}	Per-phase stored energy
W_i^{Δ}	Differential stored energy
W_{tot}^{Σ}	Total 3-phases stored energy
p_{ACi}	Average per-phase active power
p_{AC}	Total 3-phases active power
p_{DCi}	Per-phase dc power
R_{arm}	Arm Resistance
L_{arm}	Arm Inductance
R	AC filter Resistance
L	AC filter Inductance
θ_s	Grid Angular
t	Time

T	Period-time of periodic signal
f	Frequency
ζ	Damping Ratio

Subscripts

ul	Upper or Lower Arm
g	Grid variable
i	‘a’ or ‘b’ or ‘c’ phase in a three-phase quantities in natural refrence frame
K	Generic phase ‘K’
dq	Quantities in the rotating synchronous dq reference frame
pu	Variable in per unit system
SI	Variable in SI system
Σ	Sum between the upper and lower arm
Δ	Difference between the upper and lower arm
ref	Reference Value

Abbreviations

SM	Sub-Module
HB	Half Bridge
FB	Full Bridge
THD	Total harmonic Distortion
PWM	Pulse Width Modulation
NLC	Nearest Level Control
BCA	Balancing Control Algorithm
HVDC	High Voltage Direct Current
VSC	Voltage Source Converter
MMC	Modular Multilevel Converter
CCSC	Circulation Current Suppression Controller

List of the Figures & Tables

CONTENTS

INTRODUCTION

1 CONTEXT AND MOTIVATION FOR AN HVDC TRANSMISSION

Over the last century, AC has been the dominant form of electrical transmission systems. Since then, high-voltage AC transmission has some limitations, starting with transmission capacity and distance constrains and the impossibility of directly connecting two AC power networks of different frequencies. With the penetration of the new energy sources and the world global need to transmit more and more energy for the economy growth, high-voltage DC transmission is expected to grow far beyond its traditional position as a supplement to AC transmission.

Nowadays, the HVDC transmission systems are developed as the method for subsea electrical transmission, the interconnection of asynchronous AC grids and in case of any geography constraints. It is also the chosen technology for the long distance power transmission, able to deliver high power with low electrical losses. That makes it a suitable technology in overcoming the problem of decentralization of the production within the renewable generation like wind and solar resources.

With the dawn of a new energy era and the need to build a smarter grid, the European leaders agreed to develop the renewable energies in Europe. The fixed target by the European Council in 2008 [1] is to have a 20 % share of renewable energies in EU energy consumption by 2020.To reach this target, large offshore wind farms have already been installed and others are expected in the coming years, notably in the North Sea due to shallow water. Following EWEA's recommendations (see Figure 1), the European Network Transmission System Operators (ENTSO-E) has sketched a grid development plan for the next ten years [2]. The scenario proposed by ENTSO-E until 2020 is the building of 9600 km of new HVDC lines in Europe, which should be compared to the 32500 km of new and refurbished HVAC lines. .

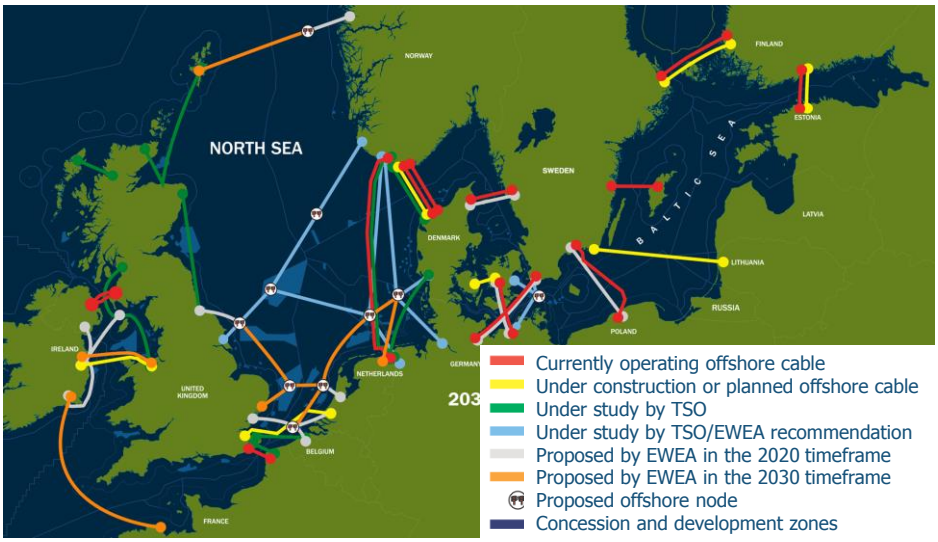

Figure 1: EWEA's 20 year offshore network development master plan [2].

In Europe HVDC transmission has been used since 1954, mostly for submarine cable transmission, as shown Figure 2 [3]. Current HVDC options are: point-to-point link, back-to-

back link and multi-terminal link (MTDC). The latter configuration is progressing toward the super-grids by interconnecting multiple HVDC and MTDCs associated to large wind farms.

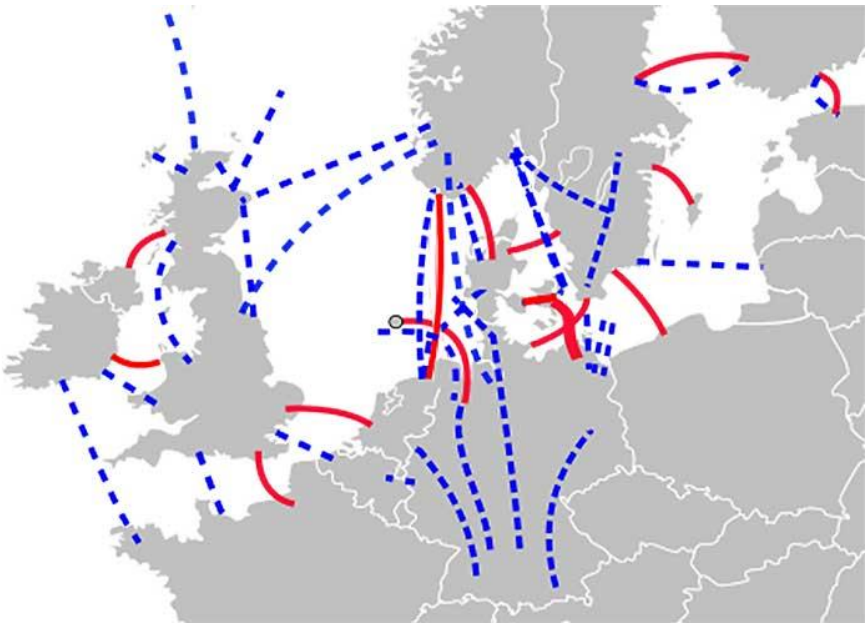

Figure 2: HVDC connections in Europe [3]

HVDC provides efficient, stable transmission and control capability. Definitely the power electronic interfaces between AC and DC system play a key role. Power electronic interfaces are changing through the introduction of new components as transistors. They play an important role to achieve high efficiency and performance in power systems

The use of power electronics in transmission systems is not a new idea since it has been used for decades, but mostly with thyristor components. The first thyristor-based link was built in the early seventies for the Eel River project (2×80 MW). Capacity rose quickly (e.g. the IFA 2000 France-UK link was built in 1986 with a power capability of 2 GW).The capacity of the newest thyristor based links installed in 2013 exceeds 7 GW. Transistors have also been used in HVDC applications for about 15 years, with the first installation on the Island of Gotland at the end of the previous century. These first installations used "simple" 2-level converters. The Cross Sound Cable (330 MW, 150 kV) between Long Island and the American continent was installed in 2002 using a 3-level converter. Because of the high voltage levels, a very large number of transistors are placed in series. However, this large stack of series switches needs to have nearly identical parameters and synchronized ignition to avoid excessive stresses on single components during switching actions. The high frequency switching operation of the PWM (≈1 kHz) was also responsible for significant losses in the range of 3 % per converter for the first generation down to 1.4 % per converter for the 3rd generation PWM based converters [5]

The appearance of VSC-HVDC, having a smaller converter size, reduced filters, dynamic reactive power support and fast power reversal, has facilitated the implementation of HVDC technology in a wider range of applications [6, 7]. Since the first successful application of VSC-

HVDC in 1997 in Gotland, Sweden; many other installations provided asynchronous interconnections of AC grids all-over the world. Due to its smaller footprint and ability to act as a virtual synchronous generator, VSC is especially suitable for connecting offshore wind power plants.

In 2002, Marquardt and Lesnicar proposed the modular multilevel converter (MMC) topology [8]. Due to the fact that it can achieve high power and high voltage levels using proven semiconductor technology, MMC has been widely accepted in the industry [9].The HVDC-from Siemens, HVDC-Light from ABB and HVDC-MaxSine from Alstom are examples of the implementation of the MMC concept in applications for HVDC transmission [10, 11, 12].

With advantages such as modularity, increased efficiency and reliability, the MMCs is now the preferred power electronic topology that has replaced the three-level converters in VSC-HVDC applications, becoming a suitable solution for the HVDC transmission systems [13].

2 PROJECT OBJECTIVES AND OUTLINE OF THIS THESIS

The motivation for this work is drawn from MMC application for the HVDC transmission. As its name implies, the main characteristics of such a converter topology regards the series connection of dozens to hundreds of identical sub-modules within a branch. This characteristic makes the suitability of MMC application for high power and high voltage transmission. However, the important number of MMC variables creates significant difficulties for synthetizing a control system. With high numbers of level, the control of SMs (balancing SM capacitor voltages) can be separated from the global control (current and power controls) [14, 15].

The aim of this work is to assess the global control of the MMC and its integration in an HVDC transmission system. This work develops and discusses control strategies used for MMC to assume its dynamics. In-depth analyses were performed to achieve control of all MMC states variables. The outline of this thesis is organized as follows:

Chapter 1 is an introduction of MMC topology; it explains the different MMC configurations. Since this topology is complex, two different control levels are distinguished: the control of the switches mainly orientated on the balance of hundreds of voltage on the elementary submodules, the higher level control whose aim is to control the currents, power, and energy in the system. Finally as a step before MMC high-level control, the MMC main parameters are introduced.

Chapter 2 is focused on the control of MMC current variables: the grid and differential currents. Several methods for control of these currents are investigated. A comparison of the presented control with the well-known control scheme of CCSC is provided. At the end of this chapter, different existing methods of linearization in the literature have been discussed and compared.

Chapter 3 investigates the different types of energy based control of the MMC. Firstly different topologies for MMC energy-based model are introduced. Then, the fundamentals of the different control strategies in order to control the stored energy in an MMC are provided. Finally a comparison between CCSC scheme as a well-known MMC control and the proposed energy based control is exposed by simulation results.

Chapter 4 deals with the connection of the two MMC stations in an HVDC link. This chapter is divided in two main sections; one is dealing with the control of the MMC station which controls the DC bus voltage in an HVDC and the other is analyzing interactions caused by its connection to the MMC station which controls the power flow. Once studied the MMC connected to a variable DC-bus, the DC bus voltage control is used to manage the DC-bus voltage and the MMC system dynamics. In the second section, a control strategy based on the MMC energy based control enables to achieve the desired dynamics for DC bus and MMCs dynamic in an HVDC link. This study shows that the way to manage the energy in the MMC may have a critical role in the DC voltage stability in an HVDC link.

Conclusions and perspectives chapter summarizes the work findings, and recommend some improvements and further investigations.

3 SCIENTIFIC CONTRIBUTION OF THIS WORK

Many works have already been achieved on the MMC control with already very good dynamic performances. We do not claim a higher performance of the current or energy controls developed in this PhD but the main contribution of this work is to propose a rigorous methodology to build step by step the control based on the principle of inversion of the model, developed for many years in the lab. The methodology allows identifying clearly all the degrees of freedom in the control and outlines the influence of the choices on the dynamic behavior of an MMC alone or integrated in an HVDC system.

The main contributions of this work are summarized below:

- A rigorous methodology to design the current controllers from the MMC model including the discussion on different linearization methodologies (Chapter 2).
- The development of the mathematical model of MMC energy variables: per-phased stored energy (W_i^{Σ}) and per-phased balanced energy (W_i^{Δ}) (Chapter 3).
- Different strategies for control of MMC energy variables: per-phased stored energy (W_i^{Σ}) and per-phased balanced energy (W_i^{Δ}) (Chapter 3).
- An in-depth analysis on DC–bus voltage variation based on different strategies to manage the energy in the MMC. It may have a critical role in the DC voltage stability in an HVDC link. This analysis has led to the idea of exchanging the MMC stored energy with the DC link which improves the DC bus voltage dynamics (Chapter 4).

- A comparison of proposed energy based control and the well-known CCSC scheme for an MMC associated to a variable DC-bus voltage.(Chapter 4).

4 LIST OF PUBLICATION DERIVED FROM THIS WORK

This work has resulted in the following publications:

SAMIMI Shabab, GRUSON François, DELARUE Philippe, GUILLAUD Xavier, COLAS Frédéric P. "Représentation Energétique Macroscopique et Diagramme PQ des Convertisseurs Modulaires Multi-niveaux," *in Symposium de Génie Électrique France,2014*.

SAMIMI Shabab, GRUSON François, DELARUE Philippe, GUILLAUD Xavier, "Synthesis of different types of energy based controllers for a modular multilevel converter integrated in an HVDC link," *in Proc. IEEE ,ADDC Conf. Birmangham,UK,2015*.

SAMIMI Shabab, GRUSON François, DELARUE Philippe, GUILLAUD Xavier, "Control of DC bus voltage with a Modular Multilevel Converter," in *Proc. IEEE PowerTech. Conf.Eidenhoven, 2015*.

GRUSON François, FREYTES Julian, SAMIMI Shabab, DELARUE Philippe, GUILLAUD Xavier, COLAS Frédéric, BELHAOUNE Moez, "Impact of control algorithm solutions on Modular Multilevel Converters electrical waveforms and losses," *in 15th EPE ECCE Europe 2015*.

SAMIMI Shabab, GRUSON François, DELARUE Philippe, COLAS Frédéric, BELHAOUNE Moez, GUILLAUD Xavier, "MMC stored energy participation to the DC bus voltage control in an HVDC link," *Revue,IEEE Trans. Power Del.*2016.

CHAPTER 1 : MMC State of the Art

1.1 HVDC CONVERTER TOPOLOGY

1.1.1. Introduction

During the last years, several multilevel converter topologies, as synthesized on Figure 1-1 [16] have been introduced for high power and medium or high voltage solutions like grid application and electrical drives [17]. The main characteristics of such multilevel converters were to achieve higher power by using power semiconductor switches in series with several lower voltage DC sources to perform power conversion via a staircase voltage waveform. The commutation of the power switches permits the addition of the DC sources which reach high voltage at the output.

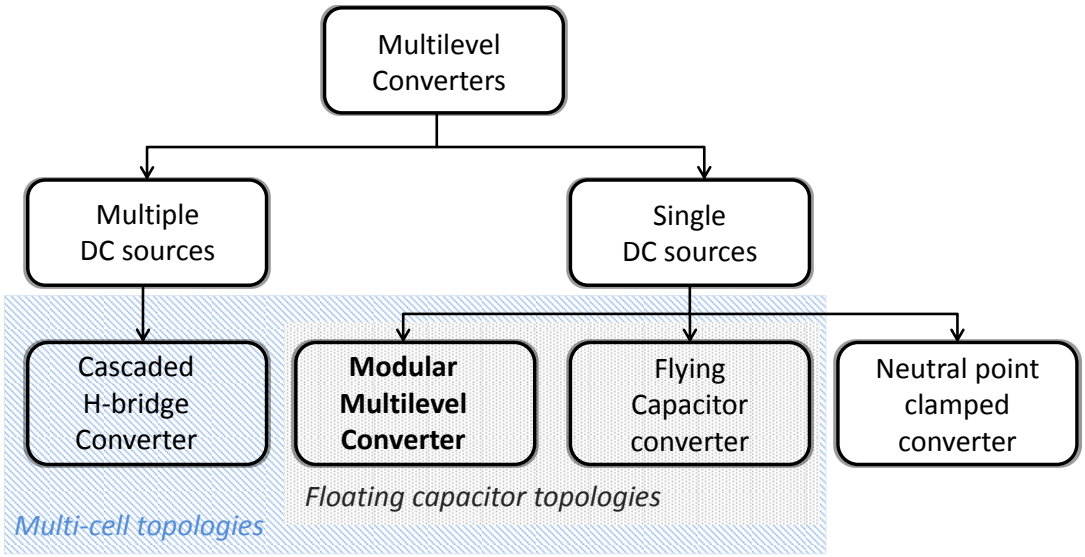

Figure 1-1: Multilevel converter topology classification [16]

Compared to two-level converters, multilevel converters present great advantages such as:

- Staircase waveform quality: Multilevel converters output voltage improves, the quality of the modulated voltage since the number of levels increases, reducing the total harmonic distortion (THD) and reducing the dv/dt stresses. Therefore electromagnetic compatibility (EMC) problems can be reduced.
- Input current: Multilevel converters can draw input current with low distortion.

The classical VSC topologies (flying capacitor converter, neutral point clamped converter) were developed long time ago for low voltage or medium voltage electrical drive applications. They were limited to three levels or five levels application at most. The increase on the number of levels was limited by the complexity on the possible topologies.

In the same time, the increase on the DC voltage induced to use many standard switches in series. The Modular Multilevel Converter represents a real breakthrough compared with the previous converters. It brings some new capabilities:

- Modularity quality: MMC stability meets different voltage level requirements
- Efficiency: MMC high efficiency is a significant importance for high power applications
- Harmonic Performance: MMC has a superior harmonic performance for high voltage applications where a large number of identical SMs with low voltage ratings are stacked up, thereby the size of passive filters can be reduced

1.1.2. MMC topologies

The MMC was initially used for AC/DC applications [8]. Today, although a wide range of applications have been considered, leading to the MMC family [18-21], as illustrated in Figure 1-2

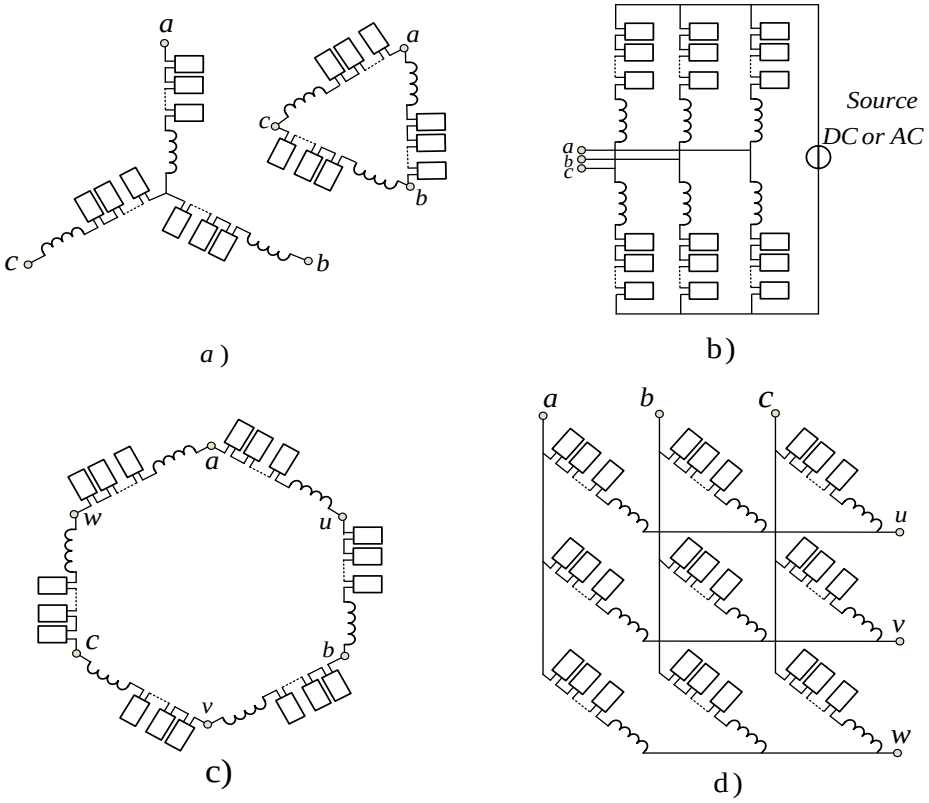

Figure 1-2: Multilevel converter topology classification [18-21]

Figure 1-2 (a) shows cases of the three-phase Cascaded H-Bridge converter in either star or delta configurations whose implementation requires only three converter branches. This topology has started being investigated for static synchronous compensator (STATCOM) applications [22].

Figure 1-2 (b) is the most frequently encountered member of the MMC family proposed by Marquardt in [21]. This variant is used in systems requiring a AC/DC conversion. This topology developed mainly for HVDC systems [23] as well as medium voltage electric drives [24].

The common DC link can be substituted by an AC source. This leads to a single/three-phase direct AC/AC conversion structure, which can be used for the interconnection of a three-phase industrial grid with a single-phase railway supply (16.33 Hz) available in several European countries [20].

Finally, the Hexverter [25] and Matrix converter [26, 27] topologies are shown in Figure 1-2(c) and (d) respectively. These MMC topologies directly connect two three phase systems, for example the supply grid and an electrical machine, in contrast to two DC/AC inverters connected in back-to-back configuration. They seem to be a candidate for AC/AC converters with a low to medium power applications.

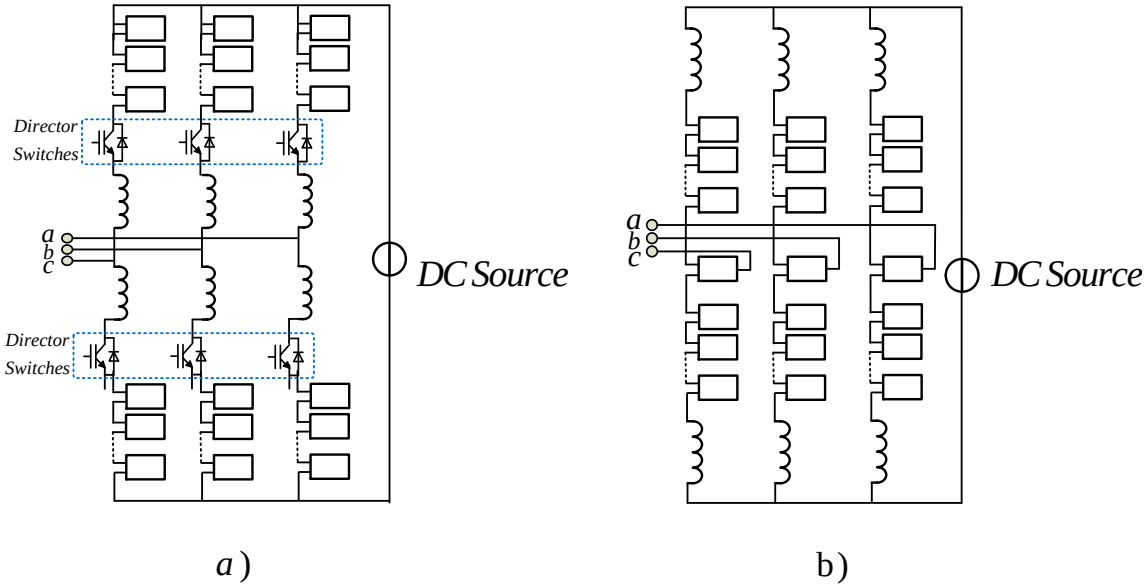

Figure 1-3: MMC –hybrid topologies found in the literature

In addition to above topologies in order to achieve more features, such as implementation with a lower number of required submodules, a number of hybrid MMC related topologies have been proposed in literature especially for AC/DC operation such as: the Alternate Arm Converter (AAC) developed by Alstom Grid [28],as well as the MMC with a middle cell [29] as shown in Figure 1-3 (a) and (b) respectively.

Since starting this thesis the available topologies are constantly evolving and changing depends on the pursued objectives. Due to the objective of this thesis, this work deals with the well-known structure labeled as MMC by its inventor illustrated in Figure 1-2(b) which is applied wildly for HVDC systems.

The general structure constituted by three legs, each of them consists of two arms per phase-leg. The upper arm and the lower one are denoted by the sub index "u" and "l" respectively. Each arm comprises N series-connected, nominally identical submodules (SMs) and a series inductor (R_{arm}, L_{arm}), as shown in Figure 1-4. Inside the arms, each submodule is individually controllable therefore the converter can act as a controllable voltage source, with a large number of available discrete voltage steps. While the SMs in each arm are controlled to generate the required phase voltage, the arm inductor filters the high-frequency components in

the arm current and is mainly used in case of DC short-circuit to limit the gradient of the DC current.

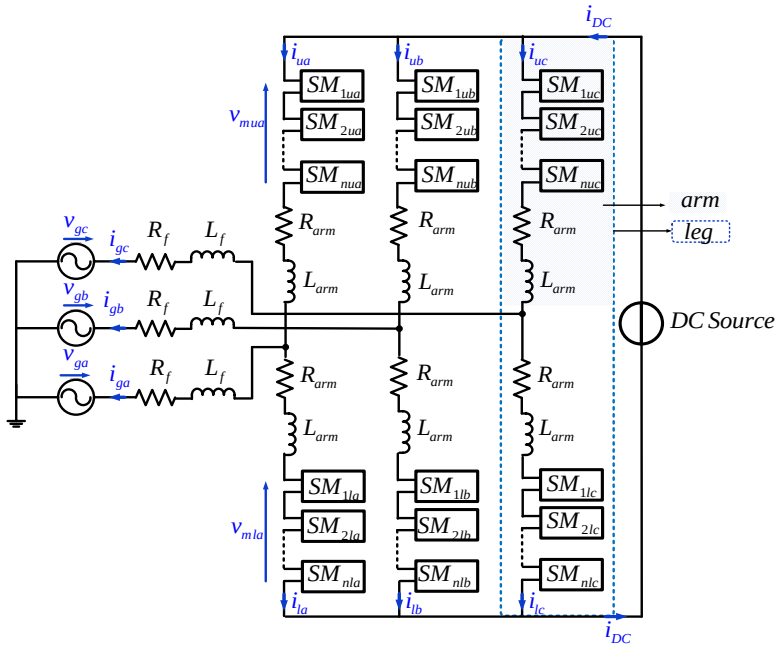

Figure 1-4: A general topology of 3-phased MMC

1.1.3. Submodules topologies

Depending on the MMC application and its topology, different types of SMs can be used.

1) The half-bridge circuit or chopper-cell shown in Figure 1-5(a): The output voltage of an half-bridge SM is either equal to its capacitor voltage v_c. (switched- on/inserted state) or zero (switched-off/bypassed state), depending on the switching states of the complimentary switch pairs, i.e., S1 and S2. This structure is the most evident choice for AC/DC applications, where only unipolar arm voltage is required. It is simultaneously the simplest option and the one that features the lowest conduction losses [21, 30, 31]. However, the antiparallel diodes are creating an uncontrollable current path in case of a DC-bus short circuit fault, what leads to a unsatisfying behavior under such conditions, as for any other VSC topologies.

2) The full-bridge circuit or bridge-cell shown in Figure 1-5(b): The output voltage of a full-bridge SM is either equal to its capacitor voltage v_c (switched-on/inserted state) or zeros (switched-off/bypassed state), depending on the switching states of the four switches S1 to S4. Since the number of semiconductor devices of a full-bridge SM is twice of a half-bridge SM, the power losses as well as the cost of an MMC based on the full-bridge SMs are significantly higher than that of an MMC based on the half-bridge SMs [21, 32].Certain applications require bipolar arm voltages such as direct AC/AC, matrix topologies or the AAC topology). Since full-bridges can actively break arm currents by imposing appropriate voltages in the arms, they can provide DC short –circuit current breaking capability. However, the double number of power switches almost doubles the conduction losses,

what seriously restrains their attractiveness for AC/DC applications and is the main motivation for the development of the clamped double submodules.

3) The clamp-double circuit shown in Figure 1-5(c): A clamp-double SM consists of two half-bridge SMs, two additional diodes and one extra integrated gate bipolar transistor (IGBT) with its anti-parallel diode. During normal operation, the switch S5 is always switched –on and the clamp-double SM acts equivalent to two series connected half-bridge SMs. Compared to the half- and full-bridge MMCs with the same number of voltage levels, the clamp-double MMC has higher semiconductor losses than the half-bridge MMC and lower than the full-bridge MMC. This cell structure was proposed by Marquardt in 2010 [21] as a specific answer to DC short circuit protection issues. In fact, with an additional switch that can temporarily reconfigure two half-bridges as one full-bridge, the converter arms can impose counter-voltages up to half their nominal blocking voltage. In addition, since the additional switch is not operated in normal conditions, it can be considered with good conduction characteristics and hence, contribute only marginally to the conduction losses [21].

4) The five-level cross-connected circuit shown in Figure 1-5 (d), a five-level cross-connected SM also consists of two half-bridge SMs connected back-to-back by two extra IGBTs with their anti-parallel diodes. Its semiconductor losses are the same as the clamp double SM [33].

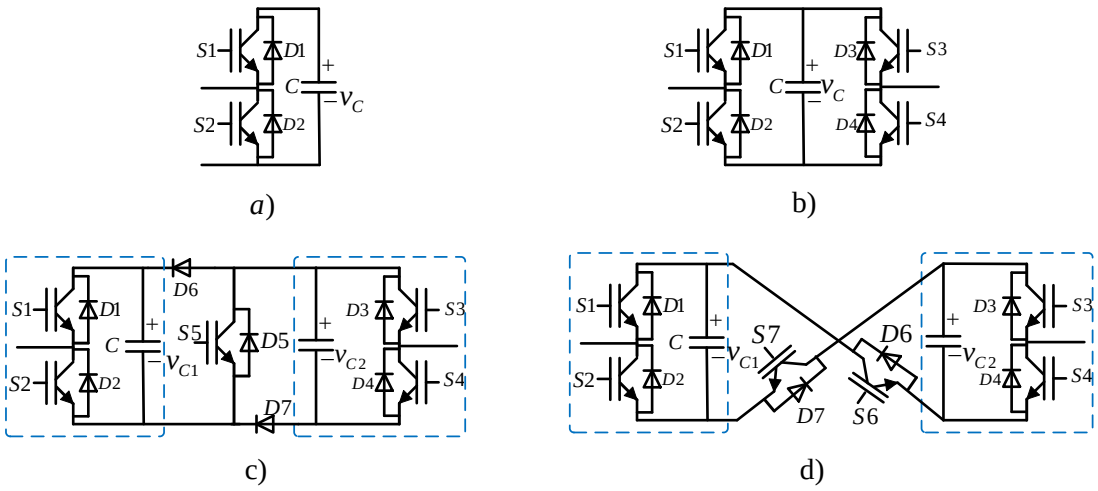

Figure 1-5: The MMC main sub-module topologies

A comparison of various SM circuits, in terms of voltage levels, DC-side short-circuit fault handling capability, and power losses, is provided in Table 1-1.

Among all of the SM circuit configurations, the half-bridge topology has been wildly applied in the MMC-HVDC applications. This is due to the presence of only two switches in the SM which results in a lower number of components and higher efficiency for the MMC.

Hereafter, the MMC based on the half-bridge SM is considered since the losses are regarded as the first priority in MMC-HVDC applications.

Table 1-1: Comparisons of various SM circuits

SM circuit	Voltage levels	DC-fault handling	Losses
Half-Bridge	$0,\ v_C$	No	Low
Full-Bridge	$0,\pm v_C$	Yes	High
Clamp-double	$0,\pm v_{C1},\pm v_{C2},(v_{C1}+v_{C2})$	Yes	Moderate
Five–level cross connected	$0,\pm v_{C1},\pm v_{C2},+(v_{C1}+v_{C2})$	Yes	Moderate

Among all of the SM circuit configurations, the half-bridge topology has been widely applied in the MMC-HVDC applications. However, ULTRANET project in Germany is expected to be realized with full bridge MMC to improve the behavior in case of DC short-circuit [34].This is due to the presence of only two switches in the SM which results in a lower number of components and higher efficiency for the MMC. Hereafter, the MMC based on the half-bridge SM is considered since the losses are regarded as the first priority in MMC-HVDC applications.

1.1.4. Half–bridge SM operating principles

The SMs have three possible states (without short-circuiting the capacitor):

• Active state: The IGBT S1 is turned ON while the IGBT S2 is turned OFF.

This SM state leads to two different electrical paths depending on the sign of the current that is entering into the SM (i_{SM}). For a positive current $i_{SM} > 0$, when the capacitor charges through the diode D1 (Figure 1-6(a)) and for a negative current $i_{SM} < 0$; when the current is leaving the SM, the capacitor discharges through the IGBT S1 (Figure 1-6(b)). For both cases, the output voltage of the SM will be equal to the voltage of the capacitor v_C , hence the SM is considered in the active state, irrespective of the direction of the SM current.

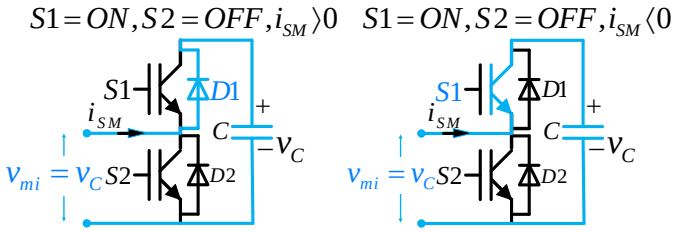

Figure 1-6: The SM active state

• Bypassed State: The IGBT S2 is turned ON while the IGBT S1 is turned OFF.

This case, depending on the sign of i_{SM}, has two electrical paths. For positive currents $i_{SM} > 0$, the current flow will pass through IGBT S2 (Figure 1-7(a)), whereas negative currents will circulate through the diode D2 (Figure 1-7(b)). The bypassed state refers to the voltage output of the SM (v_c) which is zero irrespectively of the direction of the current. In this state the SM capacitor will neither charge nor discharge since it is "isolated" from the rest of the system.

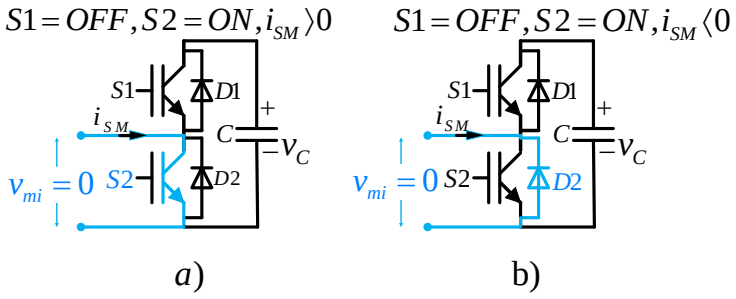

Figure 1-7:The SM bypassed state

• Blocked State: Both IGBTs S1 and S2 are turned OFF.

For this state, only the free wheel diodes operate and it can be seen in Figure 1-8 that the SM capacitor can be charged through D1 for positive currents and for negative currents the diode D2 offers a path, even if the SM is blocked. It can be conclude that the SM capacitor never can be discharged in blocked state. This state refers to MMC DC short-circuit situations.

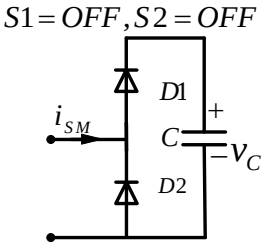

Figure 1-8:The SM blocked state

Based on mentioned SM normal operations, only active state and bypassed state are considered. A general function of theSM_i based on "SM insertion index" (n_i) can be derived as following:

- n_i=1 when SM_i is in active state then $v_{mi_i} = v_c$
- n_i=0 when SM_i is in bypassed state then $v_{mi} = 0$

Then it is possible to write general function of SM_i capacitor voltage:

$$C\frac{dv_{mi}}{dt} = n_i\, i_{SMi} \qquad \textbf{(1.1)}$$

1.1.5. Description of MMC with half bridge SMs

A three phase MMC converter connected to the grid is depicted in Figure 1-9.

Let the sum of the SMs voltages with in an arm be $v_{mu/l\,i}$ with phase index of i=a,b,c .

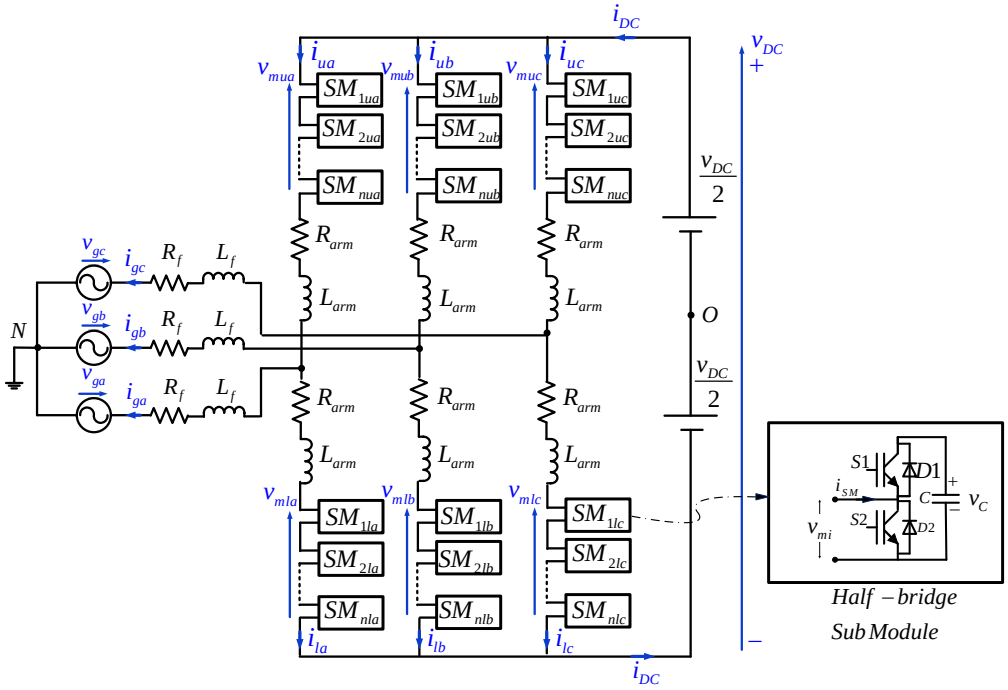

Figure 1-9:The MMC based on half bridge SM

By applying Kirchhoff current and voltage equations to the upper and lower loops of the MMC in Figure 1-9 result in (1.2), (1.3) and (1.4)

$$i_{gi} = i_{ui} - i_{li} \tag{1.2}$$

$$\frac{v_{DC}}{2} - v_{mui} - R_{arm}\, i_{ui} - L_{arm}\frac{di_{ui}}{dt} = v_{gi} + R_f\, i_{gi} + L_f\frac{di_{gi}}{dt} + v_{NO} \tag{1.3}$$

$$-\frac{v_{DC}}{2} + v_{mli} + R_{arm}\, i_{li} + L_{arm}\frac{di_{li}}{dt} = v_{gi} + R_f\, i_{gi} + L_f\frac{di_{gi}}{dt} + v_{NO} \tag{1.4}$$

From above equations it is possible to present the MMC in the matrix form:

$$\begin{bmatrix} L_f + L_{arm} & L_f \\ -L_f & -L_f - L_{arm} \end{bmatrix} \begin{bmatrix} \frac{di_{ui}}{dt} \\ \frac{di_{li}}{dt} \end{bmatrix} = \begin{bmatrix} -R_f - R_{arm} & -R_f \\ R_f & R_f + R_{arm} \end{bmatrix} \begin{bmatrix} i_{ui} \\ i_{li} \end{bmatrix} + \begin{bmatrix} \frac{v_{DC}}{2} - v_{mui} - v_{gi} - v_{NO} \\ -\frac{v_{DC}}{2} + v_{mli} - v_{gi} - v_{NO} \end{bmatrix} \tag{1.5}$$

It can be noticed from (1.5) that the MMC system matrixes are not diagonal which means that the MMC converter is a coupled system. In order to control the inner dynamics as well as to control the AC and DC power exchange in the MMC system, it is interesting to decouple the AC and DC parts.

- MMC AC part:

By adding term by term the main equations of (1.3) and (1.4) it can obtain:

$$-v_{mui}+v_{mli}-2v_{NO}+R_{arm}\left(-i_{ui}+i_{li}\right)+L_{arm}\left(-\frac{di_{ui}}{dt}+\frac{di_{li}}{dt}\right)=2v_{gi}+2L_f\frac{di_{gi}}{dt}+2R_f\,i_{gi} \tag{1.6}$$

- MMC DC part:

By subtracting term by term the main equations of (1.3) and (1.4) it results:

$$v_{DC}-\left(v_{mui}+v_{mli}\right)-R_{arm}\left(i_{ui}+i_{li}\right)-L_{arm}\left(\frac{di_{ui}}{dt}+\frac{di_{li}}{dt}\right)=0 \tag{1.7}$$

Regarding to (1.2), (1.6) and (1.7) it is possible to present system in the matrix form:

$$\begin{bmatrix} 2L_f-L_{arm} & -2L_f+L_{arm} \\ -L_{arm} & -L_{arm} \end{bmatrix}\begin{bmatrix} \frac{di_{ui}}{dt} \\ \frac{di_{li}}{dt} \end{bmatrix}= \begin{bmatrix} 2R_f+R_{arm} & -2R_f-R_{arm} \\ R_{arm} & R_{arm} \end{bmatrix}\begin{bmatrix} i_{ui} \\ i_{li} \end{bmatrix}+\begin{bmatrix} 2v_{gi}+2v_{NO}+v_{mui}-v_{mli} \\ v_{mui}+v_{mli}-v_{DC} \end{bmatrix} \tag{1.8}$$

The matrix diagonalization procedure leads to the variable changes that clearly reveal the MMC inner parameters participate in power exchange between AC grid and DC link.

Matrix diagonalization leads to the following variable changes:

$$i_{diff\,i}=\left(\frac{i_{ui}+i_{li}}{2}\right) \tag{1.9}$$

$$v_{diff\,i}=\left(\frac{v_{mui}+v_{mli}}{2}\right) \tag{1.10}$$

$$v_{v\,i}=\left(\frac{-v_{mui}+v_{mli}}{2}\right) \tag{1.11}$$

$$v'_{v\,i}=v_{vi}+v_{NO} \tag{1.12}$$

With:

i_{diff} : MMC inner difference current of phase i which circulates between the MMC legs

v_{diff} : MMC inner unbalance voltage of phase i which relates to i_{diff} flows through MMC leg

v_{vi} : MMC inner AC voltage of phase i

Regarding the above MMC variables, (1.6) and (1.7) can be written as following:

$$v'_{vi} - v_{gi} = \left(\frac{R_{arm} + 2R_f}{2}\right) i_{gi} + \left(\frac{L_{arm} + 2L_f}{2}\right) \frac{di_{gi}}{dt} \tag{1.13}$$

$$\frac{v_{DC}}{2} - v_{diff} = R_{arm}\, i_{diff\,i} + L_{arm} \frac{di_{diff\,i}}{dt} \tag{1.14}$$

Representation of the system presented in (1.15) demonstrates the decoupled MMC system:

$$\begin{bmatrix} \frac{di_{gi}}{dt} \\ \frac{di_{diff\,i}}{dt} \end{bmatrix} = \begin{bmatrix} \frac{2R_f + R_{arm}}{2L_f + L_{arm}} & 0 \\ 0 & \frac{-R_{arm}}{L_{arm}} \end{bmatrix} \begin{bmatrix} i_{gi} \\ i_{diff\,i} \end{bmatrix} + \begin{bmatrix} \frac{2}{2L_f + L_{arm}} \left(v'_{vi} - v_{gi}\right) \\ \frac{1}{L_{arm}} \left(v_{diffi} - \frac{v_{DC}}{2}\right) \end{bmatrix} \tag{1.15}$$

It is important to notice that ,since the sum of the grid currents is equal to zero there are 5 state values ($i_{g\,a}$, $i_{g\,b}$, $i_{diff\,a}$, $i_{diff\,b}$, $i_{diff\,c}$).

1.2 DIFFERENT LEVELS OF MMC MODELING

There are many variables in a MMC due to the high number of IGBT's. Different modeling approaches can be used according to the type of study and required accuracy. Model evolution in decreasing complexity is depicted in Figure 1-10 [35]. It is expected that by decreasing model complexity, computational performance can be increased. Model 1 is the most detailed. Model 2 uses a simplified power switch circuit model. Model 3 makes a simplified arm circuit equivalent.

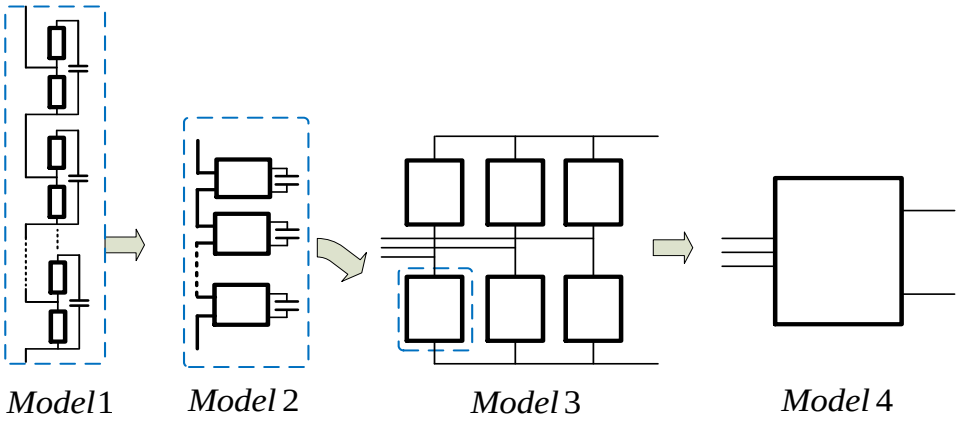

Figure 1-10:MMC model evolution in decreasing complexity

A. Model 1: Detailed IGBT-Based Model

This model considers a detailed representation of power switches. The model presented in [36] uses an ideal controlled switch, based on the half-bridge SM topology, and using the classical V-I characteristics of the power switches besides manufacturer data sheets or field measurements for non-linear characteristics.

High and Low Level controls can be implemented with this model and it is suitable model for switching and conduction losses study with any topological conditions in the converter. Although, the detailed model has a high degree of fidelity and accuracy for related switching studies it requires a large computation time in order to simulate the MMC power system with a large number of SMs. In this thesis this model will be considered as the reference model.

B. Model 2: Equivalent Circuit-Based Model [37]

In this model the SM power switches are replaced by ON/OFF resistors: R_{ON}(small value in milliohms) and R_{OFF} (large value in mega ohms). This approach allows performing an arm circuit reduction for eliminating internal electrical nodes and allowing the creation of a Norton equivalent for each MMC arm. The resistances are controlled and used for replacing the two IGTB/diode combinations. With the trapezoidal integration rule, each SM capacitor is replaced by an equivalent current source in parallel with a resistance; where is the numerical integration time-step. The derivation of these equations can be found in [37]. However, the blocked state condition and other implementation details have not been addressed. The main advantage of Model 2 is the significant reduction in the number of electrical nodes in the main system of network equations. The algorithm still considers each SM separately and maintains a record for individual capacitor voltages. It is applicable to any number of SMs per arm.

C. Model 3: MMC Arm Switching Function

In this model, each MMC arm is averaged by using the switching function concept of a half-bridge converter based on equation (1.1) and SM index.

Assuming that there is an ideal capacitor voltage balancing with in each arm, the following assumption can be made:

$$v_{C_1} = v_{C2} = \ldots = v_{C_i} = \frac{v_{C_{tot}}}{N} \tag{1.16}$$

Where $v_{C\,tot}$ represents the sum of all capacitor voltages within an arm. The accuracy of assumption increases when the number of SMs per arm is increased and/or when the fluctuation amplitudes of capacitor voltages are decreased. This assumption allows deducing an equivalent capacitance $C_{arm} = C/N$ for each arm. By defining the switching functions of an arm as follows:

$$\frac{1}{N}\sum_{i=1}^{N} n_i = m_i \tag{1.17}$$

Including the linear conductivity losses for each SM, the following switching functions can be derived for each arm when the SMs are in ON/OFF states [38]:

$$v_{mi} = m_i\, v_{ctot\,i}$$
$$i_{ctot\,i} = m_i\, i_{mi} \qquad \textbf{(1.18)}$$

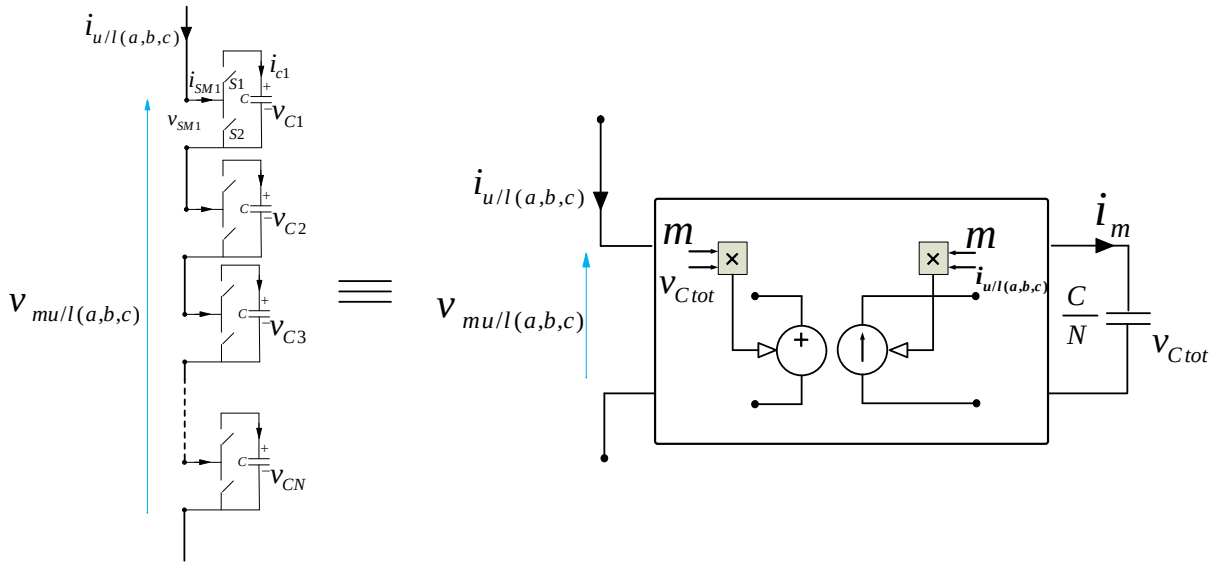

Figure 1-11:switching function model of MMC arm

$v_{mu/l}$ is defined as the modulated arm voltage for the upper or lower arm. Figure 1-11 presents a simple model of the arm. A more complex is presented in [38] which can take into account the blocked state.

By reducing each arm to an equivalent switching function model, power switches are no longer represented. This means that the balancing control of capacitor voltages in each arm and redundant SM impacts (low-level control) cannot be studied using this approach. However, the energy transferred from AC and DC sides into each arm of the MMC is taken into account, which is useful for control system strategies based on internal MMC energy balance (high-level control). Therefore, in high level control the equivalent arm capacitor voltages ($v_{c\,ul\,tot\,i}$) should be controlled (6 state variables).

$$i_{mi} = \frac{C}{N}\frac{dv_{Cul\,itot}}{dt} \qquad \textbf{(1.19)}$$

D. Model 4: Average Model of MMC

In the average model, the IGBTs and their diodes are not explicitly represented and the MMC behavior is modeled using controlled voltage and current sources. The classical AVM approach is developed for 2- and 3-level VSCs in [39] and extended to MMCs in [36, 37, 40]. In this model the whole MMC is replaced by a classic two-level-VSC converter, i.e. an equivalent capacitor is directly connected between the DC terminals. Therefore the energy stored in the

MMC cannot be controlled independently to the DC voltage level. This type of model is valid only for one high-level control strategy similar to VSC voltage control.

1.3 LOW LEVEL CONTROL

The MMC output voltage is created by the insertion and the bypassing of SMs capacitors. The arm current flows through the inserted SM capacitors and thereby changes their voltage, or equivalently, their energy content. Therefore a control is needed to switch on and off the SMs to maintaining a proper voltage balancing between the different capacitors in each SM.

Regarding the mentioned requirements, the control of such a converter presents interesting challenges, especially when it comes to operating a large number of SMs within one arm. This is the reason that in case of a MMC-HVDC with several hundreds of SMs, the modulation techniques and balancing algorithm are considered as the low-level control, and they are studied independently from the power and DC or AC voltage/current controls named as the high-level control shown in Figure 1-12.

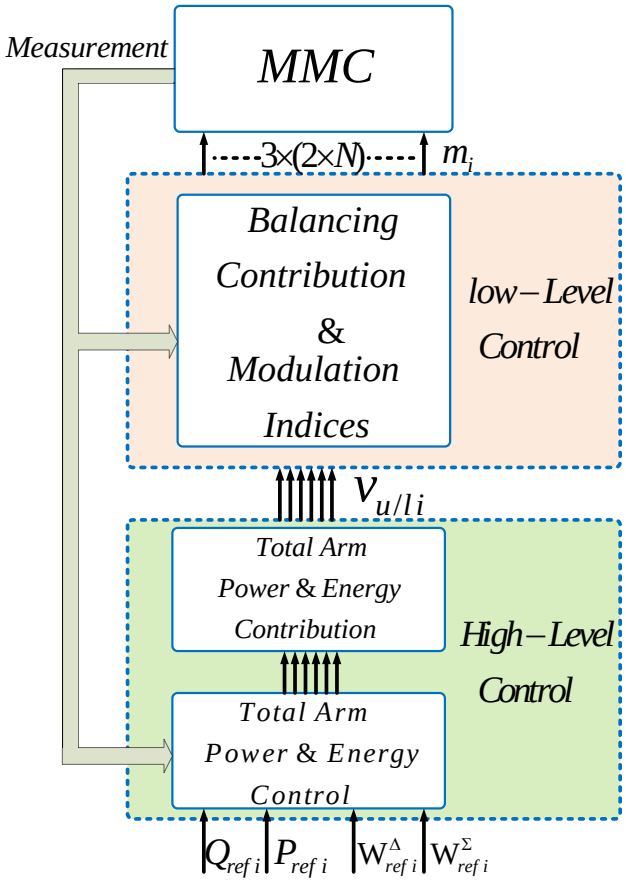

Figure 1-12:The general MMC control structure

Different techniques for low-level control are briefly presented in the following to give an overview of existing methods.

One of the possibilities is to regulate every SM individually with one PI controller per SM. Each SM is associated with a reference that combines the output voltage of the upper control layer and balancing voltages, this reference is then compared with a time-shifted triangular waveform (CPS-PWM) [41, 42]. This approach is simple and efficient for a small level of SM but its computational burden increase with the number of SM to balance.

Other methods are used for high power MMC which requires a very larg number of SMs. Two steps are identified in these methods.

The modulation technique

This function determines the number of SMs to be inserted or bypassed according to the voltage reference given by the current-control. There are several modulation approaches based on the PWM, like the CPS-PWM that can also be used with a unique unmodified reference or the Phase-Disposition PWM (PD-PWM), but also other techniques like the Selective Harmonic Elimination (SHE) or the Nearest Level Control (NLC) [43] The NLC being the simplest method it is widely used for MMCs with a large number of SM.

The principle of the NLC is the following:

$$n_i = round(N * m_i)$$

With n_i the number of SM to activate in arm i, N the number of SM per arm and m_i the duty cycle obtained from the high level control.

The Balancing Control Algorithm

This algorithm chooses between all the SMs in the arm which ones have to be switched on to respect the voltage balancing. The first BCA for MMC [44] (see Figure 1-13) implies a sorting and a selection of the SM with the lowest voltages if the current is positive (i.e. charging the capacitors) or with the highest voltages (i.e. discharging the capacitors). This BCA is very simple but it involves a very high switching frequency and thus increased losses compared to other BCAs.

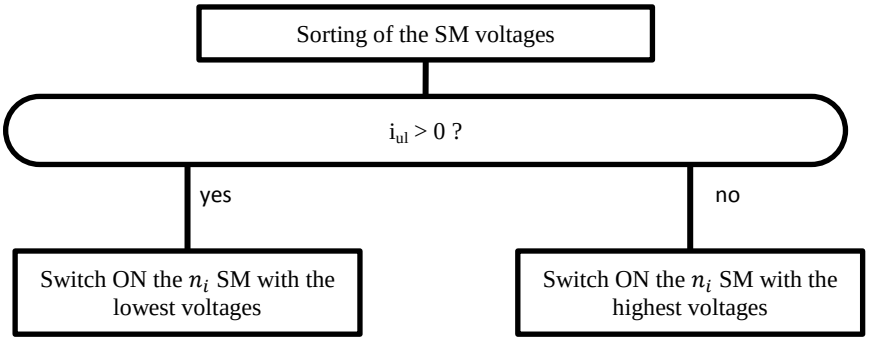

Figure 1-13:Basic BCA flowchart

To reduce the losses, voltage tolerance can be added [45] (Figure 1-14). If the voltage difference between the highest and the lowest capacitor voltages is below the tolerance the previous activated SM is kept or slightly modified by inserting or bypassing the exact number of SMs required regarding the modification on n_i. If the difference is bigger than the tolerance, the previously seen algorithm is used.

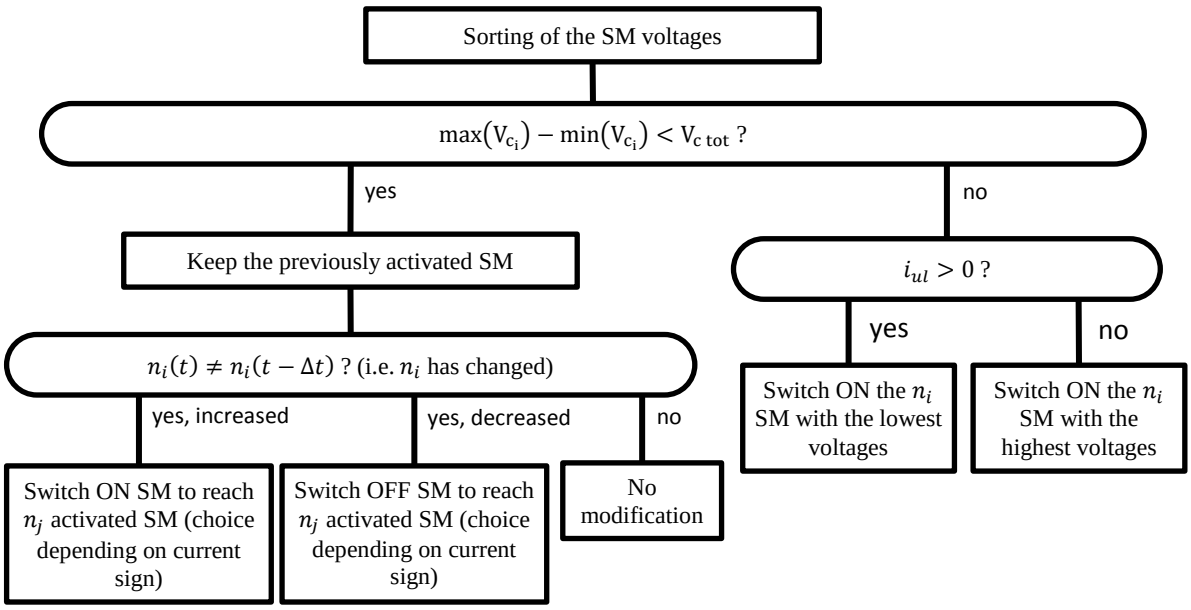

Figure 1-14:BCA with Voltage tolerance

It is also possible to avoid the sorting step, by considering a BCA that would only insert or bypass one SM at a time [46] (see Figure 1-15). The selection of this SM is made by considering only the previously inserted (resp. bypassed) SMs if we need to bypass (resp. insert) one, then according to the sign of the current the one with the lowest or highest voltage is chosen.

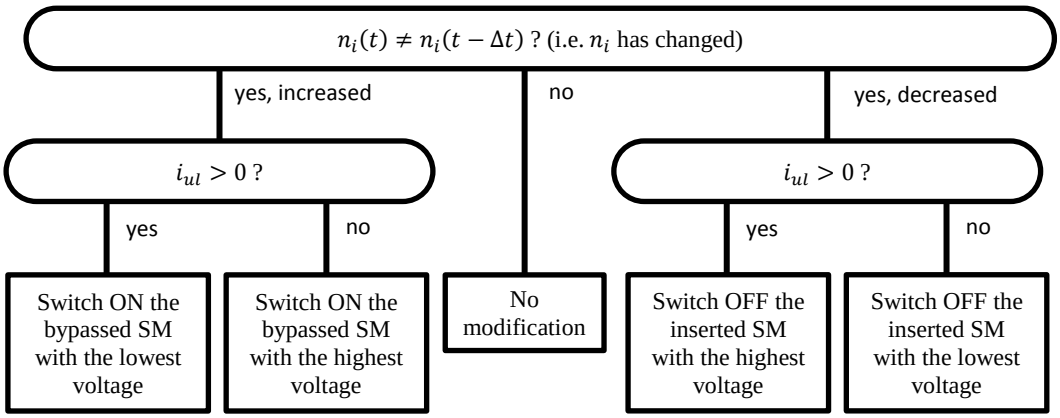

Figure 1-15:Min-Max BCA

In the sequel, balancing control algorithm is supposed to be ideal and it will be taken into account. For high number of SMs [36] has shown that the simulation results with model 2 or model 3 are very similar.

1.4 STATE OF ART ON THE HIGH LEVEL CONTROL

The high level control aims to control the currents, power and energy in the MMC. There are numerous publications in this area; however most of these publications tend to focus on an MMC alone rather than considering the overall system in an HVDC. In the literature, two main control solutions for this converter can be distinct: non-energy based control strategies and energy-based control strategies. In this subsection these two categories are explained briefly and at the last an overview of the advanced control applied on the MMC is proposed.

1.4.1. Non energy based control

The non-energy based control schemes are based on the inner current controllers which produce the voltage references for the modulators which communicate with the low level control. In this concept, different modulation methods have been proposed [8, 15, 47, 48]. The basic non-energy based control structures are based on positive sequence dq control of AC currents regarding the active power reference. These schemes are very simple but they can lead to non-sinusoidal output voltages and high voltage ripples on capacitor voltages [48-50]. To improve voltage quality and reduce capacitor voltage ripples, it can be used the CCSC (Circulating Current Suppression Controller) [51-55]. In this control scheme the second harmonic component of the circulating current of the MMC may be suppressed by means of Park's transform at -2ω. Such component does not contribute to the average power transfer at the DC terminals of the converter; yet it dissipates power since it circulates through the MMC internal resistances increasing the converter losses. Therefore, this current aimed to be minimized so that it will only have a DC component.

This control strategy leads to satisfying characteristics under normal operation but it is still difficult to predict the behavior in particular operating conditions as presented in [56]. In addition, this strategy is based on dq-coordinates, and there is no control of the zero-sequence component of the circulating current. Where, the zero sequence can be used to control the total capacitive energy of the converter. [57, 58]

However, this strategy has provided a very influential starting point for the HVDC projects and therefore in this work is analyzed in details in chapter 2.

1.4.2. Energy based control

To have a full control of the MMC inner dynamics and the stored energy in the system, the number of controllers must be equal to the number of independent state variables(11 state variables) of the system. If not, some state variables may be out of control that can take unacceptable values and lead to unstable modes in particular operating conditions as mentioned

briefly in the previous part. To solve this problem, the control scheme named "energy based control" have been developed [15, 59-62] in which all the state variables of the system are controlled. A general structure of such a control approached is depicted in Figure 1-16

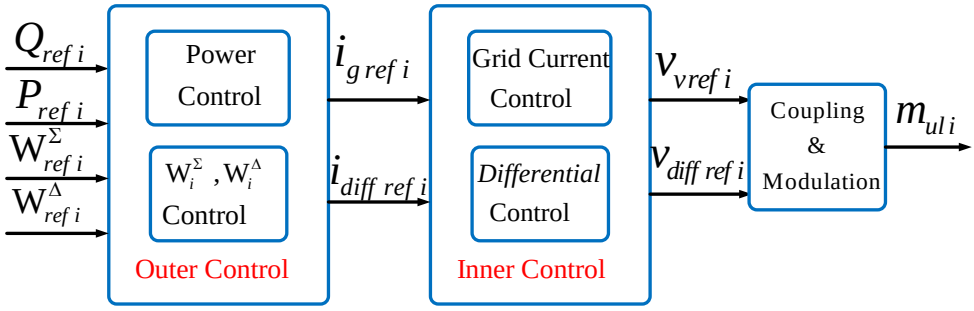

Figure 1-16: A general structure of the energy based scheme.

Due to the fact that the MMC energy and current variables have various frequencies, this task is not straightforward, and decoupling the MMC variables into its different frequency components becomes necessary. Based on this notion different energy based scheme are developed. The energy based control proposed in [60] is an attempt to extend the CCSC by including a feedback control loop in the arm capacitor energies of the MMC. The first drawback of this control method is that, since it is based on "dq0" rotating reference frame, it needs several reference frame transformations at the different frequencies where they are naturally coupled in the MMC. The second drawback refers to its inability to control the stored energy per phase independently. In other words, only the sum of the stored energy is controlled. However due to the DC current components it is important to control the stored energy of each phase independently.

1.4.3. Advanced control

Since MC converter is a multi-input multi-output (MIMO) system it may require the adoption of advanced control strategies, due to the strong coupling between the states for nonlinear dynamics. Recently, several efforts have been deployed in this direction including model predictive control [51, 61, 63] The main results concern the indirect FCS-MPC (Finite Control Set – Model Predictive Control) control strategy which allows achieving AC-side current control, capacitor voltage balancing and circulating current suppression control at the same time [64]. In [60], the Lagrange multiplier in the "abc" frame is suggested for the control of internal dynamics of the MMC converter. This mathematical optimization technique is exploited in order to instantaneously control the average capacitive energy sum and difference, stored in the upper and lower arms, while minimizing the fluctuations in either the circulating currents or sum of the stored energy in capacitors. To improve the performance of the proposed method, adaptive filters are used in [65] for estimating the input variables needed by the controller. A state space control approach based on linear quadratic regulator (LQR) controller with integral action for a three phase multi cells MMC is developed and detailed in [66]. To improve the robustness, a state space controller is designed in [67], based on input output linearization.

In fact, simultaneous control of the AC-side currents, differential currents, and stored energy of the MMC turns out to be a bilinear modeling on which some advanced control techniques can be used. Based on bilinear state space model, the trajectory tracking problem for power converters based on passivity foundations has been solved [68]. Due to the use of passivity theory, the controller is a simple conventional PI controller. The stability results are global and hold for all positive definite gains of conventional controllers

In [69], a periodic bilinear time-varying model of the MMC in the rotating reference frame is developed. Based on this PBTI (Periodic Bilinear Time Invariant) model, Ph. Münch has proposed a Periodic Linear Quadratic Regulator (PLQR) with an extended and least squares (LS) estimator to determine the currents and energies. The PLQR controller is proposed to control the currents and stored energy of the MMC. The PLQR regulator is used to achieve optimal control. Using lifting procedure, the problem becomes a time-invariant state feedback control.

In [70, 71], a global asymptotic stability of the system is investigated. Using the passivity-based methods, the controller design and stability analysis of the MMC is given in [72]. Most of these methods lead to a linear controller but a few results in literature concern advanced control strategies based on nonlinear control law. In [73], the Sum of Squares (SOS) decomposition method is used to design a nonlinear controller for the discrete-time bilinear model of the MMC. However, the proposed approach leads to a complex control law, where the practical implementation is not obvious.

1.5 CONCLUSION

Evolution of HVDC convert topologies over time has shown a great improvement by innovation of the new converter structure named MMC. In this chapter different MMC topologies with the possible SM circuit configuration are presented. Since, focus of this work is to study the control of the MMC in an HVDC, the well-known structure of the MMC based on the half-bridge SMs is considered. The basics of such a MMC are provided as well.MMC has a complex topology to control, two level controls are established: low-level and high-level controls which the latter is the subject of this work.

Although, the trend of MMC high –level control is to use advanced controllers, the classical PI or PID controllers are considered in this work to study and analysis the dynamic of all MMC state variables. This study leads to profound comprehension the dynamic interaction between inner and outer loops in the MMC which are detailed in chapter 2,3 and 4.

CHAPTER 2 : MMC Current control design

2.1 INTRODUCTION

This chapter is focused on the control of the grid and differential MMC currents. Regarding section 1.1.6, the MMC current variables are deduced directly as three grid currents (i_{gi}) and three differential currents (i_{diffi}). The dynamic of these MMC state variables should be the fastest compare to control of other MMC variables. In this chapter these currents and their proper controls are discussed.

Until the end of this chapter, the converter balancing voltage of SMs is considered as ideal, therefore the arm-averaged model, as shown in Figure 2-1, is used in order to not take into account the harmonics which are not a matter of interest of this thesis.

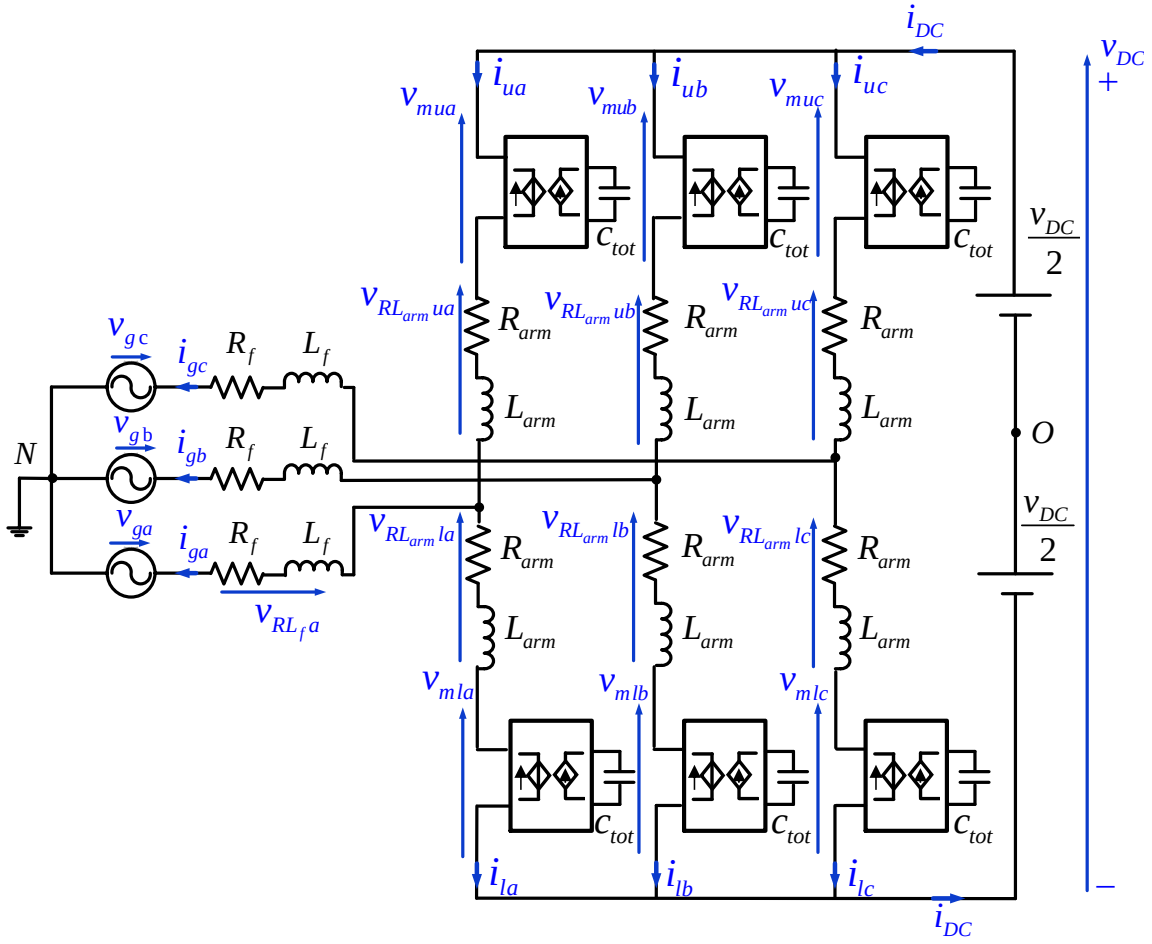

Figure 2-1: MMC based on the arm-average model

For the sake of simplicity the main equations are recalled in Table 2-1 (see chapter 1). From these differential equations the block diagram of a three phased MMC can be derived. The MMC block diagram of phase-a is presented in the upper part of Figure 2-2 .

To address the control synthesis, a general structure of MMC inner currents closed loops based on the concept of inverse model is presented in lower part of Figure 2-2. In the next subsections the control principles of current controllers: $C_{r\,i_g}$ and $C_{r\,i_{diff}}$ are discussed.

Table 2-1: MMC main equations

MMC differential equations	
$v_{m\,u/l\,i} = m_{u/l\,i} v_{c\,u/l\,i\,tot}$	(2.1)
$v_{diff\,i} = \left(\frac{v_{mu\,i} + v_{ml\,i}}{2}\right), v_{v\,i} = \left(\frac{-v_{mu\,i} + v_{ml\,i}}{2}\right)$	(2.2)
$\acute{v}_{vi} - v_{gi} = \left(\frac{R_{arm} + 2R_f}{2}\right) i_{gi} + \left(\frac{L_{arm} + 2L_f}{2}\right) \frac{di_{gi}}{dt}$	(2.3)
$\frac{v_{DC}}{2} - v_{diff\,i} = R_{arm} i_{diff\,i} + L_{arm} \frac{di_{diff\,i}}{dt}$	(2.4)
$i_{gi} = i_{u\,i} + i_{l\,i}\,,\; i_{diff\,i} = \left(\frac{i_{u\,i} + i_{l\,i}}{2}\right)$	(2.5)
$m_{u/l\,i}\, i_{u/l\,i} = C_{tot} \frac{dv_{cu/l\,i}}{dt}$	(2.6)
With $i = a, b, c$	

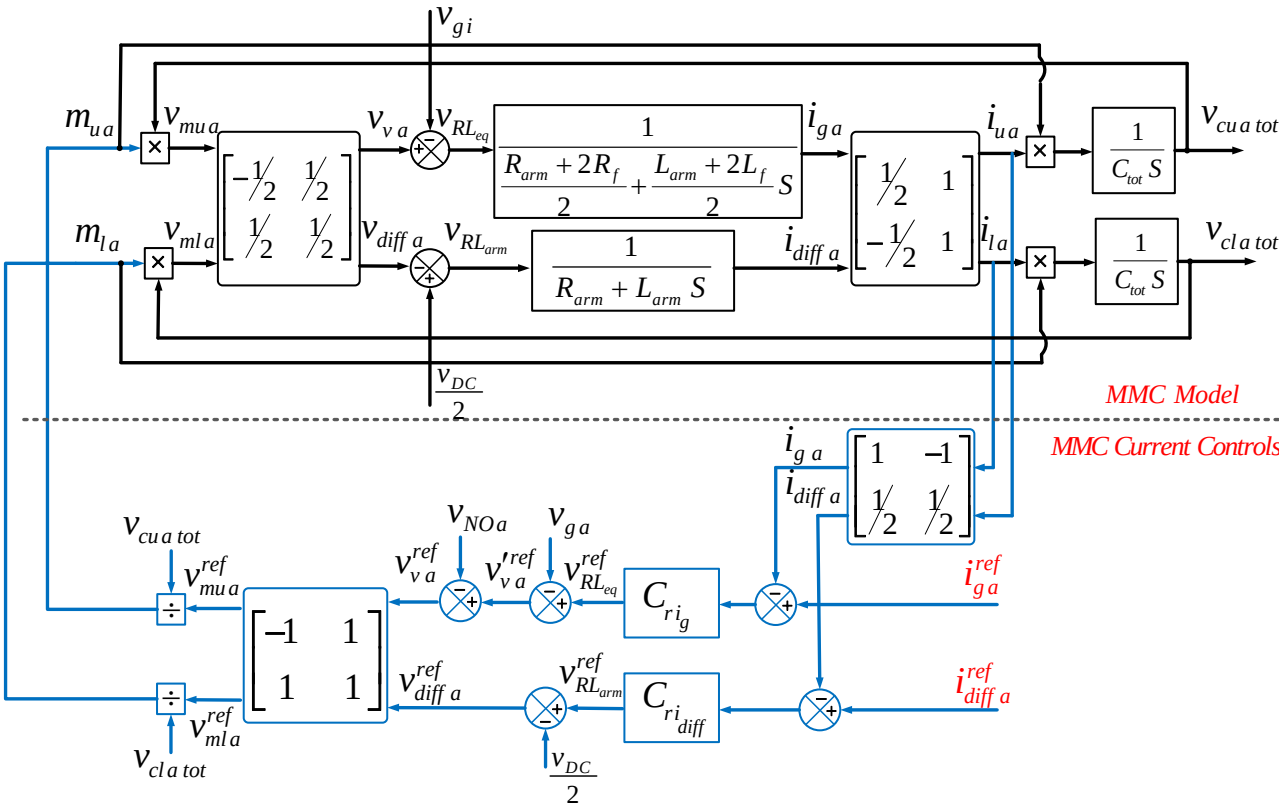

Figure 2-2: Bock diagram of current loops via model inversion

2.2 AC CURRENT CONTROL STRUCTURE

The general organization of the AC current control is deduced from the inversion of the part of the MMC block diagram which establishes the link between the currents to control and the control signals: $m_{u\,i}$ and $m_{l\,i}$. For each current and voltage in the MMC model a reference signal is defined in the control. In steady state, each current or voltage is supposed to be equal to its reference. Depending on the type of equation, the inversion may be adjusted. In case of an instantaneous relation, a direct inversion may be derived, in case of a differential equation is involved, a closed loop is needed.

The different inversions are now detailed.

- Inversion of equation (2.1):

$$m_{u/l\,i}^{ref} = v_{mu/l\,i}^{ref} / v_{c\,u/l\,i\,tot} \tag{2.7}$$

Equation (2.1) is nonlinear. The new system whose inputs are $v_{mu/l\,i}^{ref}$ and outputs are the grid and differential currents, can be considered as linear. This linearization plays an important role on the MMC control performance, a discussion on this point will be proposed in section 2.6.

- Inversion of equation (2.2):

$$v_{mu\,i}^{ref} = \left(v_{diff\,i}^{ref} - v_{v\,i}^{ref}\right), \qquad v_{ml\,i}^{ref} = \left(v_{diff\,i}^{ref} + v_{v\,i}^{ref}\right) \tag{2.8}$$

Equation (2.2) highlights the coupling between $m_{u\,i}$ and $m_{l\,i}$ to control the grid and differential currents. The new system composed whose inputs are $v_{v\,i}^{ref}$ and $v_{diff\,i}^{ref}$ is now decoupled.

- Inversion of equation (2.3)and(2.4):

$$v_{v\,i}^{ref} = v_{RL_{eq}\,i}^{ref} + v_{gi} \tag{2.9}$$

$$v_{diff\,i}^{ref} = \frac{v_{DC}}{2} - v_{RL_{arm}\,i}^{ref} \tag{2.10}$$

Equations (2.3) (2.4) are the differential equations that they necessitate the closed loops for their inversion. For the control of $i_{g\,i}$, $v_{g\,i}$ is considered as a disturbance, this operation is proposing a compensation of the disturbance. The same way in equation (2.4), $v_{DC}/2$ is compensated as a disturbance.

The new system composed whose inputs are $v_{v\,i}^{ref}$ and $v_{diff\,i}^{ref}$ is now linearized and decoupled.

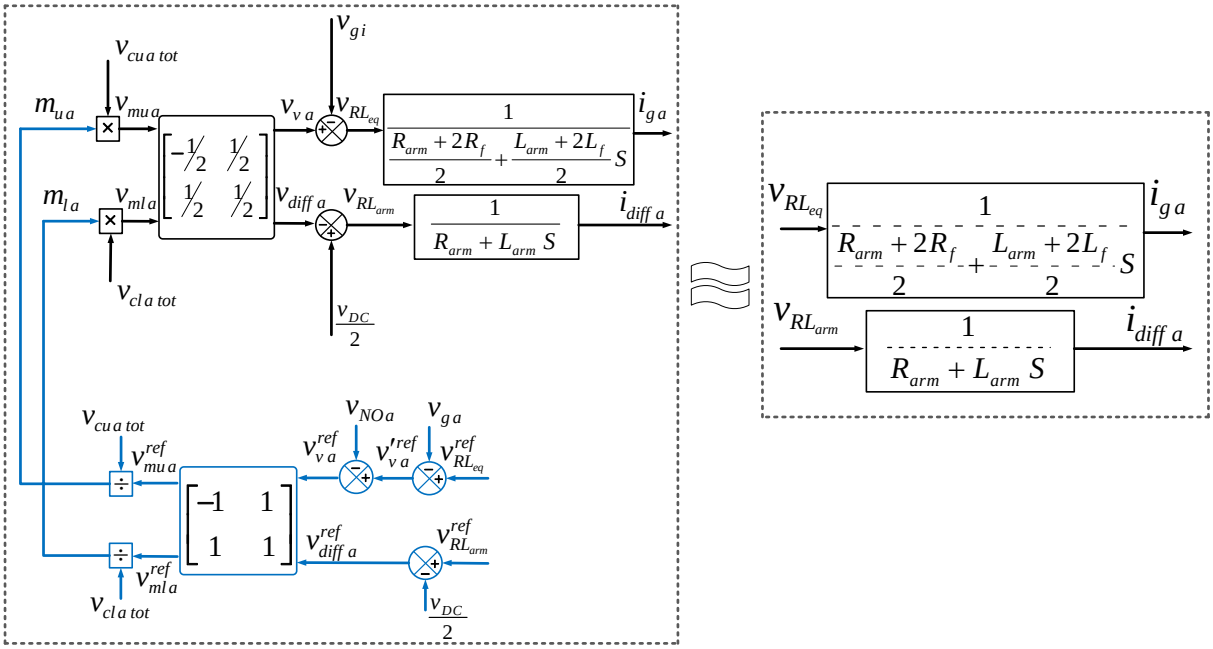

Figure 2-3: Equivalent model of MMC currents via model inversion

In conclusion, the different actions detailed in (2.7), (2.8), (2.9) and (2.10) simplify the design of the controllers. Hence the control system can be considered equal to (2.9) and (2.10) as shown in write part of Figure 2-3, it behaves as if it were two decoupled simple first orders system to control.

In reality, the actual system behavior is never the same as its model representation but the controller is able to cope with these small uncertainties.

To address the control design, a general structure of MMC inner currents closed loops based on the concept of inverse model is presented in lower part of Figure 2-2. In the next subsections the control principles of current controllers $C_{r\,i_g}$ and $C_{r\,i_{diff}}$ are discussed.

2.3 DESIGN OF THE AC CURRENT CONTROLLER

Based on the grid current equations (2.3), and the inversion method described in previous section, it can be deduced that control of these currents is possible via a classical PI first order controller.

The control scheme of AC grid currents proposed in this thesis is a well-known approach in the literature [50]. In this method, two current axes: direct and quadrature, (dq)-axes are defined, and a control strategy is designed based on the mathematical model of the system. Using feedforward signals and PI regulators, the dq axes can be independently controlled this leads to control the active power and the reactive power separately.

2.3.1. Structure of the controller

Applying PI controllers for the AC currents necessitate the dq coordination that they can be obtained by Park transformation. This transformation is commonly used in three-phase rotating system to convert the three phase rotating domain to two phase's stationary domain. The Park transformation used in this thesis is the power invariant one. The transformation matrix and its inverse are described as following:

$$P=\frac{2}{3}\begin{bmatrix} \cos(\theta) & \cos\left(\theta-\frac{2\pi}{3}\right) & \cos\left(\theta+\frac{2\pi}{3}\right) \\ -\sin(\theta) & -\sin\left(\theta-\frac{2\pi}{3}\right) & -\sin\left(\theta+\frac{2\pi}{3}\right) \\ \frac{1}{2} & \frac{1}{2} & \frac{1}{2} \end{bmatrix} \quad (2.11)$$

$$P^{-1}=\begin{bmatrix} \cos(\theta) & -\sin(\theta) & 1 \\ \cos\left(\theta-\frac{2\pi}{3}\right) & -\sin\left(\theta-\frac{2\pi}{3}\right) & 1 \\ \cos\left(\theta+\frac{2\pi}{3}\right) & -\sin\left(\theta+\frac{2\pi}{3}\right) & 1 \end{bmatrix} \quad (2.12)$$

The angle θ_s is linked to the grid angle and it is determined thanks to a PLL (Phase Lock Loop). More details can be found in appendix II. The description of the system after applying the Park transformation can be split in two sets of decoupled equations. The zero sequence component of the current is equal to zero since the sum of the grid currents are always equal to zero.

$$v_{vd}-v_{gd}=\left(L+\frac{L_{arm}}{2}\right)\frac{di_{gd}}{2}+\left(R+\frac{R_{arm}}{2}\right)i_{gd}+\left(L+\frac{L_{arm}}{2}\right)\omega i_{gq} \quad (2.13)$$

$$v_{vq}-v_{gq}=\left(L+\frac{L_{arm}}{2}\right)\frac{di_{gq}}{2}+\left(R+\frac{R_{arm}}{2}\right)i_{vq}+\left(L+\frac{L_{arm}}{2}\right)\omega i_{gd} \quad (2.14)$$

At this stage, the choice has been done to design the controller based on a per unit model. Since synthesis of the control schemes are more comprehensive in per unit system, the control schemes are designed in per unit. The MMC AC parameters in per unit are described as follow:

2.3.2. Design of the AC current controller based on per unit model

At this stage, the choice has been done to design the controller based on a per unit model. Since synthesis of the control schemes are more comprehensive in per unit system, the control schemes are designed in per unit. The MMC AC parameters in per unit are described as follow:

$$S_b = S_n \text{ (Apparent power)} \quad (2.15)$$

$$V_b = V_n \text{ (RMS value of the phase to neutral voltage)} \quad (2.16)$$

$$\omega_b = \omega_n = 2\pi f_n \quad (2.17)$$

$$I_b = \frac{S_b}{3V_b} \quad (2.18)$$

$$Z_b = \frac{V_b}{I_b} \tag{2.19}$$

$$L_b = \frac{Z_b}{\omega_b} \tag{2.20}$$

With

$$V_{dq_b} = \sqrt{3}V_n = \sqrt{3}V_b \tag{2.21}$$

$$I_{dq_b} = \sqrt{3}I_n = \sqrt{3}I_b \tag{2.22}$$

It can be deduced that:

$$V_{dq_b} I_{dq_b} = 3V_n I_n = S_b \tag{2.23}$$

Then the equations of the AC current model in per unit are as following:

$$\begin{aligned} v_{vd_{pu}} - v_{gd_{pu}} = &\left(\frac{L_{pu}}{\omega_b} + \frac{L_{arm_{pu}}}{2\omega_b}\right)\frac{di_{gd_{pu}}}{dt} + \left(R_{pu} + \frac{R_{arm_{pu}}}{2}\right) i_{gd_{pu}} \\ &+ \left(L_{pu} + \frac{L_{arm_{pu}}}{2}\right)\omega_{pu} i_{gq_{pu}} \end{aligned} \tag{2.24}$$

$$\begin{aligned} v_{vq_{pu}} - v_{gq_{pu}} = &\left(\frac{L_{pu}}{\omega_b} + \frac{L_{arm_{pu}}}{2\omega_b}\right)\frac{di_{gq_{pu}}}{dt} + \left(R_{pu} + \frac{R_{arm_{pu}}}{2}\right) i_{gq_{pu}} \\ &+ \left(L_{pu} + \frac{L_{arm_{pu}}}{2}\right)\omega_{pu} i_{gd_{pu}} \end{aligned} \tag{2.25}$$

The structure of the AC current control in per unit is presented in Figure 2-4. It generates the reference voltages of v_v^{ref} which it can be adopted by the low level control. For PI controllers the pole compensation method can be applied. The proportional and integral coefficients for a PI controller considered as: $K_{p_{pu}}(1 + \frac{1}{T_{i_{pu}} s})$ are abstained as following:

$$T_{i_{pu}} = \frac{2\zeta}{\omega_n} \tag{2.26}$$

$$K_{P_{pu}} = \left(\frac{L_{pu}}{\omega_b} + \frac{L_{arm_{pu}}}{2\omega_b}\right) T_{i_{pu}} \omega_n^2{}_n \tag{2.27}$$

Where $\omega_n$depends on the response time with zeta =0.7. For more details see Index A.

2.3.3. Analysis of the simulation results

Based on the AC current control described in this section the simulation results are proposed: a step of 1 pu is applied on the AC power reference at t = 0.1s. The reactive power reference stays equal to zero. The simulation has been done on EMTP-RV ™ [74] and the parameters are listed in Table 2-2. The response time of current loop is 5ms

.

Table 2-2: Parameter of the simulated MMC

parameter	value
L_f	60 mH
R_f	0.5 Ω
L_{arm}	50mH
R_{arm}	1.02 Ω
C_{tot}	$32\mu F$
U_g	$320kV$
V_{DC}	$640\ kV$

The structure of this control is depicted in Figure 2-4. In this figure it can be seen that the differential currents are not controlled and $v_{RL_{arm}i}$ are considered equal to zero. It can be seen in this figure, the calculation of insert index is done by v_{DC}. This is due to the hypothesis that the average value of the $v_{C\,u/l\,i\,tot}$ are considered equal to v_{DC}.

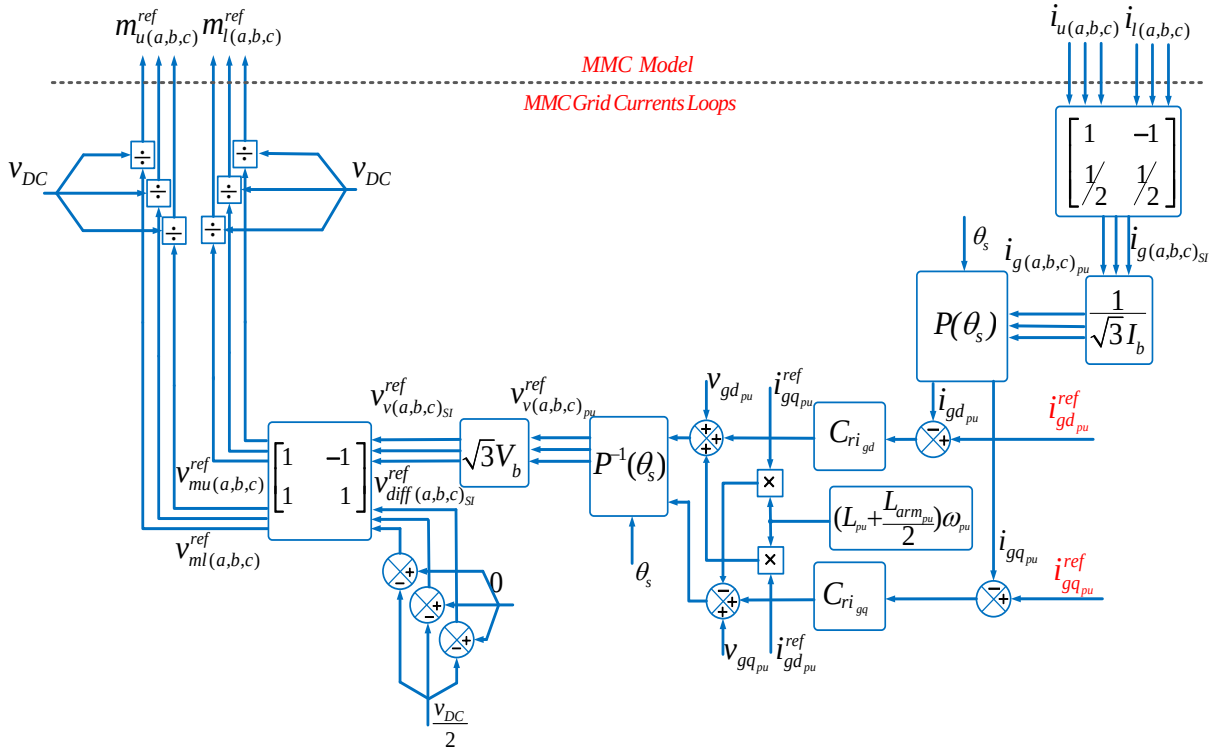

Figure 2-4: MMC Grid current loops in per unit

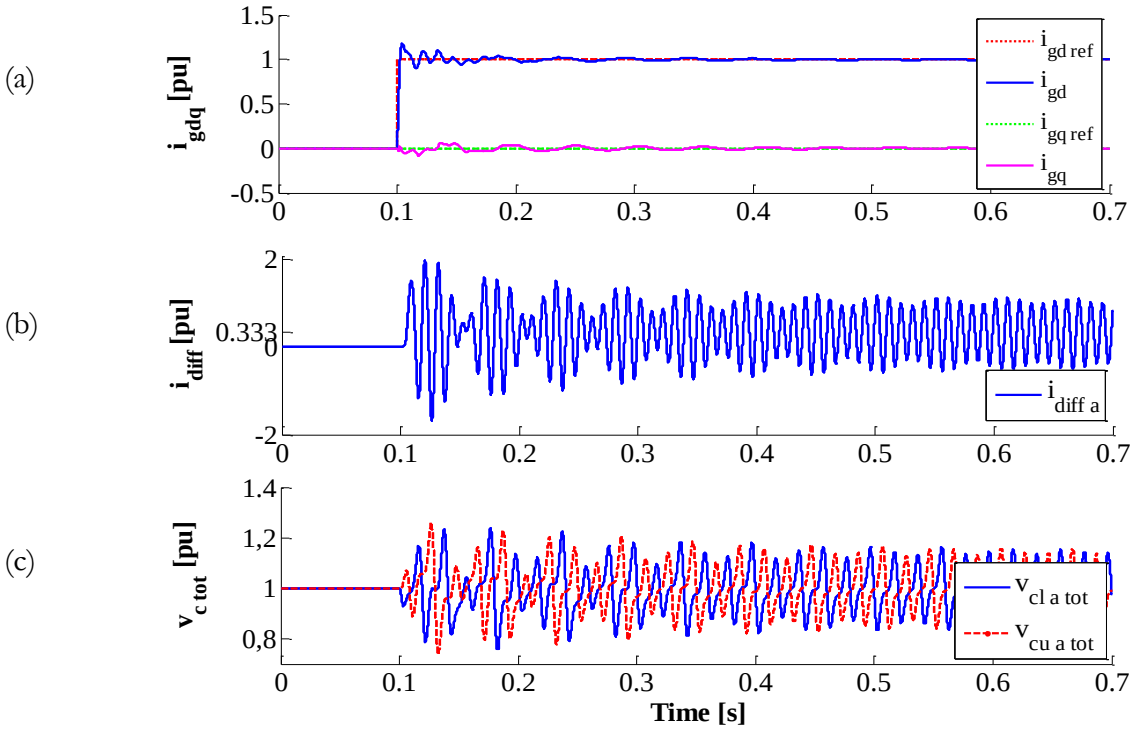

Figure 2-5: MMC AC current simulation results.

The simulation results are presented in Figure 2-5. As shows Figure 2-5(a), in this simulation only the grid currents are controlled. This figure shows that the dq components of the grid currents reach their references correctly. The few oscillations can be noticed, these oscillation are due to the method of calculation of the insert index applied in this control scheme.

Figure 2-5(b), shows the differential current of phase–a . It has important oscillations about 2 pu. Figure 2-5 (c) shows the total voltage of arm capacitors for phase-a. It can be seen that the average value of $v_{cua\,tot}$ and $v_{cla\,tot}$ are stabilized around 1 pu value.

The most important oscillations are observed for the differential currents. These oscillations on the differential currents show clearly drawback of lack of differential current control on the dynamics of the system. From the spectrum of the differential current, shown in Figure 2-6, it can be noticed that this current contains a DC part (0Hz) and the AC part principally at the double frequency (100Hz).

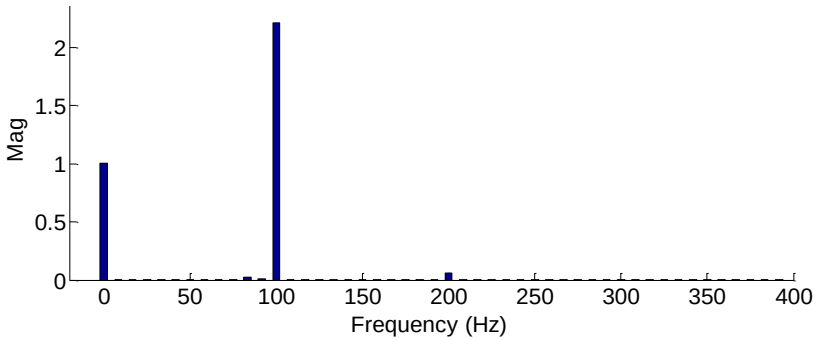

Figure 2-6: Spectrum of differential current with AC current control

As shown previously, the average level on energy stored in the capacitor is next to 1. A very simple solution of control consists in eliminating only the double fundamental frequency harmonic of the differential current a known control scheme named "Circulating Current Suppression Controller" (CCSC) has been proposed [53].This control scheme is explained in the next section. In this case, the average value of the differential current is not controlled explicitly.

2.4 CIRCULATING CURRENT SUPPRESSION CONTROLLER (CCSC)

Circulating currents are corresponding to the part of the AC component of the differential currents that circulate between MMC arms. These currents are due to the arm voltage differences with in a leg. In [75, 76] the circulating current model has investigated and it has pointed out that by considering the AC outer voltage of the MMC ($v_{vi} - v_{gi}$) as a sinusoidal voltage only with the fundamental harmonic, the excited circulation currents have an AC component at the double fundamental frequency in negative sequence. Since these circulating currents distort the arm currents and may increase the SM voltages ripples, a suppression of the second harmonic of the circulating current is proposed in the literature named as CCSC [53, 54, 77]

2.4.1. Expression of the differential current equation in per unit

In order to design the controller of the differential currents based on per unit model equation *(2.4)* recalled here:

$$\frac{v_{DC}}{2} - v_{diff\,i} = R_{arm} i_{diff\,i} + L_{arm} \frac{di_{diff\,i}}{dt}$$

Then the MMC DC parameters in per unit are described as follow

$$P_b = P_n \tag{2.28}$$

$$V_{DCb} = V_{DCn} \tag{2.29}$$

$$I_{DCb} = \frac{P_b}{V_{DCb}} \tag{2.30}$$

$$R_{DCb} = \frac{V_{DCb}}{I_{DCb}} \tag{2.31}$$

$$H_L = \frac{1}{2} L_{arm} \frac{I_{DCb}^2}{P_b} \tag{2.32}$$

Regarding to the equation of the differential current provided in Table 2-1 this equation in per unit can be obtained:

$$\frac{1}{2} - v_{diff\,i_{pu}} = R_{arm_{pu}} i_{diff\,i_{pu}} + 2H_L \frac{di_{diff\,i_{pu}}}{dt} \tag{2.33}$$

In [76] it is demonstrated that in the CCSC approach the three phase circulating currents by applying the park transformation at 2ω, can be transformed into two DC components in the double fundamental frequency in negative sequence rotational reference frame as demonstrated in the sequel:

$$v_{diff\ d_{pu}} = 2H_L \frac{di_{diff\ d_{pu}}}{dt} + R_{arm_{pu}} i_{diff\ d_{pu}} - 4H_L \omega_{pu} i_{diff\ q_{pu}} \quad (2.34)$$

$$v_{diff\ q_{pu}} = 2H_L \frac{di_{diff\ q_{pu}}}{dt} + R_{arm_{pu}} i_{diff\ q_{pu}} + 4H_L \omega_{pu} i_{diff\ d_{pu}} \quad (2.35)$$

Then structural of the proposed control is shown in Figure 2-7.

The same simulation event in AC current control is applied on the CCSC scheme with the response time of 5ms for both differential and grid current loops. The simulation results are depicted in Figure 2-8.

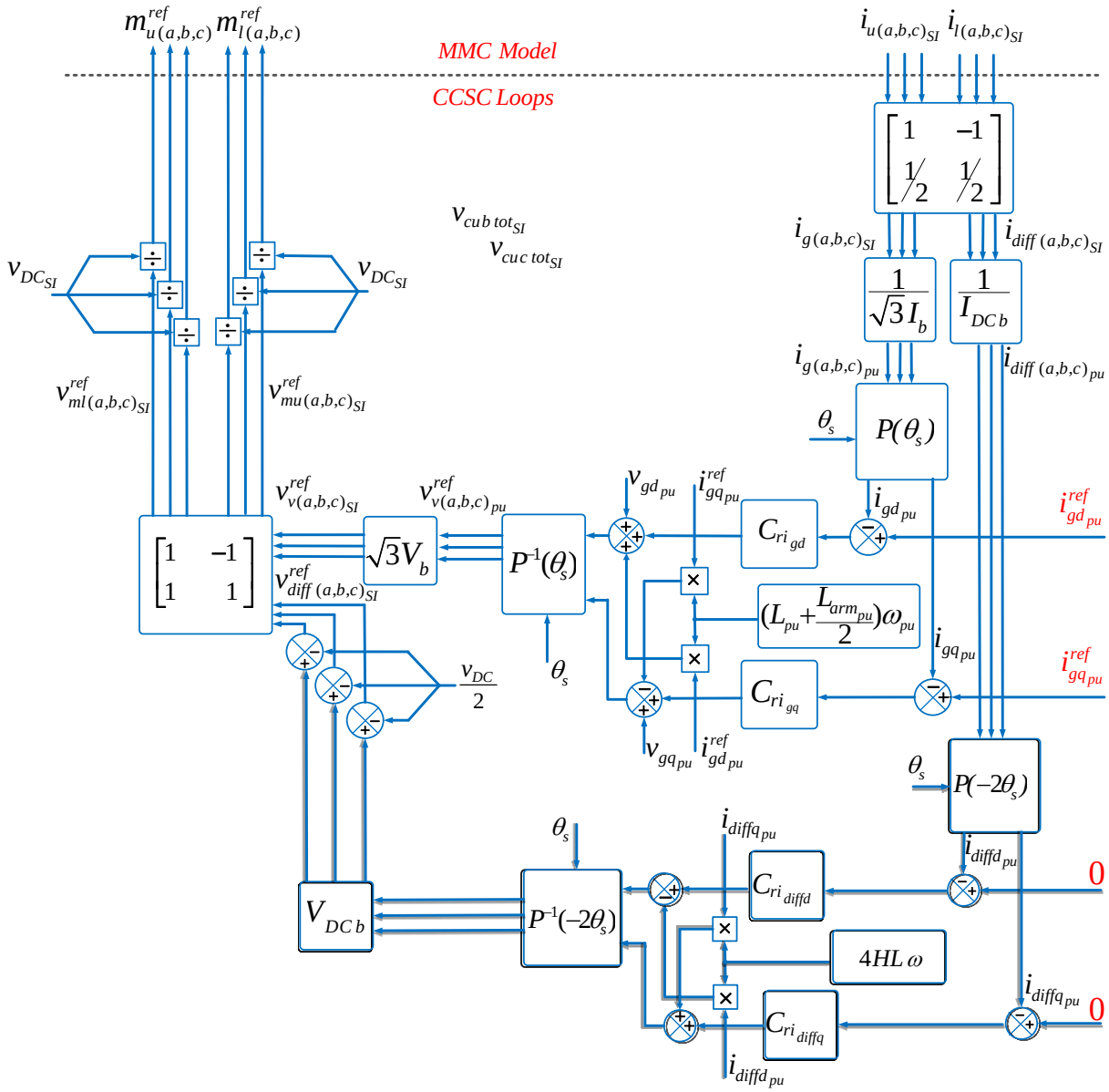

Figure 2-7: Structure of circulating current suppression controller in dq frame (CCSC)

a)

b)

c)

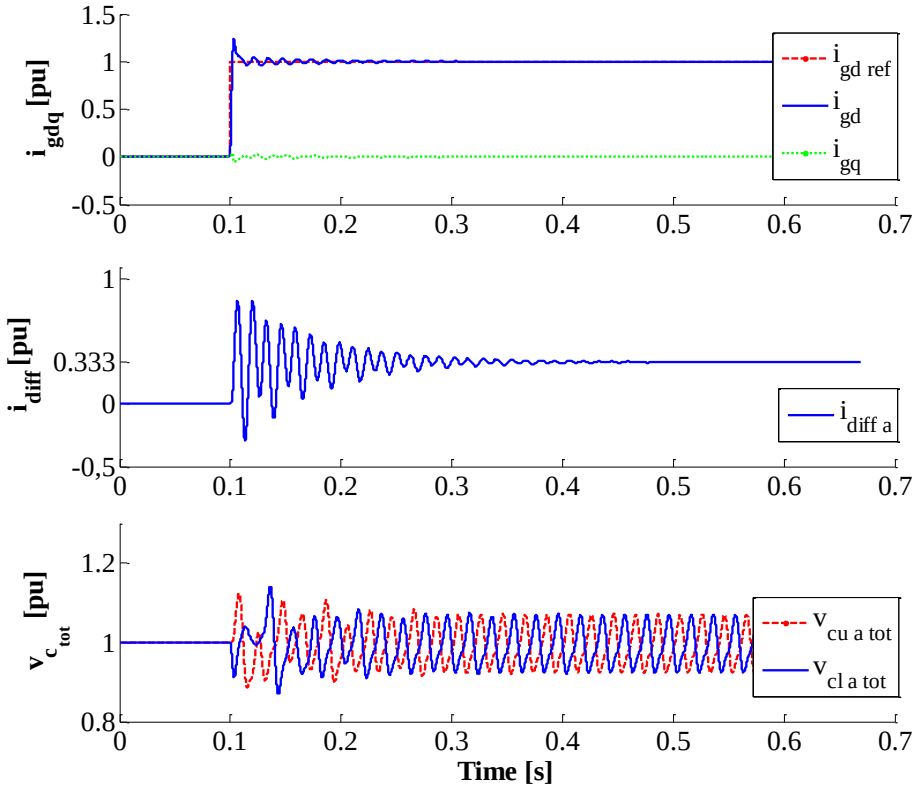

Figure 2-8: MMC AC current simulation results.

The simulation results in Figure 2-8(a) show that the AC currents are well controlled. In comparison with previous control simulation results (see Figure 2-5), the main difference can be observed on Figure 2-8(b), since there are fewer oscillations on the differential current and in the steady state a DC value is reached. Figure 2-8(c) shows that although there is no control on the average value of $v_{cua\,tot}$ and $v_{cla\,tot}$, they stabilize naturally around 1 pu value which is discussed in the next part.

Comparing to the previous control results, the voltage ripples are smaller. This is related to the mitigation of the double fundamental frequency harmonic of the differential current in CCSC scheme.

2.4.2. CCSC approach analysis

In CCSC-dq , the total voltage of SM capacitors within an arm $(v_{cu/l\,i\,tot})$ are not controlled but these voltages are stabilized naturally next to the DC link voltage (v_{DC}) .This has been depicted in the simulation results presented in Figure 2-8. Furthermore it is possible to adjust each of the MMC total arm voltages to a different value of v_{DC}. This new value can be adjusted proportionally to DC link voltage by coefficient of k that is noted as $K\,v_{DC}$ (see Figure 2-9). This mechanism is described in the sequel:

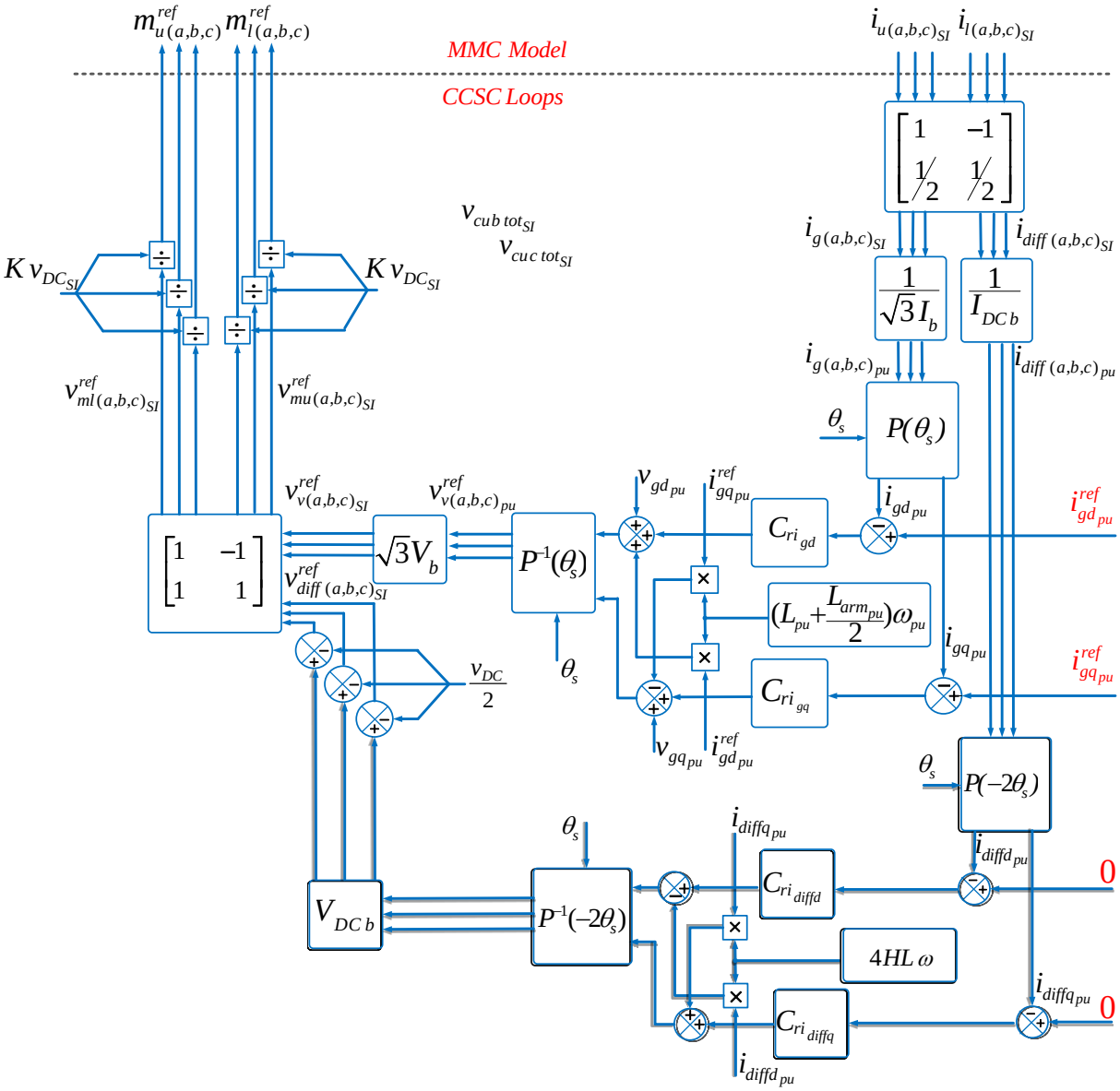

Figure 2-9: Structure of circulating current suppression controller in dq frame (CCSC) with insertion index by $K\,v_{DC}$

As depicted in Figure 2-7 the references of the insertion indices in $CCSC_{dq}$ are calculated as following:

$$m_{u\,i} = \frac{\frac{v_{DC}}{2} + v_{vi}}{K\,v_{DC}} \tag{2.36}$$

$$m_{l\,i} = \frac{\frac{v_{DC}}{2} - v_{vi}}{K\,v_{DC}} \tag{2.37}$$

As mentioned in (2.1),the modulated voltages are calculated as follow:

$$v_{u\,i} = m_{u\,i}\,v_{cu\,i\,tot}$$

$$v_{l\,i} = m_{l\,i}\,v_{cl\,i\,tot}$$

The average values of (2.36) and (2.37) with affecting $\langle v_{v\,i}\rangle = 0$ can be obtained:

$$\langle m_{u\,i}\rangle = \langle m_{l\,i}\rangle = \frac{K}{2} \tag{2.38}$$

The $v_{ctot\,ul\,i}$ and $m_{ul\,i}$ are supposed to be the superposition of a DC part and an oscillating part. Considering the ripple part of the $v_{cl\,i\,tot}$ is much smaller compare to its DC part, $v_{cu/l\,i\,tot}$ is assimilated to a pure DC signal. Then it can obtained equation (2.39):

$$\langle m_{u/l\,i}\, v_{cu/l\,i\,tot}\rangle = \langle m_{u/l\,i}\rangle\langle v_{cu/l\,i\,tot}\rangle \tag{2.39}$$

Regarding $v_{diff\,i}$ definition (see (2.2)) and (2.39), the average value of $v_{diff\,i}$ may obtained as following:

$$\langle v_{diff\,i}\rangle = \langle\frac{v_{mu\,i} + v_{ml\,i}}{2}\rangle = \frac{\langle m_{u\,i}\rangle\langle v_{cu\,i\,tot}\rangle + \langle m_{l\,i}\rangle\langle v_{cl\,i\,tot}\rangle}{2} = \frac{K}{2}\left(\frac{\langle v_{cu\,i\,tot}\rangle + \langle v_{cl\,i\,tot}\rangle}{2}\right) \tag{2.40}$$

By considering the differential current equation in (2.4), the differential voltage in steady state can be derived:

$$v_{diff\,i} = \frac{v_{DC}}{2} - R_{arm} i_{diff\,i} \tag{2.41}$$

Since the voltage of $R_{arm} i_{diffi}$ can be neglected compare to $V_{DC}/2$ then the differential voltage in steady state can be written as following:

$$v_{diff\,i} = \frac{v_{DC}}{2} \tag{2.42}$$

Regarding to (2.40) and (2.42) it can be derived that:

$$\frac{\langle v_{cu\,i\,tot}\rangle + \langle v_{cl\,i\,tot}\rangle}{2} = K\, v_{DC} \tag{2.43}$$

On the other hand regarding to v_{vi} definition provided in (2.3) its average value with neglecting the average value of their ripple parts multiplication can be obtained in:

$$\langle v_{v\,i}\rangle = 0 = \frac{-\langle m_{u\,i}\rangle\langle v_{cu\,i\,tot}\rangle + \langle m_{l\,i}\rangle\langle v_{cl\,i\,tot}\rangle}{2} = \frac{K}{2}\left(\frac{-\langle v_{cu\,i\,tot}\rangle + \langle v_{cl\,i\,tot}\rangle}{2}\right) \tag{2.44}$$

Which it means:

$$-\langle v_{cu\,i\,tot}\rangle + \langle v_{cl\,i\,tot}\rangle = 0 \tag{2.45}$$

Regarding to (2.41)and (2.43) it can obtain that:

$$\langle v_{cu\,i\,tot}\rangle = \langle v_{cl\,i\,tot}\rangle = K\, v_{DC} \tag{2.46}$$

The simulation results presented in Figure 2-10 confirmed equation (2.46). This figure indicates that the average value of output voltage of SMs within an arm are stabilized at the DC link voltage ($K = 1$) without performing any voltage control. That is why, despite the important oscillations on the differential currents, these currents achieved a constant value in the steady state regarding to MMC power balance between grid and the DC link.

This simulation results demonstrate the effect of the insertion indices in managing the SMs output voltages with in an arm in CCSC scheme. The study case is following a step of 1 pu at t=0.1s on the AC current that for $0\ s < t < 0.4\ s$.K=1 and for $0.4\ s < t < 1\ s$, K=1.3.

Similarly to above demonstration it is possible to adjust the average of $v_{ctot\ ul\ i}$ to other values proportional to v_{DC} .This can be done by modifying the value of the *K* .Adopting equation (2.36) with different value of K, leads to a proportional control of the average value of output voltage of the SMs with in an arm ($v_{c\ ul\ itot}$) without measuring or applying any control on these voltages in CCSC scheme.

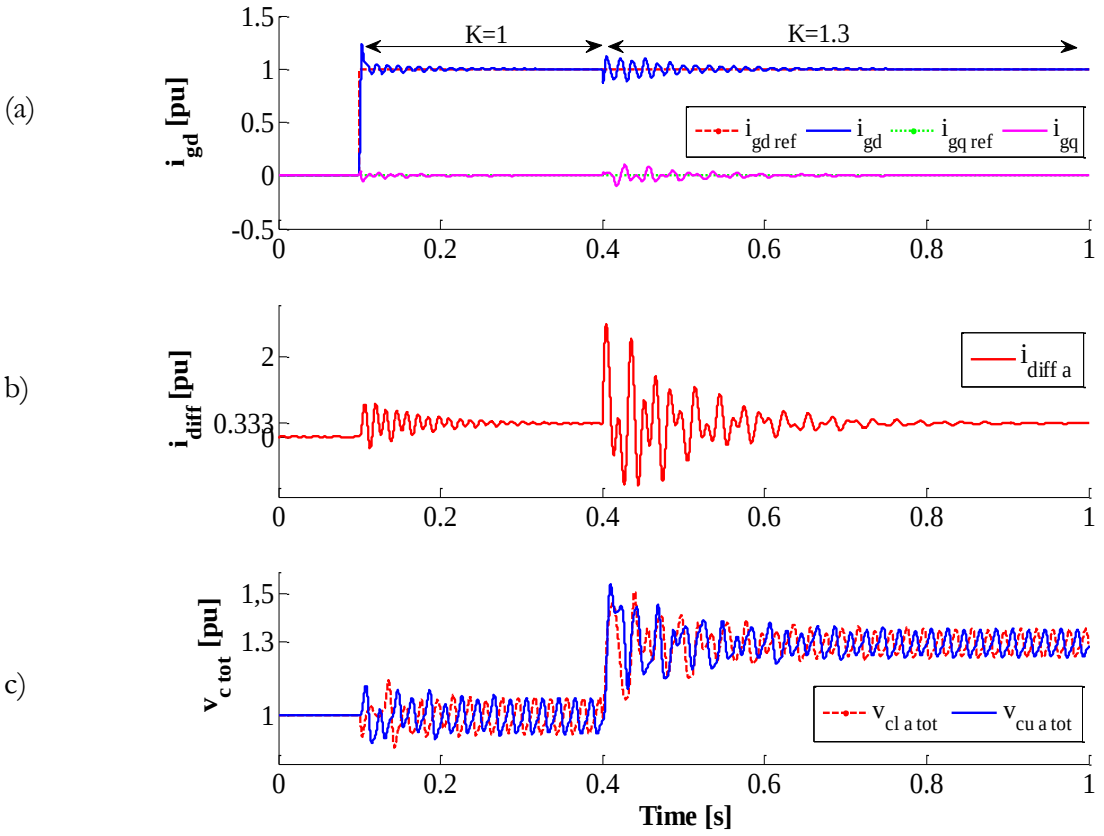

Figure 2-10:CCSCdq simulation results by modifying the insertion indices.

Figure 2-10 (a) and (b) show that by modifying the insertion index by K=1.3, the inner currents transient oscillations has increased but their steady state values have not changed since these currents are related to power transmission demanded that does not changed. However, as shown in Figure 2-10 (c) the average values of $v_{c\ ul\ i\ tot}$ are enhanced to 1.3 pu for K=1.3.

This simulation results show that the transient oscillations increased at t=0.4 s when K is changed, this oscillations are related to lack of control on the differential currents and the capacitor voltages.

In other words, in CCSC it is possible to control the average value of $v_{c\,ul\,i\,tot}$ proportional to v_{DC}. In fact by modifying the insertion indices the initial MMC stored energy changes.

2.4.3. Focus on an unstable operation point with CCSC

The previous simulations have shown that MMC dynamic is not well controlled and important oscillations occur during the transient. This section shows that, CCSC control scheme can lead to unstable behavior.

This case study highlights that since all the state values of the MMC in CCSC scheme are not controlled, it can lead to unstable states for the converter. Based on the CCSC scheme described in section 2.4 the simulation results for an unstable case are proposed.

The structure of CCSC is the same as presented in previous subsections. In order to demonstrate the unstable point in short simulation time the simulation parameters only for this case study are partly changed as listed in Table 2-3 with a step of 1 pu applied on the AC power reference at t = 0.1s. The reactive power reference stays equal to zero.

Table 2-3: Parameter for the simulated instable case

parameter	value
L_f	60 *mH*
R_f	0.6 *Ω*
L_{arm}	50*mH*
R_{arm}	0.5 *Ω*
C_{tot}	*24μF*
$U_{g_{rms}}$	*333kV*
V_{DC}	*640 kV*

. In this study case, the damping ratios for the PI controllers are considered as following:

$$\zeta_{ig} = 2.1 \ , \quad \zeta_{idiff} = 5.7 \tag{2.47}$$

The response time of current loops are 10ms.

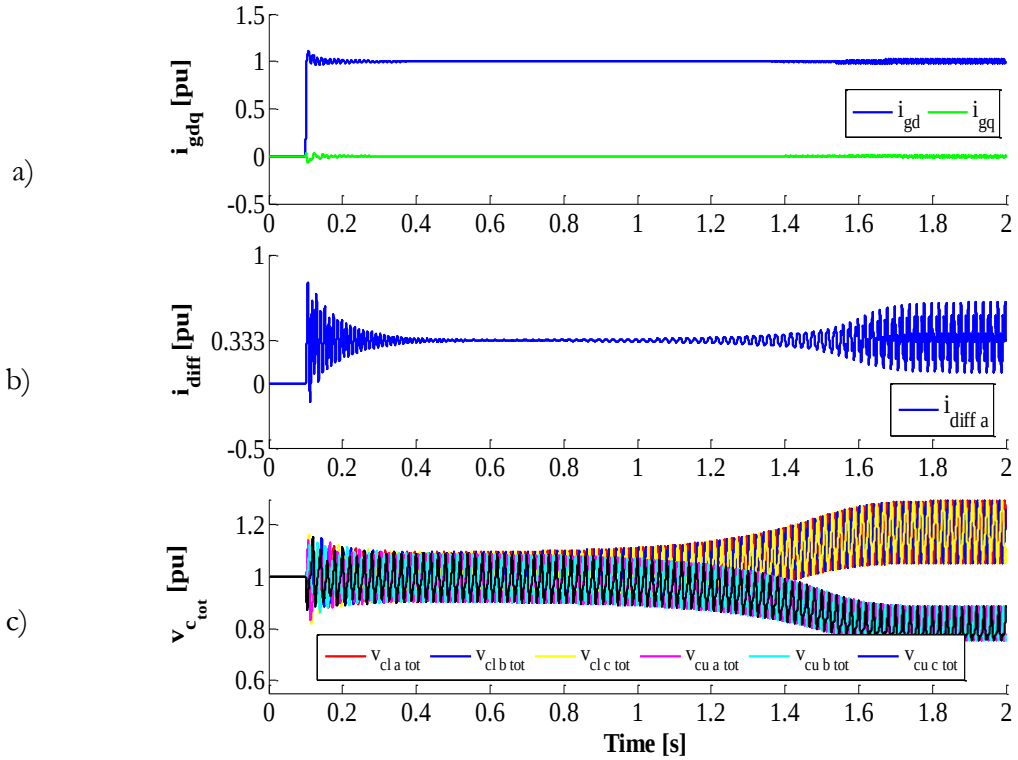

Figure 2-11: Simulation results for an MMC unstable case controlled by CCSC scheme.

The simulation results in Figure 2-11 shows that before t=0.7 s the MMC variables are well controlled. However after t=0.7 s, MMC reveals an unstable behavior on the grid currents (i_{gd}) and the differential current is observed and the average value of $v_{cu\ i\ tot}$ and $v_{cl\ i\ tot}$ becomes to diverged. These simulation results show that this simple way to control LLC is not correct since it leads to very important oscillations mainly on the differential current, during the transient. In certain case, it may even lead to unstable conditions. A better control of the differential current is needed. This is the aim of the following section.

2.5 DIFFERENTIAL CURRENT CONTROL

Considering an ideal balanced operating point, in steady state the DC link current I_{DC} is distributed equally among the legs. Consequently the inner differential current per phase is desired to be one third of the DC link current. However, according to SM voltage variations which it results the arm voltage differences, the differential currents contain the undesired AC harmonics as well.

In fact, this AC part is superposed on the DC part of the differential current and flows through the three phases without the effect on the MMC AC side voltages and currents. As a result the differential currents can be considered as following:

$$i_{diff\ i} = i_{diff\ AC\ i} + i_{diff\ DC\ i} \quad \textbf{(2.48)}$$

In the literature, several studies are investigated on the limitation or elimination of the AC component of the differential current which distort the sinusoidal arm currents. For example in [78] limitation of this current by sizing the arm inductor is discussed. In [79], the elimination of circulating current via a resonant filter is investigated, the other approaches propose an active control for suppression the double fundamental frequency of the differential currents [61].

This thesis addresses to an active control on the differential currents. It controls the instantaneous differential current per phase to control properly the differential current dynamics. These current as the MMC inner current have an important role on MMC dynamics. This scheme tries to control the differential currents per phase to provide the demanded DC current of the converter and at the same time it eliminates the transient behavior of these currents.

Regarding equation (2.4) and the MMC equivalent model depicted in Figure 2-3 it can be deduced that the control of the differential currents are possible via the first order controller per each phase as shown in Figure 2-12. This inner current controller regulates the reference voltage of $v_{RL_{arm}\,i}^{ref}$ which they provide $v_{diff\,i}^{ref}$ (see (2.10)).

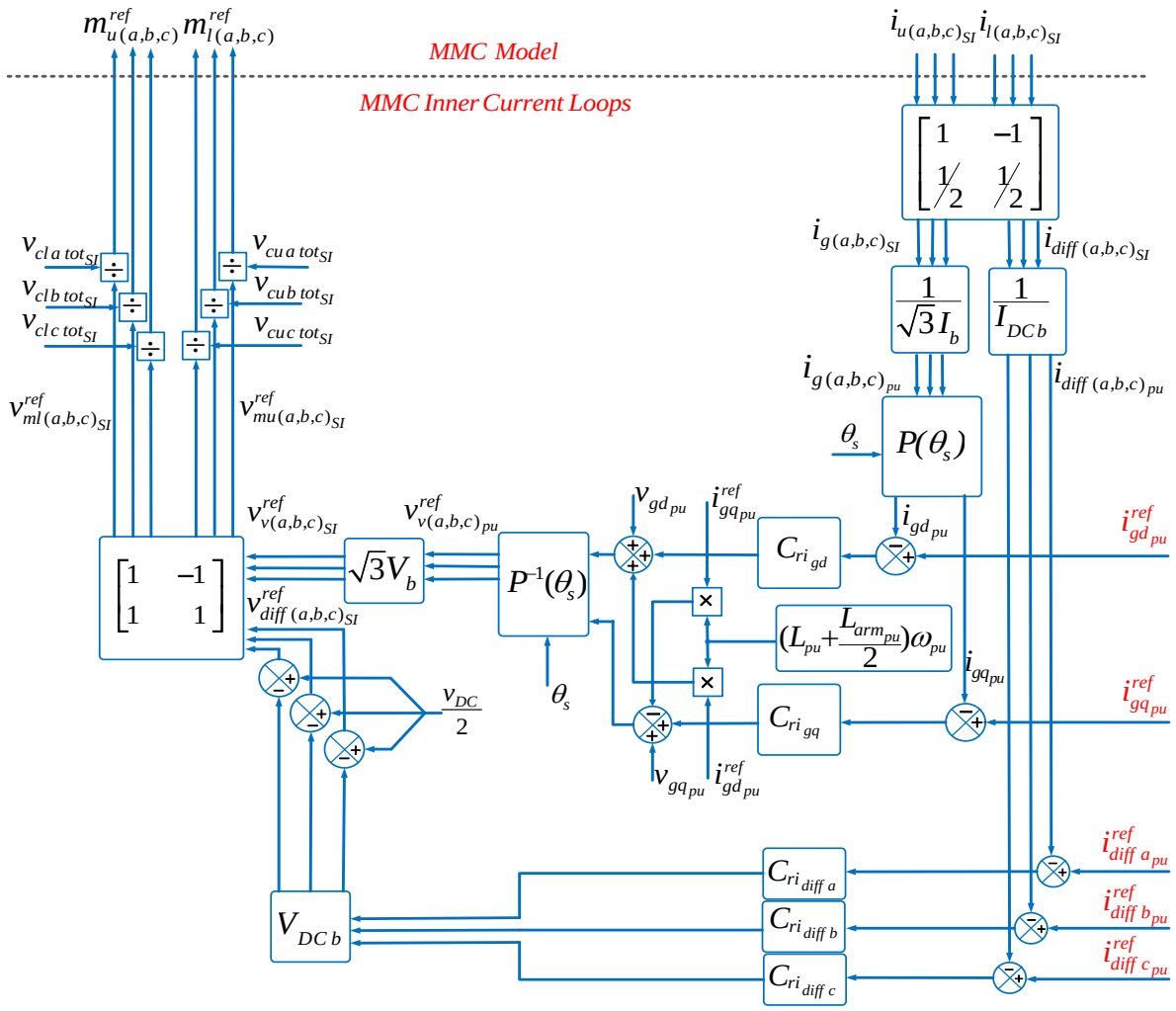

Figure 2-12: MMC Differential current loop

The simulation results for this control scheme are presented in Figure 2-13: a step of 1 pu is applied on the AC power reference at t = 0.1s, the reactive power reference stays equal to zero and a step of 1/3 pu (0.333 pu) is applied on the differential current at t=0.1s. The response time of current loops are 5ms.

a)

b)

c)

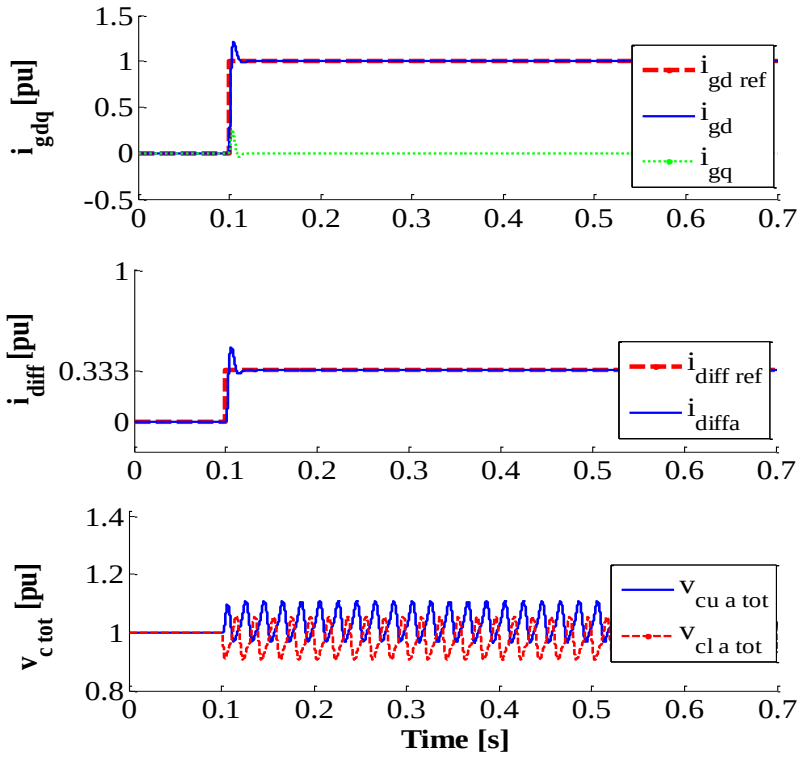

Figure 2-13: Differential current control simulation results.

In Figure 2-13 (a) it can be seen that the AC currents are well controlled and compare to Figure 2-10(a) the transient oscillations are eliminated. A significant difference can be observed on Figure 2-13(b) since transient oscillations of differential currents seen on Figure 2-10(b) in CCSC scheme are decreased dramatically. Figure 2-13 (c) shows that regarding to reference values of grid currents and differential currents based on MMC power balancing the average values of $v_{cul\ tot}$ depicted for phase-a are constant.

This figure also reveals that the average values of upper arm and lower arm are not equal.

If consider MMC control scheme contains only the MMC current controllers which its structure is shown in Figure 2-10 there is no control on the MMC equivalent arm voltages. In such a system the grid current references can be obtained based on the AC power imposed on the converter and consequently, the references of the differential currents can be calculated to achieve the power balance between AC grid and DC bus. In such a control configuration there is no link between the 6 equivalent arm capacitor voltages.

Therefore, despite the limited oscillations of the equivalent arm capacitor voltages that is related to the differential current loops, the average values of these voltages are not controlled as shown the simulation results in Figure 2-14 . In this simulation a step of .066 pu is applied on the

the differential current references at t=0.1 s and another step of 0.2 pu is applied on the AC power reference at t=0.2 s. The response time of the current loops are 5 ms.

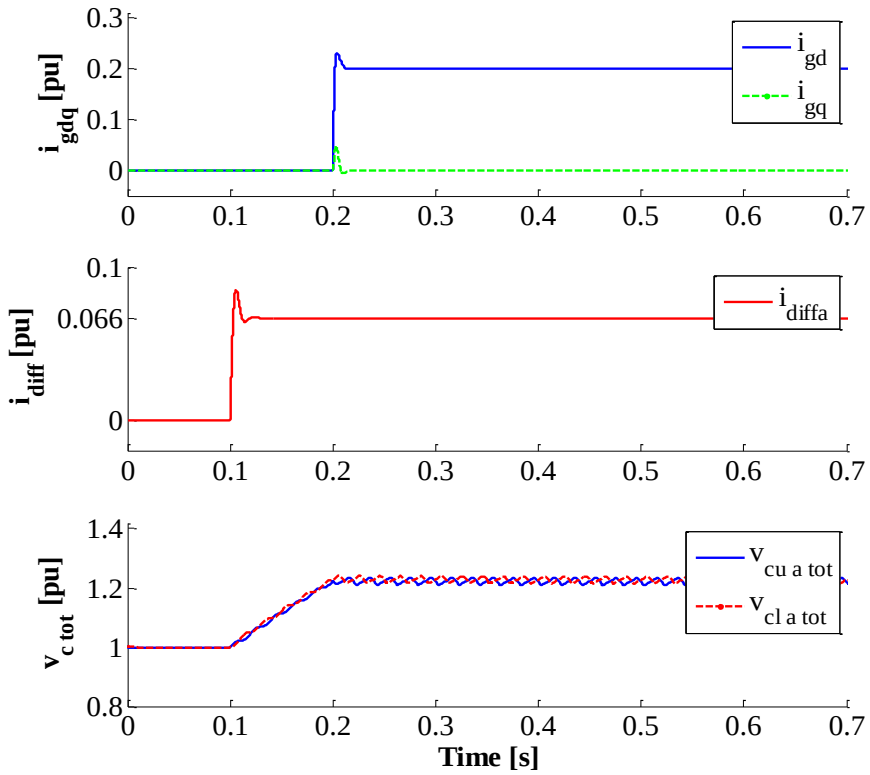

Figure 2-14: Simulation results for MMC with inner current controls.

In Figure 2-14 (a) and (b) it can be seen that the AC currents and differential currents are well controlled independently. However Figure 2-14(c) shows that the equivalent arm capacitor voltages of phase-a ($v_{cu\,a\,tot}$ and $v_{cu\,l\,tot}$) following the step on the differential currents increase. This increase is due to DC power injection to MMC that induces storage of energy in the equivalent arm capacitors. In specific case, the AC power demand is the same value as the injected DC power, the average value of these voltages is stabilized.

In other words these simulation results show that the proposed control scheme can control more efficiently the dynamic of the MMC than CCSC. However this simulation results also show clearly the lack of the control on the equivalent arm capacitor voltages. In order to control the dynamics of the equivalent arm capacitor voltages ($v_{cul\,i\,tot}$) it is necessaire to add an outer control which is discussed in chapter 3.

2.6 DIFFERENT SOLUTIONS FOR CALCULATING THE MMC INSERT INDEX

In this section the choice for calculating the insertion index is discussed. In the literature it can be found three main choices for calculating the insertion index which are demonstrated and compared in next part:

- Linearization by the model inversion (or exact):

As mentioned in (2.7) insert index definition are as follow:

$$m_{u\,i} = \frac{v_{mu\,i}^{ref}}{v_{C\,u\,i\,tot}}$$

$$m_{l\,i} = \frac{v_{ml\,i}^{ref}}{v_{C\,l\,i\,tot}}$$

As is shown in Figure 2-2 this insertion index is related to the exact inversion of the MMC model where the controllers are considered as ideal.

- Insert index calculation with v_{DC}

$$m_{u\,i} = \frac{v_{mu\,i}^{ref}}{v_{DC}} \quad \textbf{(2.49)}$$

$$m_{l\,i} = \frac{v_{ml\,i}^{ref}}{v_{DC}} \quad \textbf{(2.50)}$$

In this choice as discussed in [55] v_{DC} is substituted to $v_{C\,u/l\,i\,tot}$ in insert index definition since it considered the sum of the v_{DC} and a ripple component that the amplitude of this ripple part in neglected compare to v_{DC} amplitude which it is correct in case of CCSC schemes and not for other control schemes.

- Insert index calculation by the mean values of the SM voltages within an arm

$$m_{u\,i} = \frac{v_{mu\,i}^{ref}}{\left(\frac{v_{cu\,i\,tot} + v_{cl\,i\,tot}}{2}\right)} \quad \textbf{(2.51)}$$

$$m_{l\,i} = \frac{v_{ml\,i}^{ref}}{\left(\frac{v_{cu\,i\,tot} + v_{cl\,i\,tot}}{2}\right)} \quad \textbf{(2.52)}$$

This choice as discussed in [36] the mean value of $v_{C\,tot}$ in each arm is applied in the insert index calculation.

To highlight the differences of these calculation methods a comparison is performed. The proposed simulation results in Figure 2-15 is based on the inner current loops described in section 2.5 by performing following events: a step of 1 pu on the AC current references at t=0.1s and a step of 1/3 pu (0.333 pu) on the differential current references at t= 0.1s.

The simulation results show that the main differences of these methods are in the differential current oscillations. It can be seen in Figure 2-15(b) by exact insert index calculation method, the differential currents have not oscillations which it is applied in the rest of this thesis.

This figure also shows that in case of insert index calculation methods by v_{DC} or by the mean values of the SM voltages within an arm, the differential current contains harmonic components at double frequency of the fundamental frequency.

In order to control correctly these currents in [79] the authors investigate on a resonant controller for differential currents that control both average value of the i_{diff} and also eliminates the mentioned harmonic. This control is provided in next subsection.

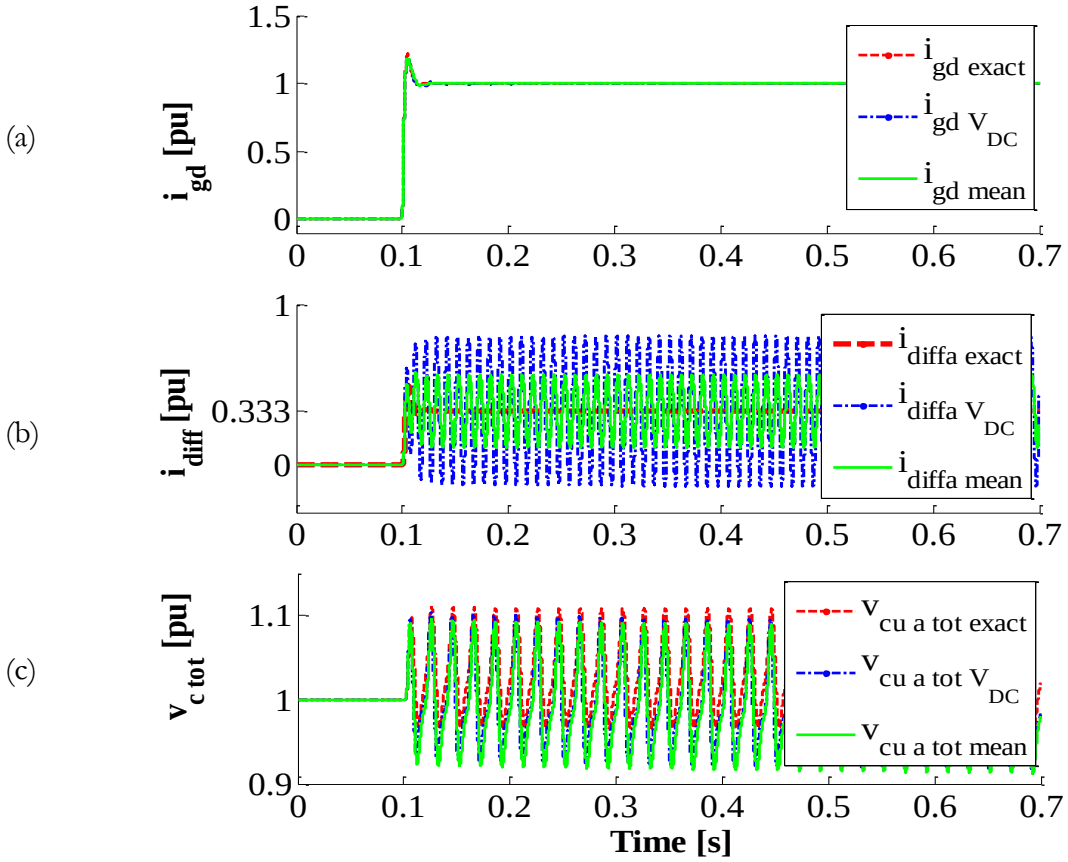

Figure 2-15: Comparison of the different types of insert index calculation.

2.7 RESONANT CONTROLLER FOR THE DIFFERENTIAL CURRENTS

Regarding simulation results presented in previous sub-section, in case of insert index calculation by v_{DC} or insert index calculation by the mean values of the SM voltages the differential currents may contain oscillation at double frequency of the fundamental frequency. However, these methods of insert index calculation have been adopted widely in the literature such as [36, 53, 55].

At first solution to avoid this problem, a control is added to CCSC schem. It means that two actions are achieved in parallel: control of the DC component on one hand with a DC component controller and control of the double frequency component with the CCSC.

Both functions may be achieved with a single controller which can manage DC and double frequency components at the same time. Such a control can be realized by a proportional resonant controller. The integral part of the controller controls the DC component whereas the resonant part, controls the double frequency component. Then the transfer function of the PIR controller can be obtained as follows: ref de system bouclé reference model inversion

$$C(s) = \frac{C_0 + C_1 s + C_2 s^2 + C_3 s^3}{s((n\omega_0)^2 + s^2)} \tag{2.53}$$

Where $\omega_\circ$ is fundamental pulsation in rad/s. This structure is to compensate the harmonic of order n.

According to transfer function of the differential currents mentioned in section 2.4, the characteristic polynomial of control loop is as following:

$$C(s) = C_0 + C_1 s + C_2 s^2 + C_3 s^3 + s\left(R_{arm_{pu}} + 2H_L s\right)((n\omega_0)^2 + s^2) \tag{2.54}$$

Considering the Naslin polynomial of order 4:

$$N(s) = 1 + \frac{s}{\omega_0} + \frac{s^2}{\alpha\omega_0^2} + \frac{s^3}{\alpha^3\omega_0^3} + \frac{s^4}{\alpha^6\omega_0^4} \tag{2.55}$$

The expressions of the coefficients of the characteristic polynomial can be obtained as following:

$$\begin{aligned} C_0 &= 2H_L\alpha^6\omega_0^4 \\ C_1 &= \frac{C_0}{\omega_0} - R_{arm_{pu}}(n\omega_0)^2 \\ C_2 &= \frac{C_0}{\alpha\omega_0^2} - 2H_L(n\omega_0)^2 \\ C_3 &= \frac{C_0}{\alpha^3\omega_0^3} - R_{arm_{pu}} \end{aligned} \tag{2.56}$$

In order to suppression of second harmonic of differential currents n is equal to 2. Simulation results for applying this controller with $\alpha = 2.2$ and over shut time equal to 10 ms is presented in Figure 2-16.

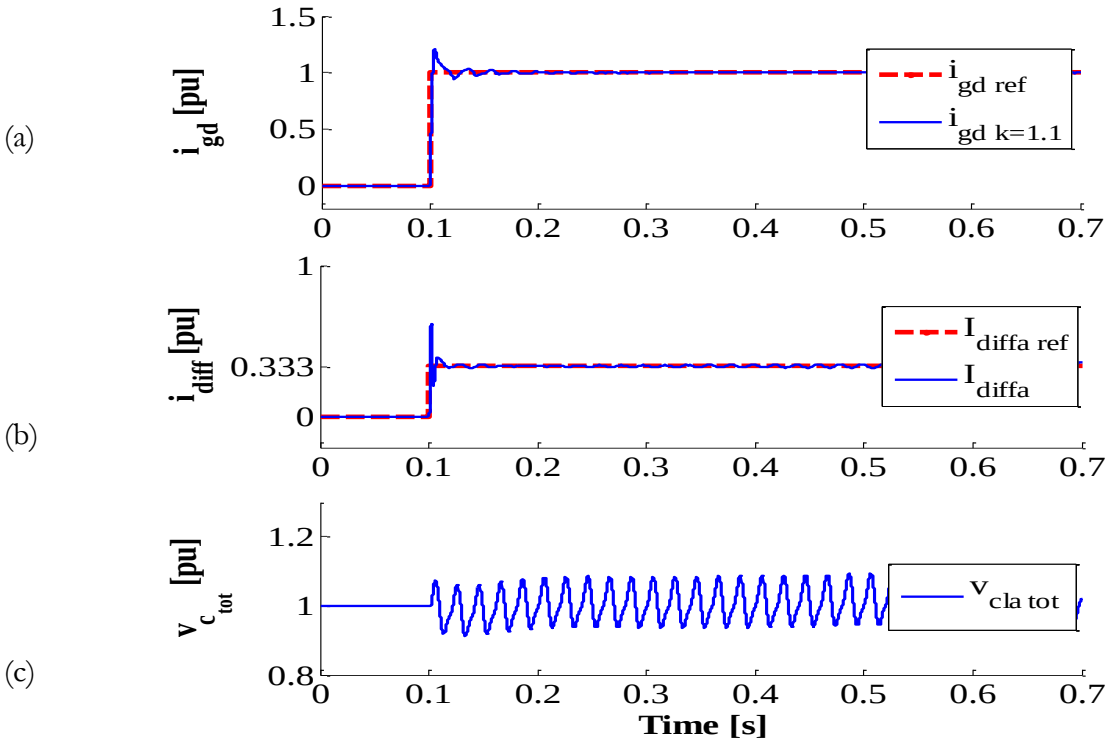

Figure 2-16: Resonant controller for differential currents in case of linearization by v_{DC}..

The simulation show the result when applying the resonant controller for the differential currents in case of insert index calculation by v_{DC}. As usual, the grid currents are well controlled. However, Figure 2-16 (b) shows that differential currents are well controlled regarding its reference and the oscillations at double frequency of the fundamental frequency are eliminated.

2.8 CONCLUSION

This chapter has presented basics for inner currents: grid currents (i_{gi}) and differential currents (i_{diffi}) mathematical model and analysis. In this chapter, several methods for control of these inner currents are investigated. The basic control method, which it includes only the control of grid currents, presents only good dynamics performance for grid currents and the oscillation on the differential currents and the total voltage of arm capacitors are rather important and it necessitate the differential current control. Then the well-known control scheme of CCSC highlighted a better performance for MMC since the steady state value of the differential currents and the average values of the total voltages of arm capacitors stabilized naturally. However, the transient oscillations on the differential currents shows clearly lack of control of the differential currents which it can lead to unstable states for the converter. From this, a control method based on an active control of the differential currents is proposed that it shows a good performance for controlling the both MMC inner currents.

To sum up with the proposed control method the transient oscillations of the differential currents and the grid currents are considerably decreased and consequently the oscillations of the total voltages of arm capacitors are reduced. But contrary to the CCSC scheme the average values of these voltages are not stabilized equally and should be controlled. Therefore, an outer voltage loop is required.

In addition in this chapter different existing methods of linearization in the literature have been discussed and compared. In case of linearization by v_{DC} and linearization by the mean value of the total voltage of upper and lower arm capacitors with in a leg, the differential currents include the second harmonics. Consequently there are different control methods. In this chapter the resonant controller in order to eliminate the second harmonics and control the differential current is studied.

As conclusion, the matter of this chapter was to bring in the methodological principles on control of the MMC inner currents, in order to introduce the whole control of the MMC dynamic in next chapter.

CHAPTER 3 : MMC energy based control design

3.1 INTRODUCTION

The principles of different types of MMC energy based control are discussed in this chapter. Various strategies have been investigated in the literature for MMC control, direct modulation strategy and CCSC [53] that does not intend to control the differential currents.

Two other control solutions are augmented with differential currents control named closed loop [48] and open loop [15]. These schemes by estimating the energy, have proposed two solutions for the insertion indices by using measured total capacitor voltages (closed loop scheme) and using estimated total capacitor voltages (open loop scheme). However, the authors of the closed-loop scheme have mentioned that this control requires two voltage control loops for stability reasons [48]

Regarding the MMC stability criteria and control robustness there is another family of MMC control schemes named energy-based control strategies [15, 59-62]. These energy-based control schemes include explicitly a feedback control loop on the arm capacitor energies which provides the references of the inner current loops. As already said in the introduction, all the proposed MMC controls in the literature do not control the same number of MMC state variables. But, to have a fully control of the stored energy in the system, the number of controllers must be equal to the number of independent state variables of the system. If not, some state variables may be out of control, can take unacceptable values.

This chapter investigated different types of energy based control of the MMC, assuming that the AC and differential currents are controlled as explained in the previous chapter and recalled in Figure 3-1. Since this chapter is focused on the control of the energy thanks to the grid or differential currents ($i_{g\,i}$ and $i_{diff\,i}$), a new model is required to design the control.

The first part of this chapter is dedicated to the presentation of different topologies for MMC energy-based model. Since the inner current loops are studied in chapter 2, they are supposed to be implemented.

Based on these models, the fundamentals of the different control strategies in order to control the whole stored energy in an MMC are provided in the second part. The principle of model inversion is used for designing the general organization of the control.

The third part investigates the methodologies to control the energy balancing between upper arm and lower arm with in a leg. Finally a comparison between CCSC scheme as a well-known MMC control and the proposed energy based control is exposed by simulation results.

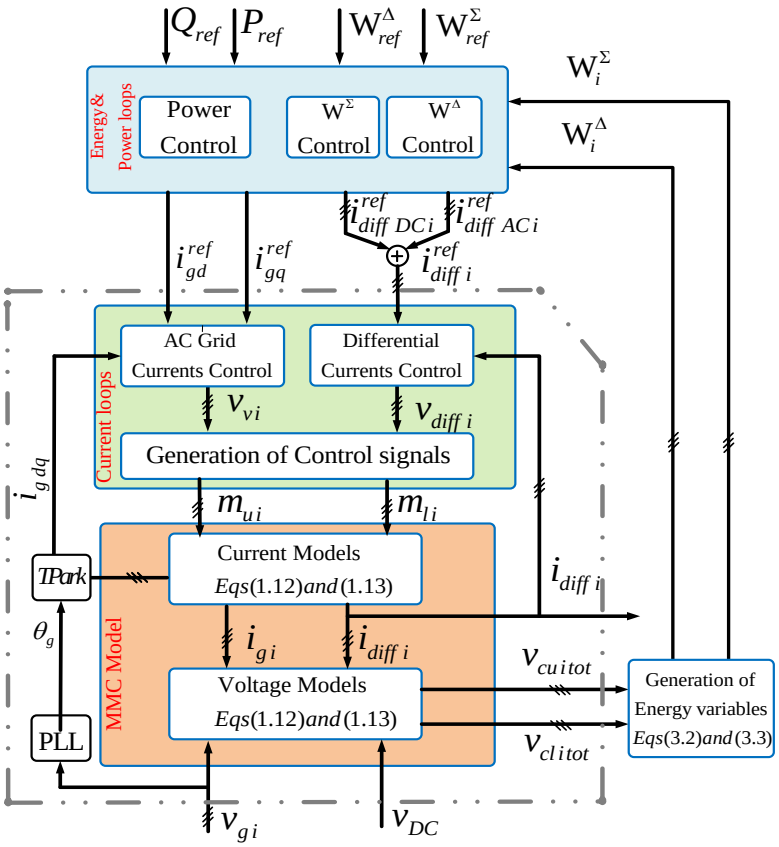

Figure 3-1: MMC energy based simulation model

3.2 DIFFERENT TYPES OF MMC ENERGY-BASED MODEL

The equivalent model of the MMC as shown in chapter 1 includes: equivalent arm capacitors, arm inductors and resistances. Considering equivalent arm capacitors as the main energy storage elements in the MMC, the equivalent circuit of each arm can be considered as shown in Figure 3-2.

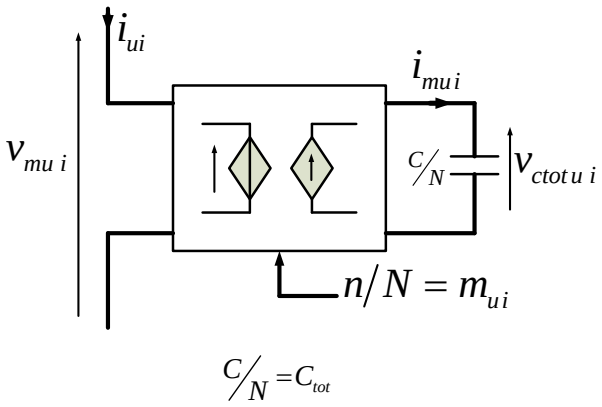

Figure 3-2: Equivalent up-arm circuit configuration

Then the stored energy in upper-arm can be calculated as:

$$W_{ctot\,u\,i} = \frac{1}{2} C_{tot} v_{ctot\,u\,i}^2 \tag{3.1}$$

the power balance in upper –arm circuit can be obtained:

$$\frac{dW_{ctot\,u\,i}}{dt} = v_{ctot\,u\,i} i_{mu\,i} \tag{3.2}$$

Where:

$$v_{ctot\,u\,i} i_{mu\,i} = v_{mu\,i} i_{u\,i} \tag{3.3}$$

In the following sub-sections, different energy based models are developed in order to establish a link between the MMC currents and the MMC energy variables.

3.2.1. Instantaneous-energy based model

This model is based on the conservation of instantaneous power for the 6 equivalent arm capacitors. Regarding the MMC model described in chapter 1 and chapter 2, the conservation of the power for phase "i" can be written as follow:

$$\begin{cases} \frac{dW_{ctot\,u\,i}}{dt} = v_{ctot\,u\,i} i_{mu\,i} = v_{mu\,i} i_{u\,i} = \left(v_{diff\,i} - v_{v\,i}\right)\left(i_{diff\,i} + \frac{i_{g\,i}}{2}\right) \\ \frac{dW_{ctot\,l\,i}}{dt} = v_{ctot\,l\,i} i_{ml\,i} = v_{ml\,i} i_{l\,i} = \left(v_{diff\,i} + v_{v\,i}\right)\left(i_{diff\,i} - \frac{i_{g\,i}}{2}\right) \end{cases} \tag{3.4}$$

Where:

$$\begin{cases} i_{mu\,i} = C_{tot} \frac{dv_{ctot\,u\,i}}{dt} \\ i_{ml\,i} = C_{tot} \frac{dv_{ctot\,l\,i}}{dt} \end{cases} \tag{3.5}$$

Inserting (3.5) in (3.4) , yields to (3.6):

$$\begin{cases} \frac{dW_{ctot\,u\,i}}{dt} = C_{tot}\left(v_{ctot\,u\,i}\frac{dv_{ctot\,u\,i}}{dt}\right) = \frac{i_{g\,i}}{2} v_{diff\,i} - \frac{i_{g\,i}}{2} v_{v\,i} - i_{diff\,i} v_{v\,i} + i_{diff\,i} v_{diff\,i} \\ \frac{dW_{ctot\,l\,i}}{dt} = C_{tot}\left(v_{ctot\,l\,i}\frac{dv_{ctot\,l\,i}}{dt}\right) = -\frac{i_{g\,i}}{2} v_{diff\,i} - \frac{i_{g\,i}}{2} v_{vi} + i_{diff\,i} v_{v\,i} + i_{diff\,i} v_{diff\,i} \end{cases} \tag{3.6}$$

For simplifying the equations, the sum and subtraction of the equations (3.6) are considered.

Per-phase stored energy (W_i^{Σ}) :

$$W_i^{\Sigma} = \frac{1}{2} C_{tot}(v_{ctot\,u\,i}^2 + v_{ctot\,l\,i}^2) \tag{3.7}$$

And the per-phase energy difference (W_i^{Δ}).

$$W_i^{\Delta} = \frac{1}{2} C_{tot}(v_{ctot\,l\,i}^2 - v_{ctot\,u\,i}^2) \tag{3.8}$$

Then MMC energy variable (W_i^{Σ} and W_i^{Δ}) equations can be derived as follow:

$$\begin{cases} \dfrac{dW_i^{\Sigma}}{dt} = \dfrac{d(W_{ctot\,u\,i} + W_{ctot\,l\,i})}{dt} = -i_{g\,i}v_{v\,i} + 2i_{diff\,i}v_{diff\,i} \\ \dfrac{dW_i^{\Delta}}{dt} = \dfrac{d(W_{ctot\,l\,i} - W_{ctot\,u\,i})}{dt} = -i_{g\,i}v_{diff\,i} + 2i_{diff\,i}v_{v\,i} \end{cases} \quad (3.9)$$

Since the energy stored in the inductance or dissipated in the resistances are small, it is possible to do the following approximations:

$v_{v\,i} \approx v_{g\,i}$ and $v_{diff\,i} \approx v_{DC}/2$

Then (3.9) can be written as:

$$\begin{cases} \dfrac{dW_i^{\Sigma}}{dt} = \dfrac{d(W_{ctot\,u\,i} + W_{ctot\,l\,i})}{dt} = -i_{g\,i}v_{g\,i} + i_{diff\,i}v_{DC} \\ \dfrac{dW_i^{\Delta}}{dt} = \dfrac{d(W_{ctot\,l\,i} - W_{ctot\,u\,i})}{dt} = -i_{g\,i}\,v_{DC}/2 + 2i_{diff\,i}v_{g\,i} \end{cases} \quad (3.10)$$

Assuming that $i_{g\,i}$ is sinusoidal (frequency ω) and $i_{diff\,i}$ constant, it is possible to have some considerations on (3.10) equations in steady state.

- $i_{g\,i}\,v_{DC}/2$: grid frequency component(ω)
- $i_{diff\,i}v_{DC}$: DC component
- $i_{g\,i}v_{g\,i}$: DC component and the second harmonics (2ω) component.
- $i_{diff\,i}v_{g\,i}$: grid frequency component(ω).

The above analysis demonstrates that the MMC energy variables are supposed to have a DC component and two other harmonic components at ω and 2ω. These properties will be used further.

Focusing on the MMC energy based model, the dynamic of the inner current loops (see the MMC model and current loops in chapter 2) are supposed to be infinite which means that $i_{diff\,DC\,i}^{ref} \cong i_{diff\,DC\,i}$ and $i_{gi}^{ref} \cong i_{gi}$.

3.2.1.1. Instantaneous model of the MMC per- phase stored energy

By merging the DC power and AC power definitions as presented by (3.11) and (3.12) in (3.9) the expression of the $W_i^{\Sigma}$and W_i^{Δ} obtains in (3.13):

Defining DC power as:

$$p_{DC\,i} = i_{diff\,i\;DC}\,v_{DC} \quad (3.11)$$

And active power as:

$$p_{AC\,i} = i_{g\,i}\;\; v_{g\,i} \quad (3.12)$$

Expression of the $W_i^{\Sigma}$and W_i^{Δ} can be obtained:

$$\begin{cases} \dfrac{dW_i^{\Sigma}}{dt} = \dfrac{1}{2} C_{tot} \dfrac{d}{dt}\left(v_{ctot\,u\,i}^2 + v_{ctot\,l\,i}^2\right) = p_{DC\,i} - p_{AC\,i} \\ \dfrac{dW_i^{\Delta}}{dt} = \dfrac{1}{2} C_{tot} \dfrac{d}{dt}\left(v_{ctot\,l\,i}^2 - v_{ctot\,u\,i}^2\right) = -i_{g\,i} \dfrac{v_{DC}}{2} + 2\, i_{diff\,i} v_{g\,i} \end{cases} \tag{3.13}$$

Based on equation (3.13) an MMC equivalent instantaneous energy based model can be derived as shown in Figure 3-3: MMC equivalent model based on instantaneous equations Figure 3-3.

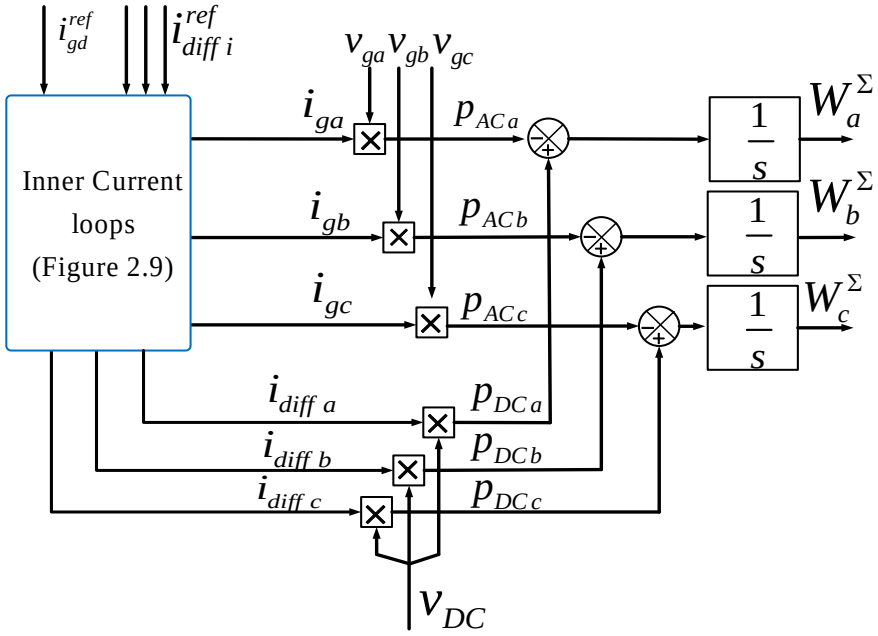

(a) Per-phase stored energy instantaneous model

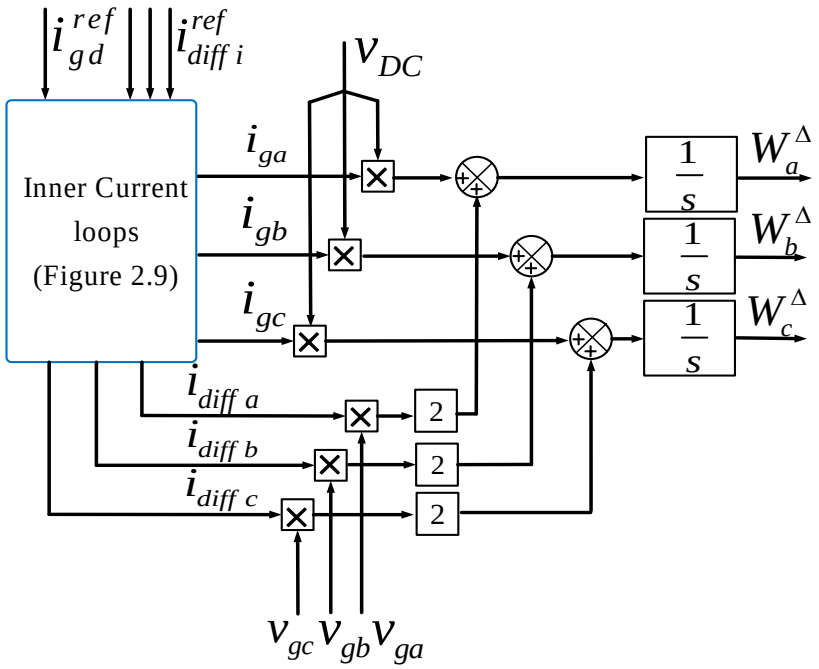

(b) Difference stored energy between up and low arms instantaneous model

Figure 3-3: MMC equivalent model based on instantaneous equations

3.2.1.2. Instantaneous model of the total energy stored in the MMC

Another solution for MMC instantaneous model is possible by considering the sum of the three equations of W_i^{Σ} in (3.13), the whole energy stored in the MMC can be obtained in (3.14)..

$$\frac{dW_{tot}^{\Sigma}}{dt} = \frac{3}{2} C_{tot} \frac{d}{dt} \left(v_{ctot\,u_{av}}^2 + v_{ctot\,l_{av}}^2 \right) = p_{DC} - p_{AC} \tag{3.14}$$

Where

$$v_{ctot\,ul_{av}}^2 = \left(\frac{v_{ctot\,ul\,a}^2 + v_{ctot\,ul\,b}^2 + v_{ctot\,ul\,c}^2}{3} \right) \tag{3.15}$$

Then another instantaneous model based on equation (3.14) can be obtained as shown in Figure 3-4:

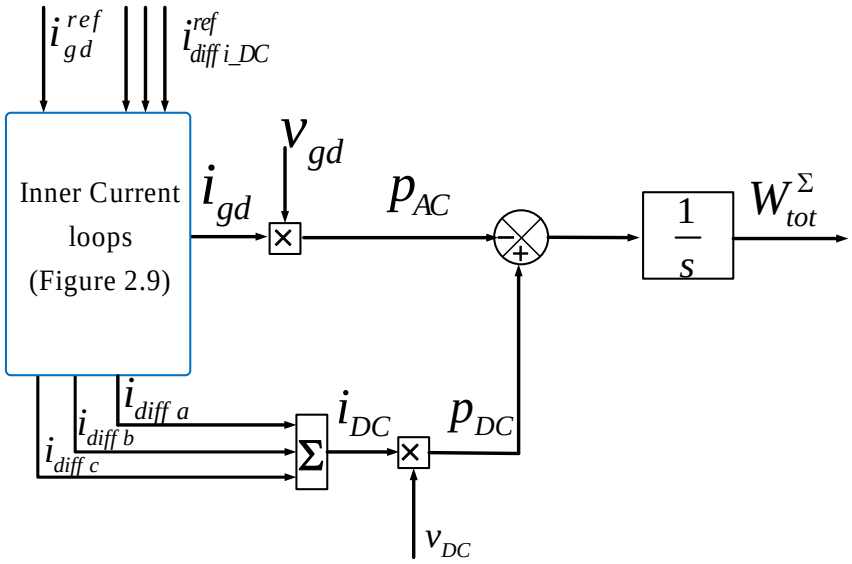

Figure 3-4: MMC Whole stored energy equivalent model based on instantaneous equations

3.2.2. MMC average energy based model

In this subsection, the methods to define MMC energy based model for controlling the average value of MMC energy variables are presented.

The average value of the energy on a grid period (T) is considered as shown in (3.16). These equations highlight the link between the stored energy in up and low arms and MMC inner currents: grid currents and the differential currents.

$$\begin{cases} \frac{1}{T}\int_0^T \left(\frac{dW_i^{\Sigma}}{dt}\right)_T = \frac{1}{T}\left(W_i^{\Sigma}(T) - W_i^{\Sigma}(0)\right) = -\langle i_{g\,i} v_{g\,i}\rangle_T + \langle v_{DC} i_{diff\,i}\rangle_T \\ \frac{1}{T}\int_0^T \left(\frac{dW_i^{\Delta}}{dt}\right)_T = \frac{1}{T}\left(W_i^{\Delta}(T) - W_i^{\Delta}(0)\right) = -\langle i_{g\,i}\frac{v_{DC}}{2}\rangle_T + 2\langle v_{g\,i} i_{diff\,i}\rangle_T \end{cases} \quad (3.16)$$

On (3.16), it can be seen that the per-phase stored energy (W_i^{Σ}) depends on the active power on this phase and the average value of the DC power on the same phase.

In case, i_{gi} is a sinusoidal current and i_{diffi} is a constant one, both terms in average value of the per-phase difference energy (W_i^{Δ}) are equal to zero:

$$\langle i_{g\,i}\frac{v_{DC}}{2}\rangle_T = 0, \qquad \langle i_{diff\,i} v_{g\,i}\rangle_T = 0 \quad (3.17)$$

A solution to avoid both terms to be null in the same time is either to add a DC component in $i_{g\,i}$ or an AC component in $i_{diff\,i}$. Since it is not allowed to add a DC component in a grid current, only the second solution is valid. Consequently, an AC current component ($i_{diff\,i\,AC}$) is added in the differential current. Then the differential current can be considered as follow:

$$i_{diff\,i} = i_{diff\,i\,DC} + i_{diff\,i\,AC} \quad (3.18)$$

By merging (3.18) in (3.16) it yields:

$$\begin{cases} \left(\frac{dW_i^{\Sigma}}{dt}\right)_T = -\langle i_{g\,i} v_{g\,i}\rangle_T + \langle i_{diff\,i\,DC} v_{DC}\rangle_T \\ \left(\frac{dW_i^{\Delta}}{dt}\right)_T = 2\langle i_{diff\,i\,AC}\, v_{g\,i}\rangle_T \end{cases} \quad (3.19)$$

Equations of (3.19) demonstrate that the average value of W_i^{Σ} can be controlled either by the DC component of the differential currents or by the DC component of $p_{AC\,i}$. The average value of W_i^{Δ} can be controlled by the AC component of the differential currents.

The same hypothesis in the previous subsection is considered in this subsection. Then it can be obtained:

$$\begin{cases} \langle\frac{dW_i^{\Sigma}}{dt}\rangle_T = \langle\frac{1}{2}C_{tot}\frac{d}{dt}(v_{ctot\,u\,i}^2 + v_{ctot\,l\,i}^2)\rangle_T = p_{DC\,i} - \langle p_{AC\,i}\rangle_T \\ \langle\frac{dW_i^{\Delta}}{dt}\rangle_T = \langle\frac{1}{2}C_{tot}\frac{d}{dt}(v_{ctot\,l\,i}^2 - v_{ctot\,u\,i}^2)\rangle_T = -\langle i_{g\,i}\frac{v_{DC}}{2}\rangle_T + 2\langle i_{diff\,i} v_{g\,i}\rangle \end{cases} \quad (3.20)$$

Based on this definition one solution for MMC average-energy based model can be derived. As shown in Figure 3-5 the average value of per-phase active power is calculated as one third of average value of the grid power. .

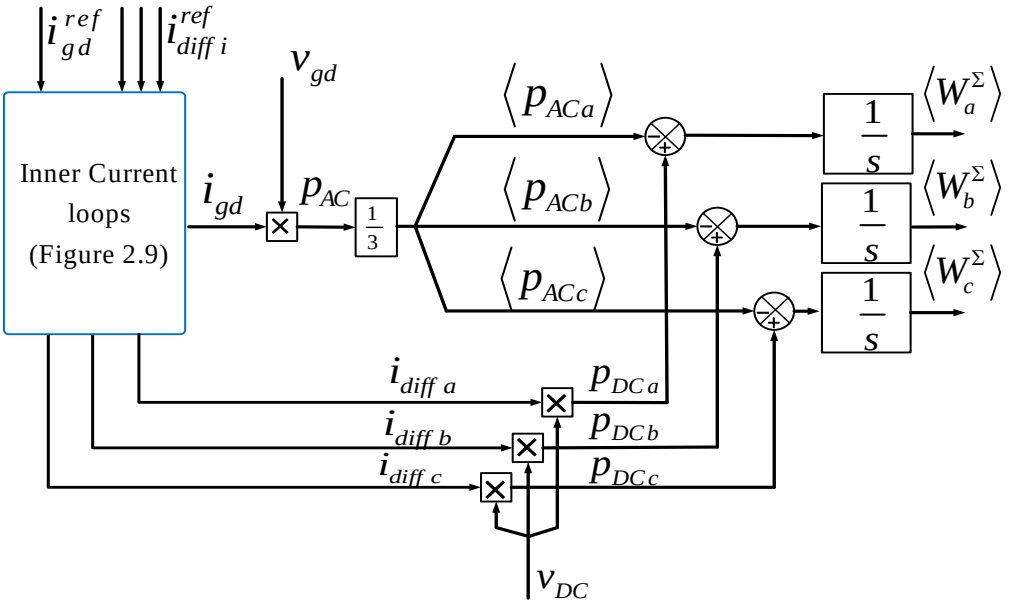

(a) Per-phase stored energy average model

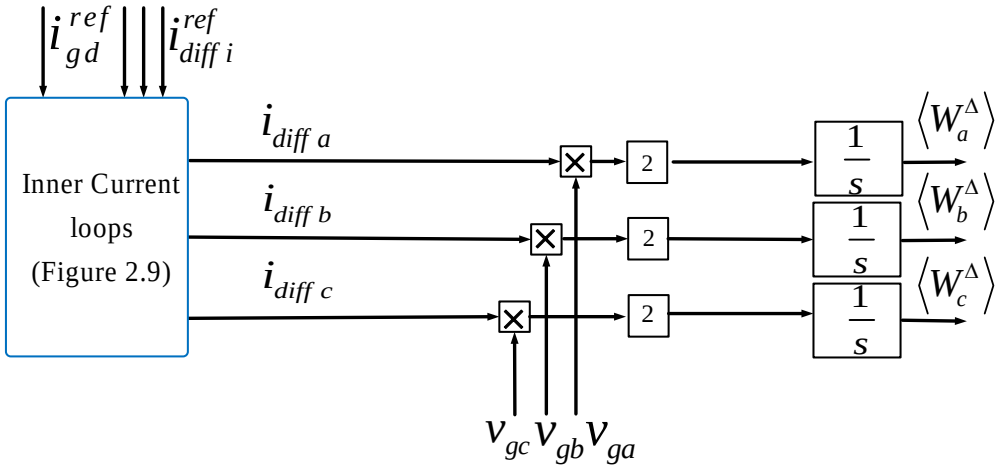

(b) Per-phase difference stored energy between up and low arms average model

Figure 3-5: MMC equivalent average model

In the previous subsections different topologies for MMC energy-based model have been presented. Based on these models, the control of the energy variables in the MMC ($W_i^{\Sigma}$and W_i^{Δ}) can be obtained. These MMC outer controls provide the references of the MMC inner currents ($i_{g\,i}$ and $i_{diff\,i}$) as shown in Figure 3-1. The MMC energy base control strategies are discussed in the next section.

3.3 MMC ENERGY BASED CONTROL STRATEGIES

The MMC energy based control strategies are presented in this subsection. This analysis includes the $W_i^{\Sigma}$and W_i^{Δ} control loops for an MMC which is connected to a DC bus with a constant voltage.

As already mentioned in the previous section, there are different possibilities for MMC energy based model: instantaneous and average models. However, control of W_i^{Δ} based on its instantaneous model is not possible since the whole system is not controllable. Therefore here after, only the control of the average value of the W_i^{Δ} is considered but different control possibilities (instantaneous value or average value) for the control of the W_i^{Σ} are studied.

From equations (3.20), it can be derived that the W_i^{Σ} can be controlled either by the p_{DC} or by the $p_{AC\,i}$ and the average value of the W_i^{Δ} can be controlled by the AC component of the differential currents. This reveals that these energy variables can be controlled independently. Since W_i^{Σ}.and $W_i^{\Delta}$are independent, control methods and analysis of these variables are studied separately in following subsections.

3.3.1. Control of the MMC stored energy

In this part, principles of MMC stored energy (W^{Σ}) control is addressed and different control schemes are proposed. As already said, the energy control part provides the references for the inner current loops that are discussed in chapter two. Here for the sake of simplicity the studied system, the dynamics of the current loops are supposed to be infinite which means that $i_{diff\,DC\,i}^{ref} \cong i_{diff\,DC\,i}$ and $i_{gd}^{ref} \cong i_{gd}$. In addition the control of the difference stored energy between phase-arms (W_i^{Δ}) is assumed to be independent from the control of W_i^{Σ} and it will be discussed further in section 3.3.2 of this chapter.

In order to be more scalable the analysis and simulation results, control schemes are developed in per unit system as follow.

Expression of per-phase stored energy equation regarding to DC per unit principals provided in index B is defined in the sequel:

$$\frac{dW_{i_{pu}}^{\Sigma}}{dt} = H_c \frac{d}{dt}\left(v_{ctot\,u\,i_{pu}}^2 + v_{ctot\,l\,i_{pu}}^2\right) = \; p_{DC\,i_{pu}} - \frac{S_b}{P_{DC_b}} p_{AC\,i_{pu}} \tag{3.21}$$

With $H_c = \frac{1}{2} C_{tot} \frac{V_{DC_b}^2}{P_{DC_b}}$

Here after, all the controls are designed in per unit regarding by inversion of its proper model in per unit.

3.3.1.1. Control of the per phase stored energy based on the instantaneous model

The first choice of control scheme is based on the instantaneous model of the MMC per-phase stored energy. The structure of this control can be obtained by inversion of the upper part of this model, depicted in Figure 3-3(a). As shown in this model W_i^{Σ} is depending on $p_{AC\,i}$ and

$p_{DC\,i}$. If the energy is chosen to be controlled via $p_{DC\,i}$, $p_{AC\,i}$ becomes a disturbance for the control of the energy. This disturbance has to be compensated. Regarding the nature of the instantaneous active power that contains second harmonics of fundamental frequency, resonant controllers are well adapted (see the details in chapter 2). Figure 3-6 shows the block diagram of this control scheme. The block diagram shows that there are three independent loops for W_i^{Σ} to define the references of the differential currents (i_{diff}^{ref}) which manage the exchange of the power between the equivalent capacitor, storage element and the DC link. In this control scenario, the power flowing through the converter is imposed by the reference on the AC power (by i_{gd}^{ref}). Therefore, the inputs of this control system are:$W_{i\,ref}^{\Sigma}$ and i_{gd}^{ref} and their out puts are $i_{diff\,i}^{ref}$.

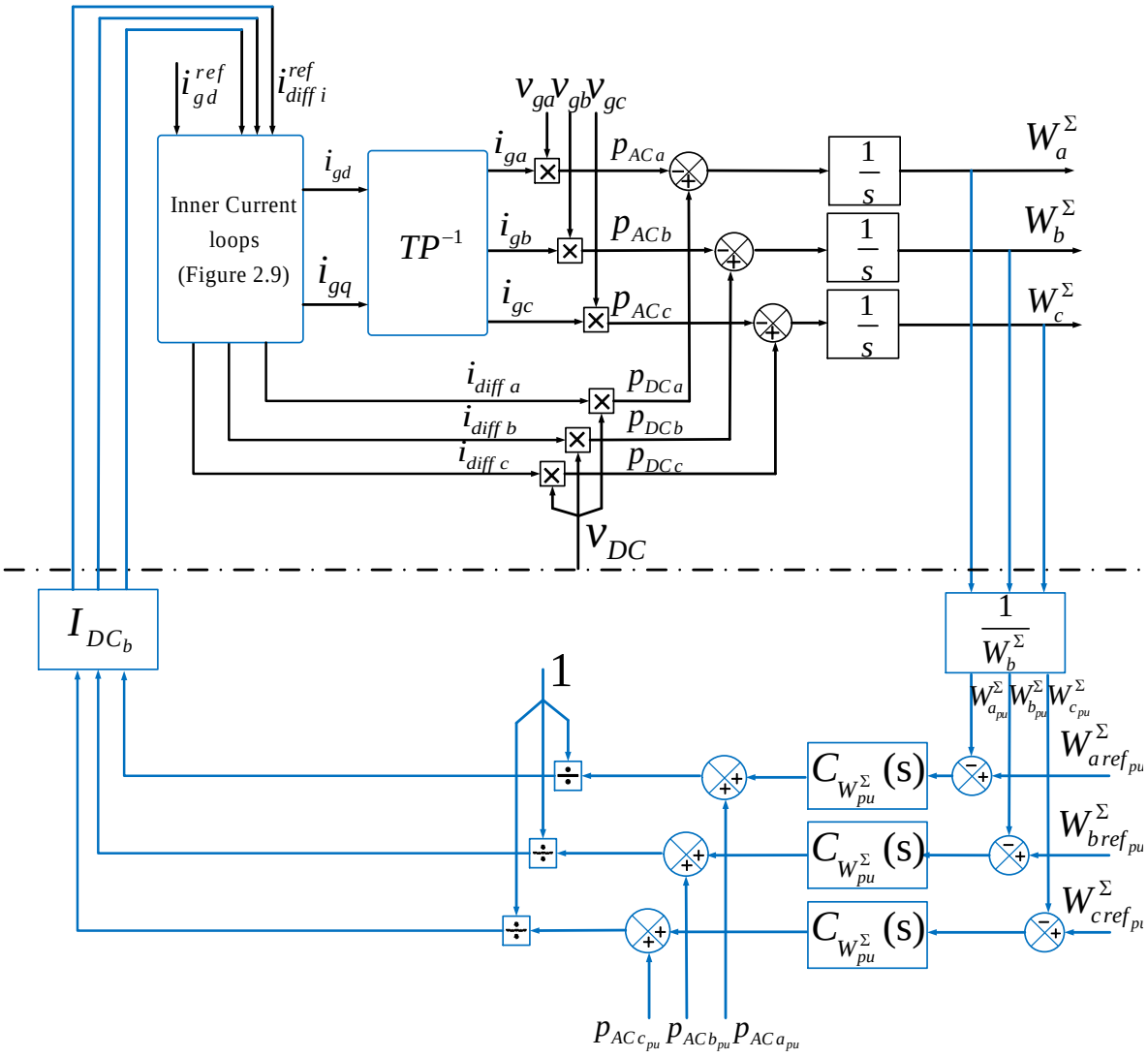

Figure 3-6: Block diagram of per-phase stored energy controlled by DC link- compensation by $p_{AC\,i}$

The simulation results for this control schemes are proposed in Figure 3-7: a step of 1 pu is applied on the AC power reference at t = 0.1s, the reactive power reference stays equal to zero and a step of 0.2 pu is applied on the $W_{i\,ref}^{\Sigma}$ at t=0.3s. A 5ms and 50 ms response times are chosen for the current loops and energy loops respectively.

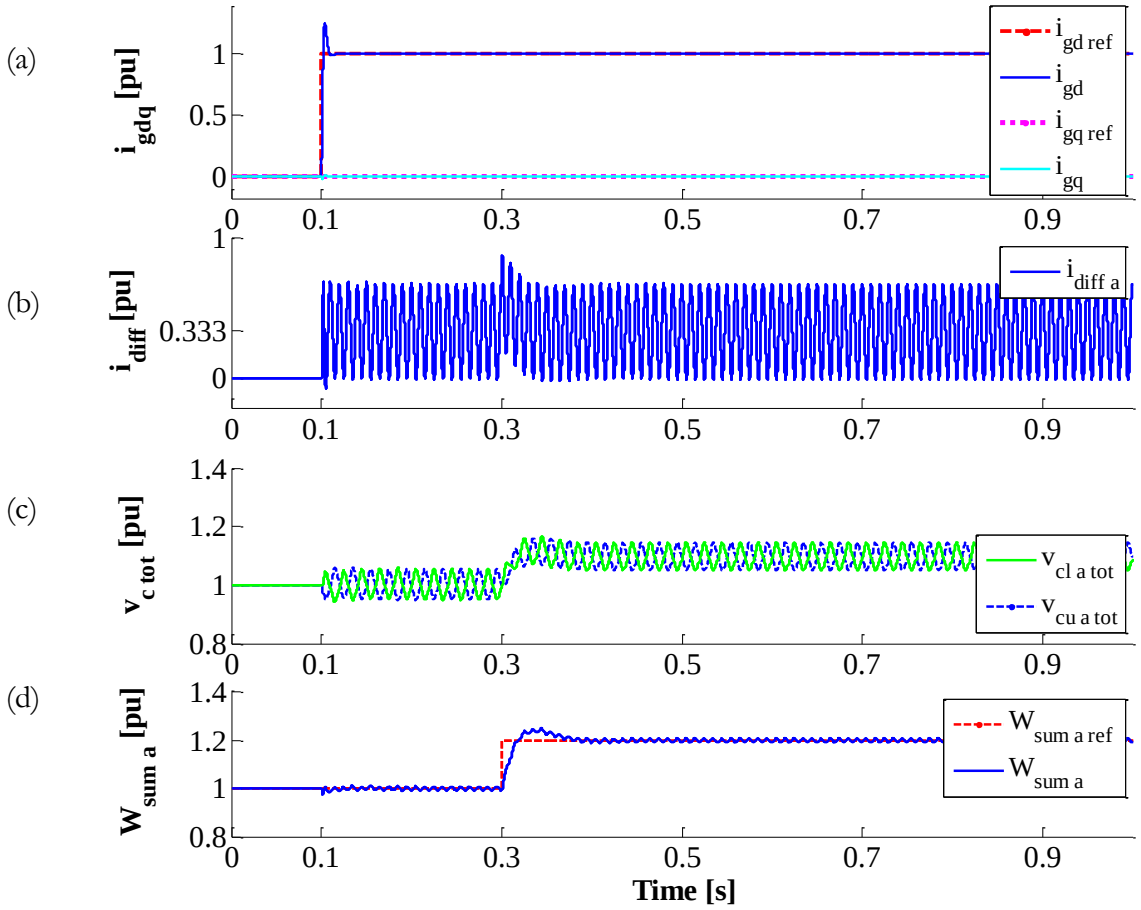

Figure 3-7: Simulation results for per phase stored energy control (W_i^{Σ}) , based on instantaneous MMC model

Figure 3-7(a) shows that the d and q components of the grid currents are well controlled regarding their references. The differential currents contain oscillations at second harmonics of fundamental frequency which depicted for phase-a in Figure 3-7(b). These oscillations are due to power fluctuation injected in current reference by the compensation of the instantaneous active power. The simulation results for the equivalent capacitor voltages for phase-a, presented in Figure 3-7(c),. This figure show that these voltages are stabilized around 1 pu after a step on active power and they are stabilized around 1.1 pu after a step of 1.2 pu on $W_{i\,ref}^{\Sigma}$. Figure 3-7(d) shows that the energy stored in phase-a follows very precisely its reference,1.1 pu, then 1.2 pu with nearly no oscillations. However, if the sum is nearly constant, it is not the case for the equivalent capacitor voltages in phase-a ($v_{cua\,tot}, v_{cla\,tot}$). Indeed, it is not possible to cancel the instantaneous fluctuation in the difference of energy between arms, so this control is not very relevant since it induces a very high level of oscillations in i_{diff} without decreasing the ripple on the $v_{cu/l\,tot}$ voltages.

3.3.1.2. Control of the MMC total stored energy based on the instantaneous model

To decrease the oscillations on the differential current seen in the previous control strategy another solution of control based on the inversion of the instantaneous model of the whole stored energy (W_{tot}^{Σ}) is proposed. Two solutions may be proposed; either to control the energy with the AC power or with the DC power. In this section, the choice is to control the energy via the AC power.

In this control methodology, contrary to the control scheme presented in the previous part, only one major control loop is implemented presented on the block diagram shown in Figure 3-8.

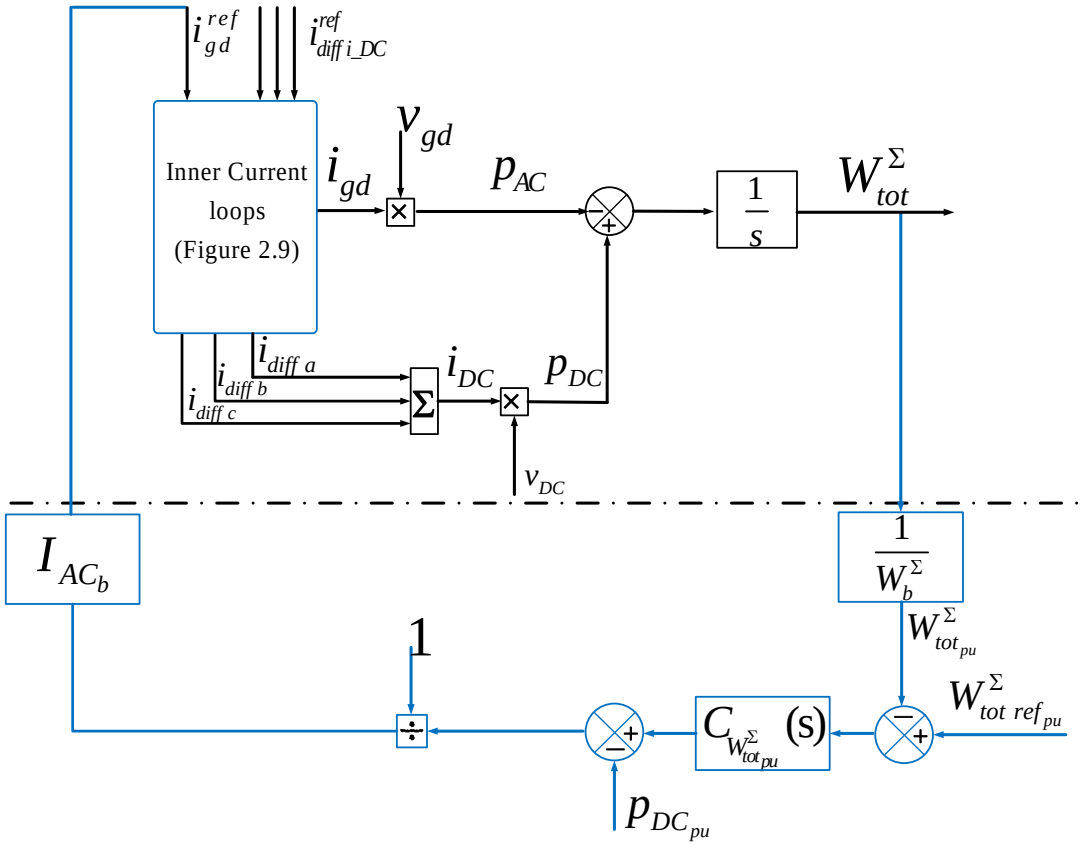

Figure 3-8: Block diagram of total MMC stored energy controlled by AC power

As shown in this block diagram, in this control scenario the power following through the converter is imposed by the reference on the DC power (by $i_{diff\ i\ DC}^{ref}$) and the reference of the MMC total stored energy regulates the AC power in the converter. In this control scenario the input of the system are: $i_{diff\ i\ DC}^{ref}$ and $W_{tot\ ref}^{\Sigma}$ and the output is i_{gd}^{ref}.

The simulation results for this control schemes are proposed in Figure 3-9: a step of 1 pu is applied on the AC power reference at t = 0.1s, the reactive power reference stays equal to zero and a step of 0.2 pu is applied on the $W_{i\ ref}^{\Sigma}$ at t=0.3s. The response times are are set to 5ms and 50 ms for the current loops and the energy loops respectively.

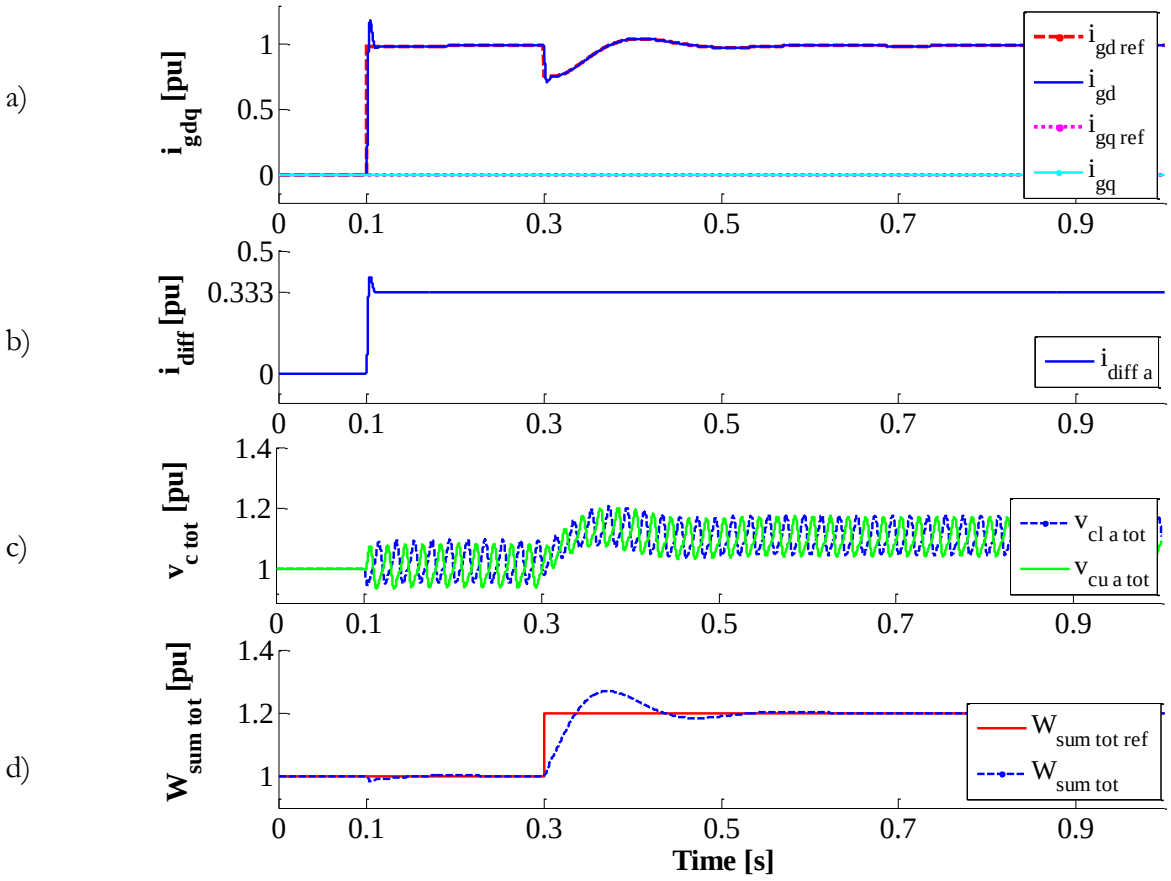

Figure 3-9: Simulation results for whole MMC stored energy: W_{tot}^{Σ}, control based on instantaneous MMC model

Figure 3-9(a) shows that the grid currents regarding to their references are well controlled. As mentioned in introduction in this control scheme the energy is controlled by the AC power This means that the energy is managed by the AC power and that explains why there is a transient at t=0.3 s when a step is applied on the energy reference. Figure 3-9(b) demonstrates that the differential current is stabilized at 1/3 pu regarding the reference of the grid currents equal to 1 pu. Figure 3-9(c), shows that the equivalent capacitor voltages for phase-a are stabilized around 1 pu after a step on the active power and they are stabilized around 1.1 pu after a step of 1.2 pu on $W_{i\,ref}^{\Sigma}$. However there is no control for each phase. Figure 3-9(d) shows that the whole stored energy stored follows correctly its reference. This simulation results demonstrate that the whole stored energy control based on the instantaneous model can control correctly W_{tot}^{Σ} and the dynamics of all parameters are well similar to per-phase stored energy control scheme.

3.3.1.3. Control of the per phase stored energy based on the averaged model

With the previous control, it is not possible to control separately the energy in each phase, the third proposed solution is to control the average value of the energy W_i^{Σ} in each phase. The

structure of this control can be obtained by inversion of the upper part of the model 2, depicted in Figure 3-5(a). In this control scheme, the $\langle W_i^{\Sigma} \rangle$ controller is tuned based on the compensation of the average value of active power per-phase that is calculated as one third of average value of the grid power. Figure 3-10: Block diagram of per-phase stored energy controlled by DC link-compensation by $p_{AC\,i}$ shows the block diagram of this control scheme.

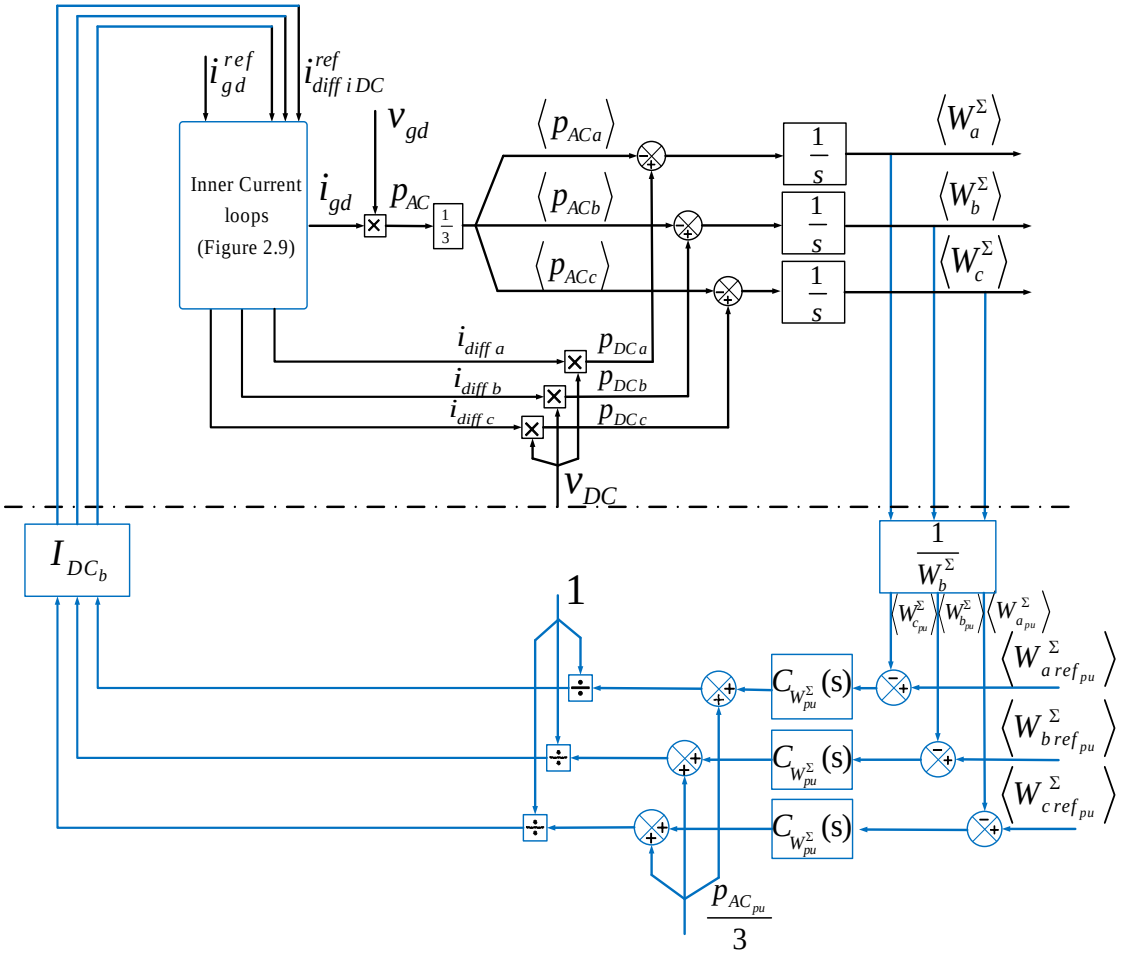

Figure 3-10: Block diagram of per-phase stored energy controlled by DC link-compensation by $p_{AC\,i}$

As it can be seen in the block diagram here, similar to the previous control scheme, the energy is supposed to be controlled by the DC power and the power flowing through the converter is imposed by the reference on the AC power (by i_{gd}^{ref}) instead of the instantaneous value.

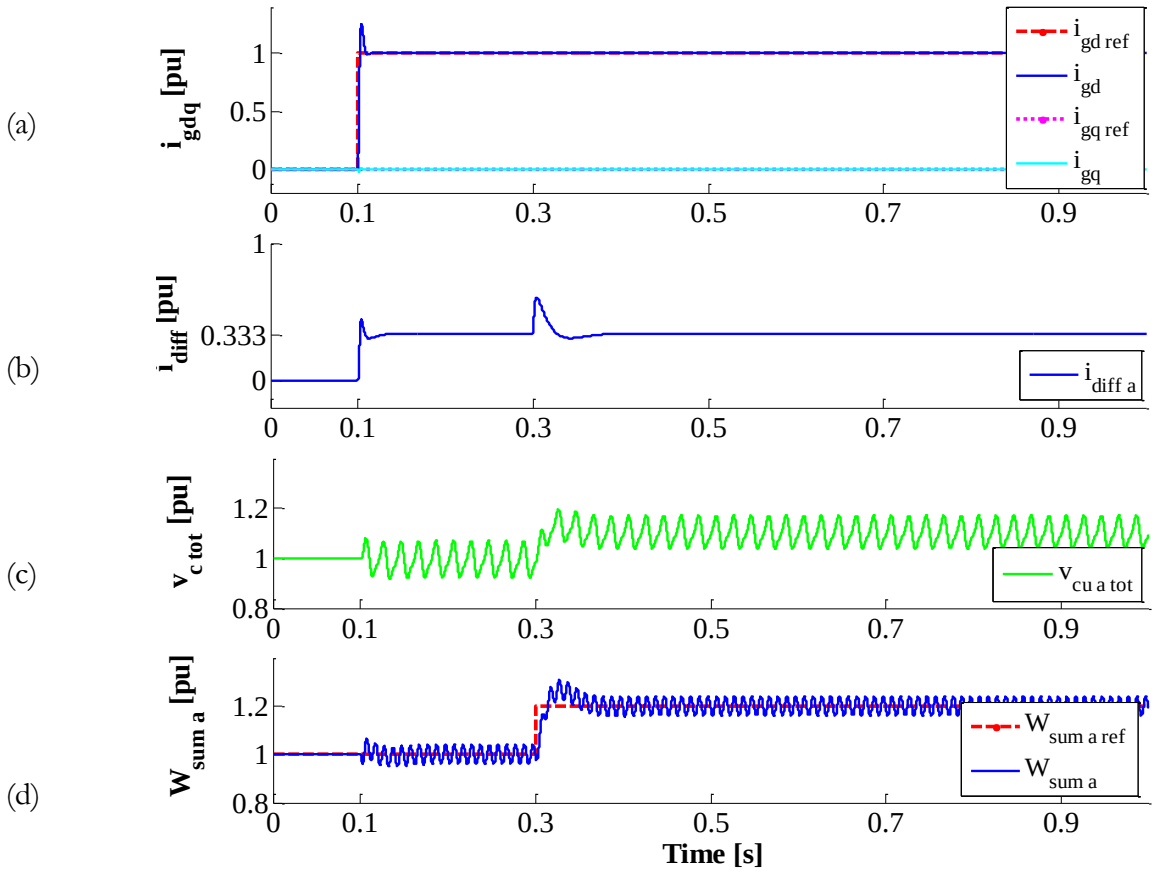

Figure 3-11: Simulation results for comparison of the MMC energy control:W_i^{Σ} controlled with compensation p_{AC} and W_i^{Σ} controlled with compensation P_{AC}

Figure 3-11(a) shows that the grid currents regarding to their references are well controlled. Figure 3-11(b) demonstrates that differential current after the transients, due to the steps on the active power and W_i^{Σ} references, is stabilized at 1/3 pu regarding the reference of the grid currents equal to 1 pu. These simulation results for the equivalent capacitor voltage for upper arm of phase a, presented in Figure 3-11(c), shows that these voltages are stabilized around 1 pu after a step on the active power and they are stabilized around 1.1 pu after a step of 1.2 pu on $W_{i\,ref}^{\Sigma}$. Figure 3-11(d) shows that the energy stored in phase-a follows correctly its reference. This simulation results demonstrate that the per-phase stored energy control based on the average model can control correctly W_i^{Σ}. The major differe.This has major consequence on the loses in the MMC.

3.3.2. Control of the difference of the stored energy between up and low arms

The three previous algorithms were focused on the control of the stored energy in a phase but it is also mandatory to control the difference the stored energy between arms in a phase (W_i^{Δ}) The same hypothesis as in section 3.3.1, are considered for the current loops $i_{diff\,DC\,i}^{ref} \cong i_{diff\,DC\,i}$ and $i_{gd}^{ref} \cong i_{gd}$

As already mentioned, control of the per-phase stored energy (W_i^{Σ}) is assumed to be independent from the control of W_i^{Δ}.

As demonstrated in section 3.3 only the average value of W_i^{Δ}can be controlled thanks to the AC component of the differential current:

$$\left\langle \frac{dW_i^{\Delta}}{dt} \right\rangle_T = \left\langle \frac{1}{2} C_{tot} \frac{d}{dt} \left(v_{cu\,tot\,i}^2 - v_{cl\,tot\,i}^2 \right) \right\rangle_T = -2 \left\langle v_{gi}\, i_{diff\,AC\,i} \right\rangle_T \tag{3.22}$$

Regarding the MMC average-energy based model, the control solution for $\langle W_i^{\Delta} \rangle$ can be obtained by the inversion of model 2 presented in Figure 3-5 (b). In order to perform the control analysis in per unit system, designing the control structure is based on the expression of $\langle W_i^{\Delta} \rangle$ in per unit as:

$$\left\langle \frac{1}{2} C_{tot} \frac{V_{DC_b}^2}{P_{DC_b}} \frac{d}{dt} \left(v_{cu\,tot\,i\,pu}^2 - v_{cl\,tot\,i\,pu}^2 \right) \right\rangle_T = -2 \frac{V_{ACb}}{V_{DCb}} \left\langle v_{gi\,pu}\, i_{diff\,AC\,i\,pu} \right\rangle_T \tag{3.23}$$

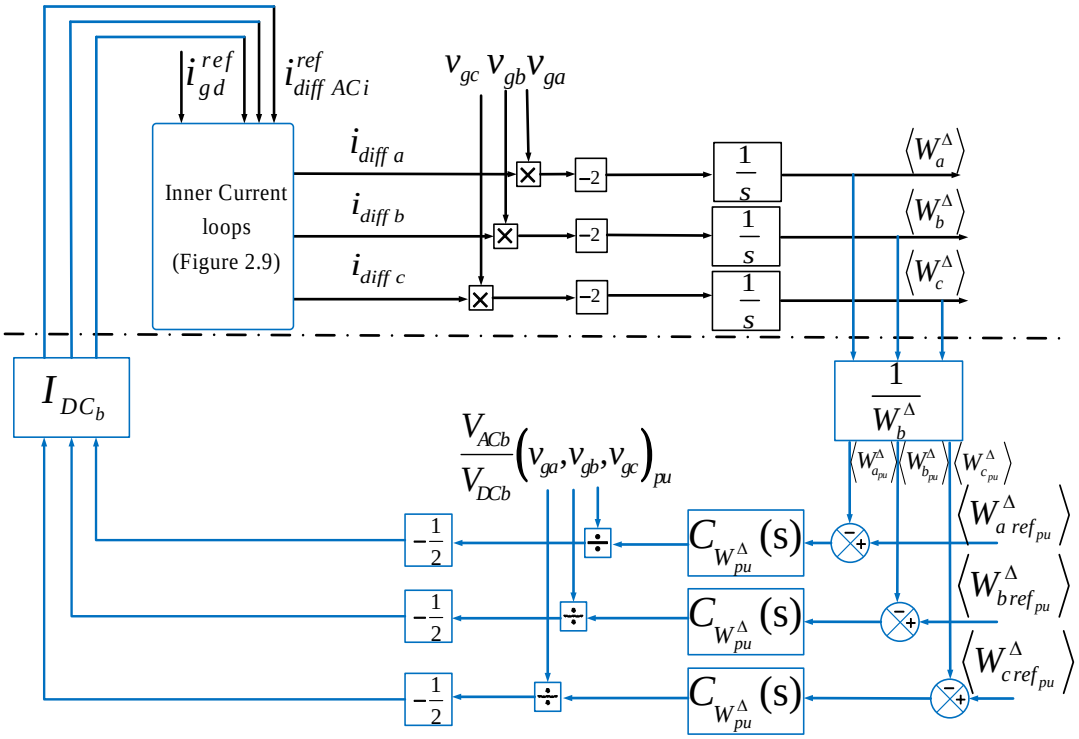

Figure 3-12: MMC equivalent model based on per-phase stored energy

Then, the block diagram of this control scheme can be obtained as shown in Figure 3-12. As it can be sketched on this figure, control of $\langle W_i^{\Delta} \rangle$ provides the references of the AC part of the differential currents.

To validate the presented control scheme, the simulation results are proposed in Figure 3-13. Since in this study, W_i^{Σ} is supposed to be controlled by the DC link a step of 1 pu is applied on the AC power reference at t = 0.1s, the reference of the W_i^{Δ} is equal to zero. Similar

to the previous simulations, the reactive power reference stays equal to zero and the response time of current and energy loops are 5 ms and 50 ms respectively.

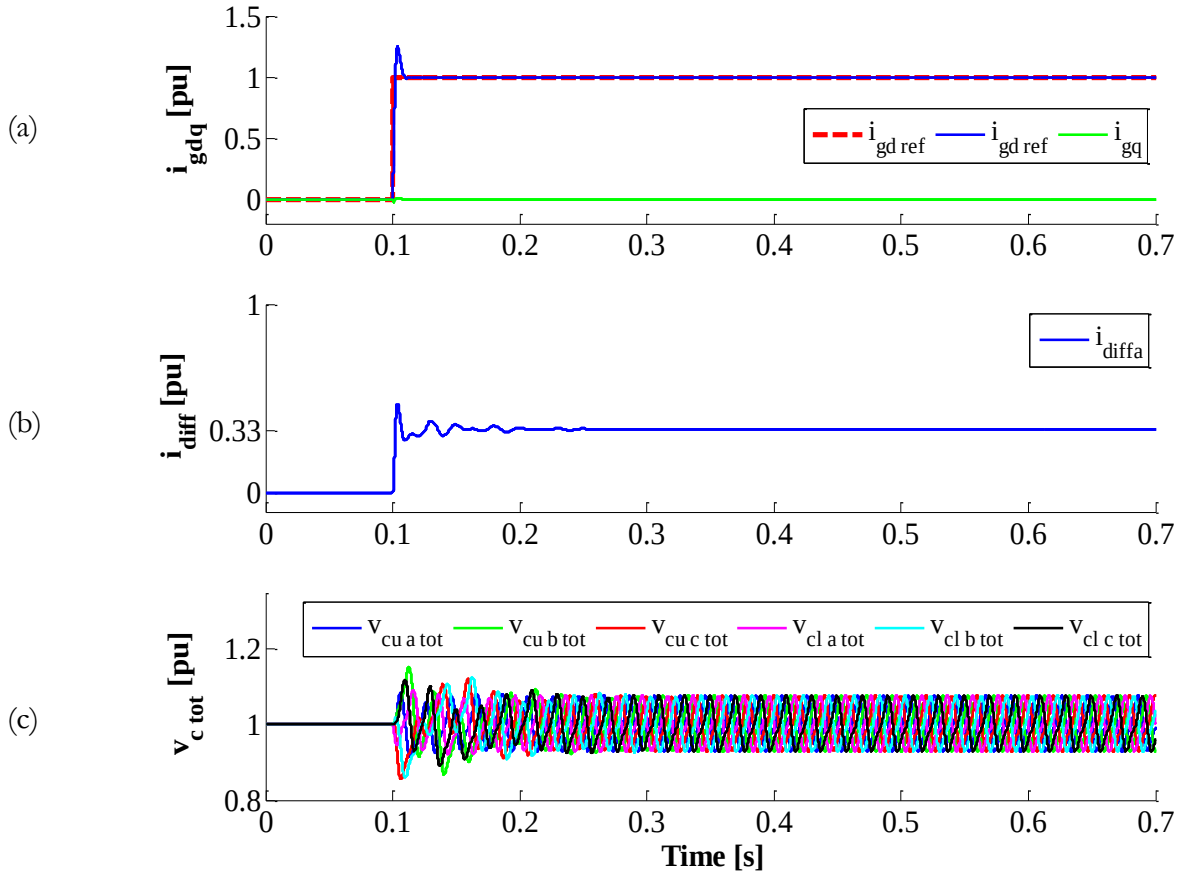

Figure 3-13: Simulation results for control of $\langle W_i^{\Delta} \rangle$.

Figure 3-13(a), shows that the grid currents regarding to its reference are well controlled

. The differential currents sum of the DC part and AC part, are depicted for phase-a in Figure 3-13(b) , this figure shows that these differential currents, for a given power reference of 1 pu are converting to 1/3 pu after the transient. The simulation results for the equivalent capacitor voltages for the 6 arms, presented in Figure 3-13(c), show that all these voltages are balanced and are stabilized around 1 pu. These simulation results validate the presented control scheme. Some more oscillations are noticed on the differential current in the transient. It is important to notice that the balancing control for each phase (control of $\langle W_i^{\Delta} \rangle$) is independent from the control of average value of these voltages (control of W_i^{Σ}) as mentioned in previous subsections.

3.4 CONCLUSION AND COMPARISON BETWEEN THE DIFFERENT PROPOSED STRATEGIES

In order to control all MMC state variables, the energy based control schemes are adopted and this chapter has presented principles of MMC energy based controls. Consequently, an energy based model for MMC is considered and the MMC energy variables are presented.

For the MMC energy variables: per-phased stored energy (W_i^{Σ}) and per-phased balanced energy (W_i^{Δ}) mathematical model and analysis are presented. This model reveals the average values of these energy variables are independent hence the whole system is controllable.

In this chapter, several methods for control of MMC stored energy are investigated. The basic control method of W^{Σ} controlled by DC link, includes the inversion of MMC instantaneous model. It presents good dynamics performance for grid currents, however the oscillations on the differential currents have a consequence on the MMC losses. This necessitates another control scheme which is based on the MMC average model that presents good dynamic performances for differential currents as well as the equivalent capacitor voltages per arm.

Comparison of the two strategies of Control of MMC per-phase energy by DC link

The simulation results for both control schemes are proposed in Figure 3-14: Simulation results for comparison of the MMC energy control:W_i^{Σ} controlled a step of 1 pu is applied on the AC power reference at t = 0.1s, the reactive power reference stays equal to zero and a step of 0.2 pu is applied on the $W_{i\,ref}^{\Sigma}$ at t=0.3s. The response times are considered 5ms and 50 ms for current loops and energy loops respectively.

Figure 3-14(a) shows that the grid currents in both simulations are well controlled and there are no differences between the two control strategies also this figure demonstrate that a step on the W_i^{Σ} has no effect on the AC currents. However as it can be seen in Figure 3-14(b) that the differential current of phase-a in case of W_i^{Σ} controlled with compensation PAC, has less oscillations. Since in both cases the differential currents are stabilize around 1pu/3 there are no differences in high level control of the converter but in point of view the SMs, less oscillations on the differential currents lead to less SMs losses. Figure 3-14(c) shows that W_a^{Σ} in both control strategies are well controlled regarding to its reference by respecting the time response of 50 ms. However W_a^{Σ} controlled with compensation p_{AC} has less oscillations since a PIR controller is used to eliminate the influence of the fluctuating active power in this control scheme. Figure 3-14(d) shows that there is no important difference between two control strategies however oscillation for total capacitor voltages in case of W_i^{Σ} controlled with compensation PAC is more important. This figure also shows that at t=0.3s the average value of the total capacitor voltages are stabilized around 1.1 pu which is correspond to t root of the $W_{i\,ref}^{\Sigma}$ =1.2 pu..

These simulation results validate the proposed control strategies and reveal that in point of view of the high level control of the converter, there is no notable difference between the controller with instantaneous AC power and average AC power. However regarding the differential currents and the capacitor voltages the SMs losses are different due to SMs currents and voltage capacitor of the SMs.

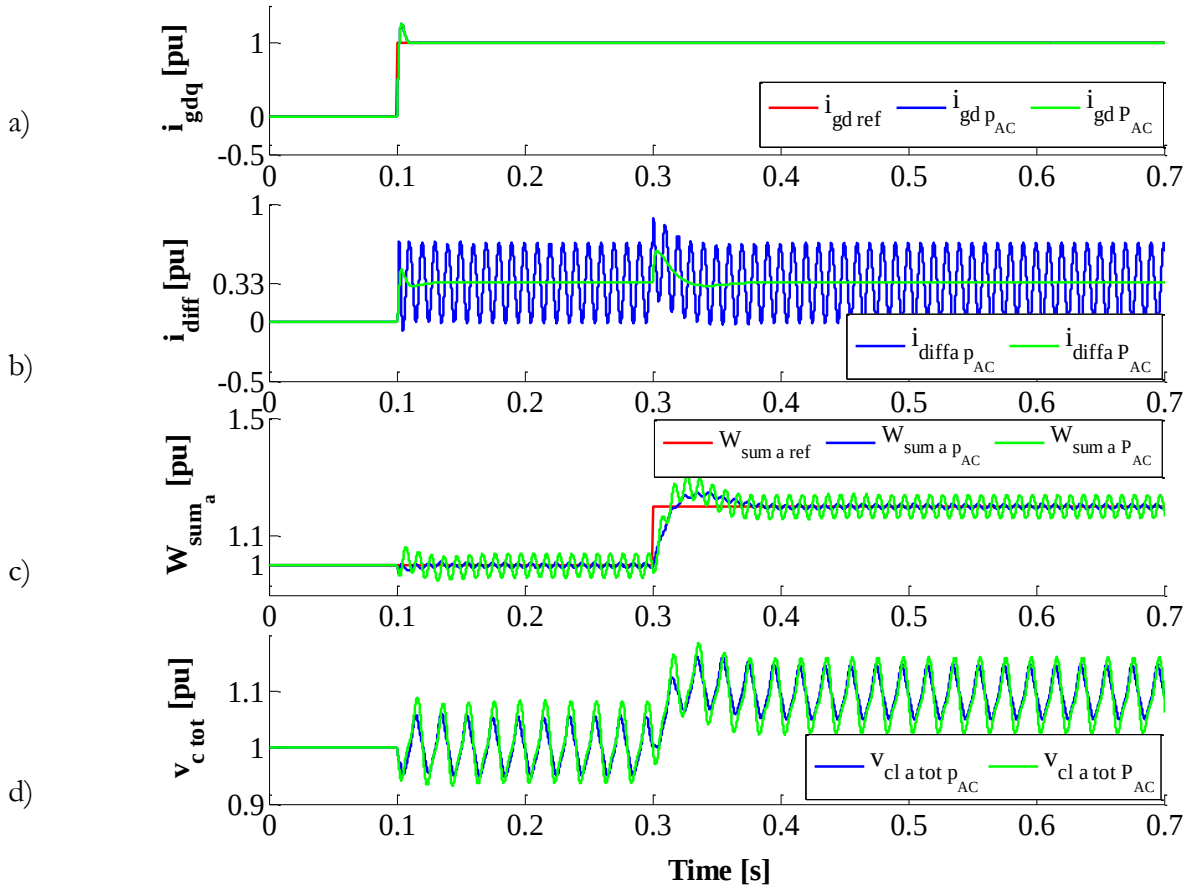

Figure 3-14: Simulation results for comparison of the MMC energy control:W_i^{Σ} controlled with compensation p_{AC} and W_i^{Σ} controlled with compensation p_{AC}

Regarding the MMC stored energy equation (3.20) there are two main control categories for W^{Σ}: MMC stored energy controlled by AC grid or by DC link are presented. Comparison of these control schemes highlight that there is notable difference between these two control solutions since the role of MMC state variables to control the energy variables change.

Comparison of two strategies of W^{Σ}Control: control by DC link or control by AC power

This comparison provides a common case study to distinguish the differences between two main controls for MMC stored energy: The studied system is composed of an MMC connected to a constant DC bus link with the same simulations' parameters as listed in (table 2-1). The response time of inner current loops are 5ms and the response time of W_i^{Σ} loop is 100 ms. The simulation are performed as follows:

- Simulation event for " W_i^{Σ} controlled by the DC power ":

  t = 0.1s, a step of 1 pu on the active power reference.

  t = 0.3s a step of 0.2 pu on the stored energy reference.

- Simulation event for " W_{tot}^{Σ} controlled by the AC power ":

  t = 0.1s, a step of 0.1 pu on the reference of DC power.

  t = 0.3s a step of 0.15 pu on the reference of the stored energy.

Figure 3-15 (I), presents the MMC variables when the energy is managed by the differential currents (DC link), in this case a step on the AC power generate the reference for the grid current ($i_{gd\,ref}$). As shown in Figure 3-15(a) the grid currents are well controlled and the step on the MMC stored energy at t=.3 s has no effect on these currents. It reveals that the demanded energy is provided by the differential currents. This can be seen in Figure 3-15(b) where the differential current of phase a (similar to other phases) are stabilized at 1pu/3 and there are transient at 0.1 s and 0.3 s. Figure 3-15(c) demonstrate that the $v_{c\,u\,a\,tot}$ is well controlled as it stabilized around 1.1pu at 0.3 regarding the step of 0.2 pu on W_{ref}^{Σ} .

Figure 3-15(II) shows the simulation results when the whole stored energy in the MMC is controlled by the AC power. In this case, the power controlled is achieved by the differential currents: a step of 1 pu is applied on its reference at t=0.1 s. Figure 3-15(d) pictures the simulation results. The grid currents are well controlled but the variation of energy is managed on the AC side by action on i_{gd}^{ref} In Figure 3-15(f) it can be seen that the differential current of phase-a is well controlled regarding its reference. This figure also shows that, since the MMC stored energy is controlled by AC power, a step on the energy reference has no consequence on the differential currents. Figure 3-15(f), demonstrates that similar to Figure 3-15(c) the voltage of the equivalent capacitor for upper arm of phase a is well controlled.

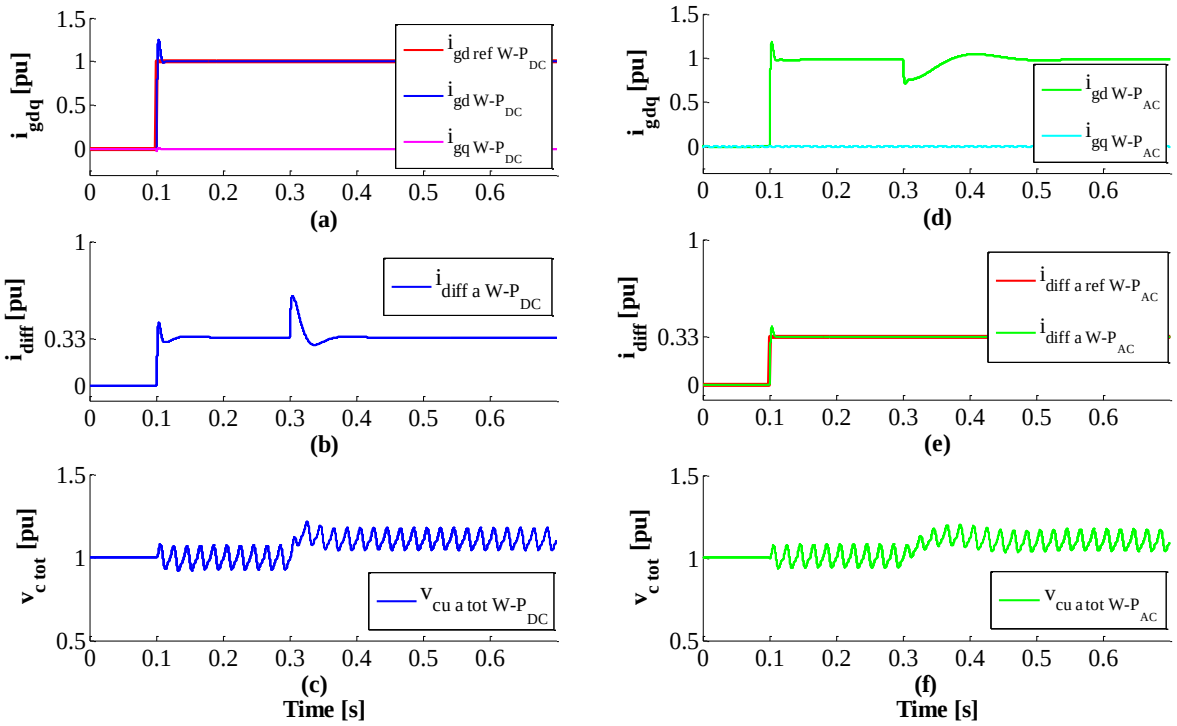

(I) W_i^{Σ} controlled by the DC power (II) W_{tot}^{Σ} controlled by the AC power

Figure 3-15: Simulation results for the MMC energy control .(I)W_i^{Σ} controlled by the DC power ,(II)W_{tot}^{Σ} controlled by the AC power

By comparison part (I) and part(II) of Figure 3-15 it can be noticed that nearly the same comments can be done in the both cases but the role of grid current and differential current are exchanged. In part (I), the MMC stored energy is managed by the differential currents: the energy stored in the capacitor comes from the DC voltage source and the power exchange is managed by the reference on the grid current. In part(II), the whole stored energy is controlled by the AC grids and there is no exchange between the energy stored in the capacitors and the DC link. In this case the power is managed by the reference on the differential currents. The comparison between two simulation results reveals that depending on the chosen solution for control of the stored energy in the MMC the exchange of power between the MMC and DC link changes.

In addition, in this chapter a control scenario for balancing the stored energy between upper and lower arms in a phase is presented and is validated by the simulation results.

CHAPTER 4 : Control of an HVDC link based on MMC

4.1 INTRODUCTION

In the majority of the MMC applications, this converter cannot be used alone. Most of the time, it is integrated in an HVDC point to point link where the two AC/DC substations have different roles: one station controls the active power flow; the other one controls the DC voltage.

The previous chapter has presented the control analysis for an MMC that controls the power flow and the voltage of the DC bus has been considered constant. In this chapter, the attention is paid on the station which controls the DC bus voltage in the HVDC link.

This control analysis enables to assess the main parameters which act on the DC voltage dynamics. Then the connection of two MMC stations is studied. This study shows that the way to manage the energy in the MMC may have a critical role in the DC voltage stability in an HVDC link.

4.2 POINT-TO-POINT HVDC LINK PRINCIPLES

Operating principles of an MMC-HVDC transmission scheme is investigated in this part. In order to transmit the electrical energy between two grids (Grid 1 and 2 in Figure 4-1) a point-to-point MMC-HVDC transmission is composed of two MMC stations connected at each ends through the DC link as shown in Figure 4-1.

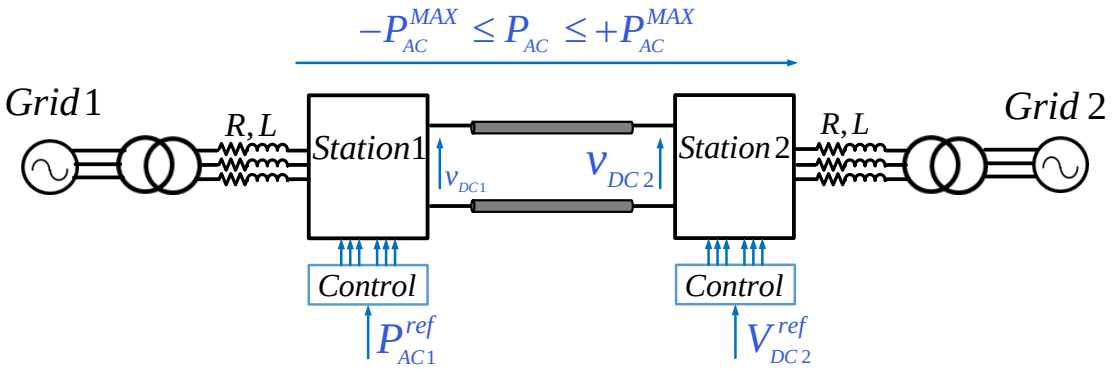

Figure 4-1: Point-to point MMC-HVDC transmission scheme

In such a transmission system, the converter is connected to the AC grid by an interface transformer which defines a specific voltage at the converter side. The role of the inductances at the AC side is mainly to limit the current in case an AC short circuit. Since the converter stations can work either as a rectifier or as an inverter, the range of power transmitted in this HVDC link comprised between $\pm P_{AC}^{MAX}$ (see Figure 4-1). On the DC side, the link between both converters can be made by an overhead line or a cable. If considered the DC link as a DC cable, the simple model is a capacitor with a small capacitance per kilo-meter. The voltage on the equivalent capacitor of the DC cable, named as the DC bus voltage, should be controlled to be constant.

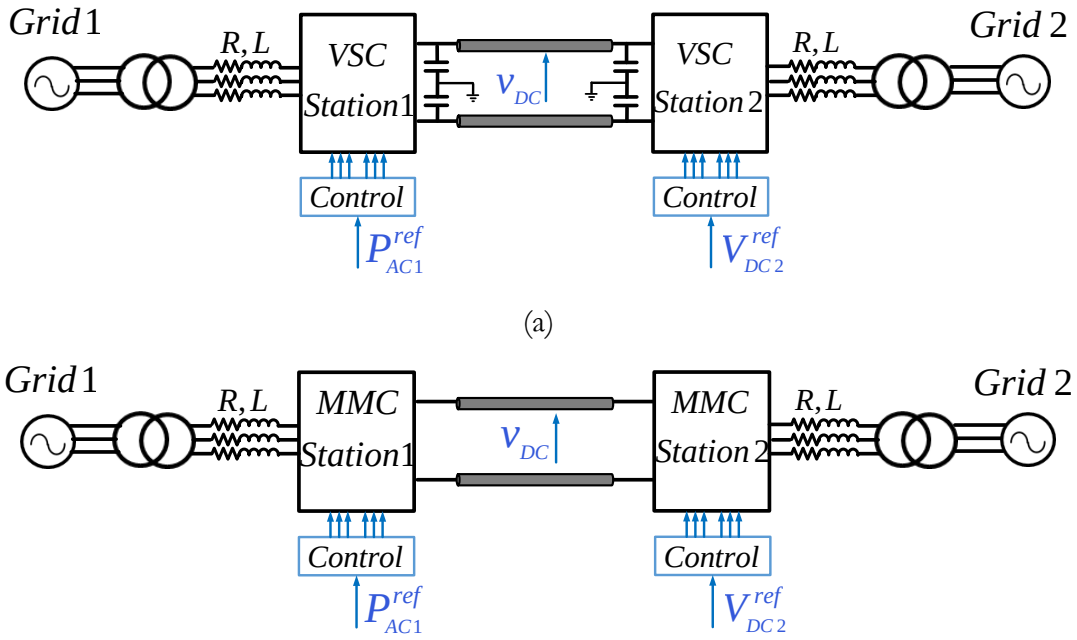

Figure 4-2: Schematic representation of an HVDC link:(a) Classical VSC applied in an HVDC link and (b) MMC applied in an HVDC link

Among the existing converter topologies applied in the HVDC transmission systems, the MMC topology is a breakthrough for high power and high voltage applications with good harmonics performances. However, there are a few draw backs as well for the MMC topology. Looking at both systems in Figure 4-2 reveals a fundamental difference in term of energy localization. In case of a classical VSC, (see Figure 4-2(a)) the capacitors are directly connected on the DC bus, which means that the storage level depends on the DC voltage [80]. In other words, these storage elements naturally participate in the DC bus voltage stability. Regarding MMC topology, (see Figure 4-2(b)) the storage elements are inside the converter [19], and no direct link exists with the DC bus. The only storage element on the DC-bus is the DC cable capacitor. In case of a large variation of power on the DC bus, this could lead to a very volatile DC voltage.

The aim of following section is to establish a link between the voltage of MMC capacitors and DC bus voltage thanks to the control. To do so, the control of the MMC station which regulates the DC voltage level has to be analyzed.

4.3 MMC DC VOLTAGE CONTROL PRINCIPLES

This section presents the control principles of the MMC station that manages the DC bus voltage. As shown in Figure 4-3, in this station, the MMC is connected to a DC link which includes the DC cable and a very simple model of the other MMC station as a power source (p_l). Therefore, in this station the DC bus voltage can vary and the only storage element is the equivalent DC cable capacitance named as C_{DC}.

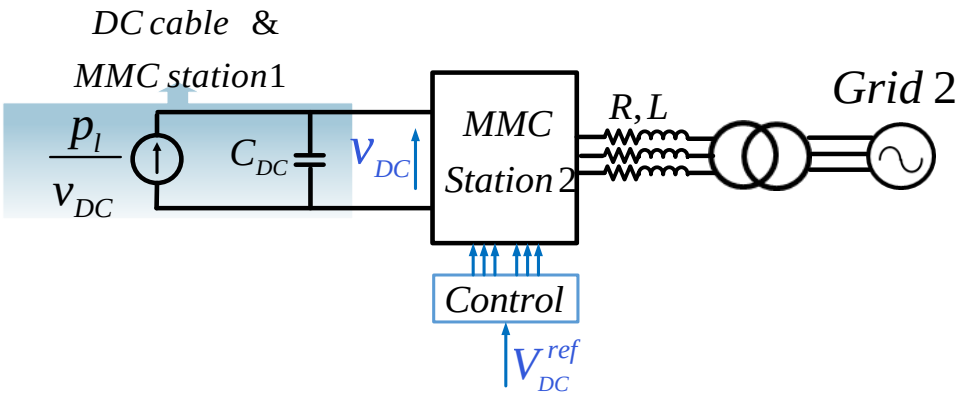

Figure 4-3: MMC station connected to a variable DC bus voltage

4.3.1. MMC model associated to a variable DC bus voltage

The model of the system has to be adapted to take into account the DC bus behavior. As shown in Figure 4-3 the DC bus is modelled by a simple capacitor C_{DC} and a current source. The energy parameter for this MMC station can be derived:

As already written in the previous chapter, the average value of per-phased stored energy can be written as following:

$$\langle \frac{dW_i^{\Sigma}}{dt} \rangle_T = \langle \frac{1}{2} C_{tot} \frac{d}{dt} (v_{c\,u\,i\,tot}^2 + v_{cl\,i\,tot}^2) \rangle_T = p_{DC\,i} - \langle p_{AC\,i} \rangle_T \quad (4.1)$$

The energy stored in C_{DC} depends on the power exchanged by the MMC (p_{DC}) with the DC bus and the power flowing from the other station (p_l) .

$$\frac{dW_{DC}}{dt} = \frac{1}{2} C_{DC} \frac{dv_{DC}^2}{dt} = -p_{DC} + p_l \quad (4.2)$$

With:

$$p_{DC} = \sum_{i=1}^{3} p_{DC\,i} \quad (4.3)$$

The DC bus voltage variation depends on the exchange of energy between the MMC stored energy and the stored energy in C_{DC}. The exchange of energy between MMC and C_{DC} depends on the MMC stored energy control strategy. In the previous chapter, two main categories for MMC stored energy control has been mentioned: control of the W_i^{Σ}. by $p_{DC\,i}$ and control of the W_{tot}^{Σ} by p_{AC} (see conclusion of chapter 3). This chapter aims to establish a link between the energy stored in the MMC and the DC bus voltage. This strategy leads to the participation of the MMC storage elements in the DC bus voltage stability. (see section 4.3.2.1)

One solution to establish a relation between the energy in the converter and the DC bus voltage level is considering the reference of energy $W_{i\,ref}^{\Sigma}$ equal to the instantaneous DC bus energy W_{DC}.

Then four study cases can be distinguished as follow:

1. DC bus voltage variation when W_i^{Σ} is controlled by $p_{DC\,i}$ with $W_{i\,ref}^{\Sigma} = Constant$
2. DC bus voltage variation when W_i^{Σ} is controlled by $p_{DC\,i}$ with $W_{i\,ref}^{\Sigma} = W_{DC}$
3. DC bus voltage variation when W_{tot}^{Σ} is controlled by p_{AC} with $W_{i\,ref}^{\Sigma} = Constant$
4. DC bus voltage variation when W_{tot}^{Σ} is controlled by p_{AC} with $W_{i\,ref}^{\Sigma} = W_{DC}$

4.3.1.1. MMC and DC bus model when the MMC energy is controlled by the DC power

Depending on the way the energy is controlled in the MMC, the DC voltage may be adjusted either by the DC power reference or the AC power reference. In this section, the energy is supposed to be controlled by the AC power. The model of this system is depicted in Figure 4-4.

The aim of this section is to establish a transfer function between the AC power reference and the DC bus voltage in order to design the controller. For doing so, equations (4.1) and (4.2) are used. First, adding the set of three equations in (4.1) leads to the following equation where w_{tot}^{Σ} is calculated:

$$\langle \frac{dW_{tot}}{dt} \rangle_T = \langle \frac{1}{2} C_{tot} \left(6 \frac{dv_{c\,tot}^2}{dt} \right) \rangle_T = p_{DC} - p_{AC} \tag{4.4}$$

With:

$$v_{c\,tot}^2 = \sum_{i=1}^{3} v_{cu\,i\,tot}^2 + \sum_{i=1}^{3} v_{cl\,i\,tot}^2 \tag{4.5}$$

Adding (4.1) and (4.2) leads to (4.6).

$$\frac{1}{2} C_{DC} \frac{dv_{DC}^2}{dt} + \langle \frac{1}{2} C_{tot} \left(6 \frac{dv_{c\,tot\,ref}^2}{dt} \right) \rangle_T = -p_{AC} + p_l \tag{4.6}$$

In the sequel, strong assumptions are required:

- The AC power is assimilated to its reference: $p_{AC} \approx p_{AC}^{ref}$
- The voltage $v_{c\,tot}^2$ is assimilated to its reference: $v_{c\,tot}^2 \approx v_{c\,tot}^{2\,ref}$ in other words: $W_{tot}^{\Sigma} \approx W_{tot}^{\Sigma\,ref}$

Equation (4.6) becomes:

$$\frac{1}{2} C_{DC} \frac{dv_{DC}^2}{dt} + \langle \frac{1}{2} C_{tot} \left(6 \frac{dv_{c\,tot\,ref}^2}{dt} \right) \rangle_T = -p_{AC}^{ref} + p_l \tag{4.7}$$

Depending on the way $v_{c\,tot\,ref}^2$ is managed, the dynamic behavior is largely modified.

When $v_{c\,tot\,ref}^2 = constant (w_{tot\,ref}^{\Sigma} = constant)$ equation (4.7) becomes:

$$\frac{1}{2}C_{DC}\frac{dv_{DC}^2}{dt} = -p_{AC}^{ref} + p_l \tag{4.8}$$

And when $v_{c\,tot\,ref}^2 = v_{DC}^2$ ($w_{tot\,ref}^{\Sigma} = w_{DC}$) equation (4.7) becomes:

$$\frac{1}{2}(6KC_{tot} + C_{dc})\frac{dv_{DC}^2}{dt} = -p_{AC}^{ref} + p_l \tag{4.9}$$

Equation (4.9) shows that the equivalent capacitor for the regulation of the DC bus now includes the capacitors of MMC. This leads to a high increase for the capacitor value. For example, in our case study, the value of the MMC capacitors ($6C_{tot}$) is 24 times the value of a 70 km DC cable capacitor. The property highlighted in (4.9),is similar to what can be found in classical CCSCdq since v_{ctot} is naturally equal to v_{dc} (see [55])

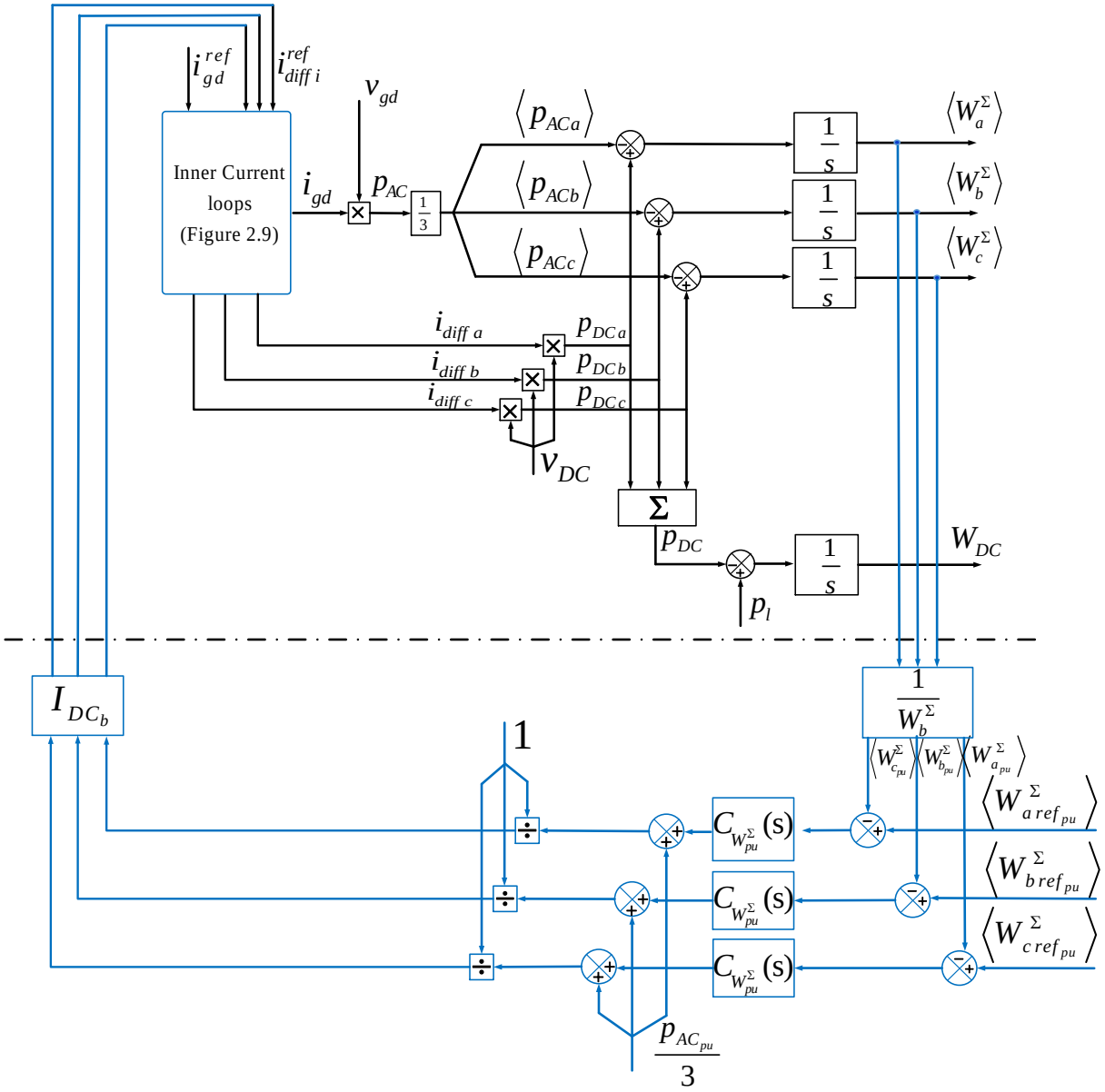

Figure 4-4: MMC connected to a variable DC bus voltage when the energy is controlled by the DC power

This equation shows that the MMC behaves as if the six capacitors were on the DC-bus which was the aim to achieve. In other words, the MMC behaves nearly as a VSC with a capacitor of $C_{DC} + 6C_{tot}$. The simulation results presented in Figure 4-5 confirm this assertion.

At t = 0.1s, a step of -0.004 pu on $P_{AC\ ref}$ is applied during 300ms.

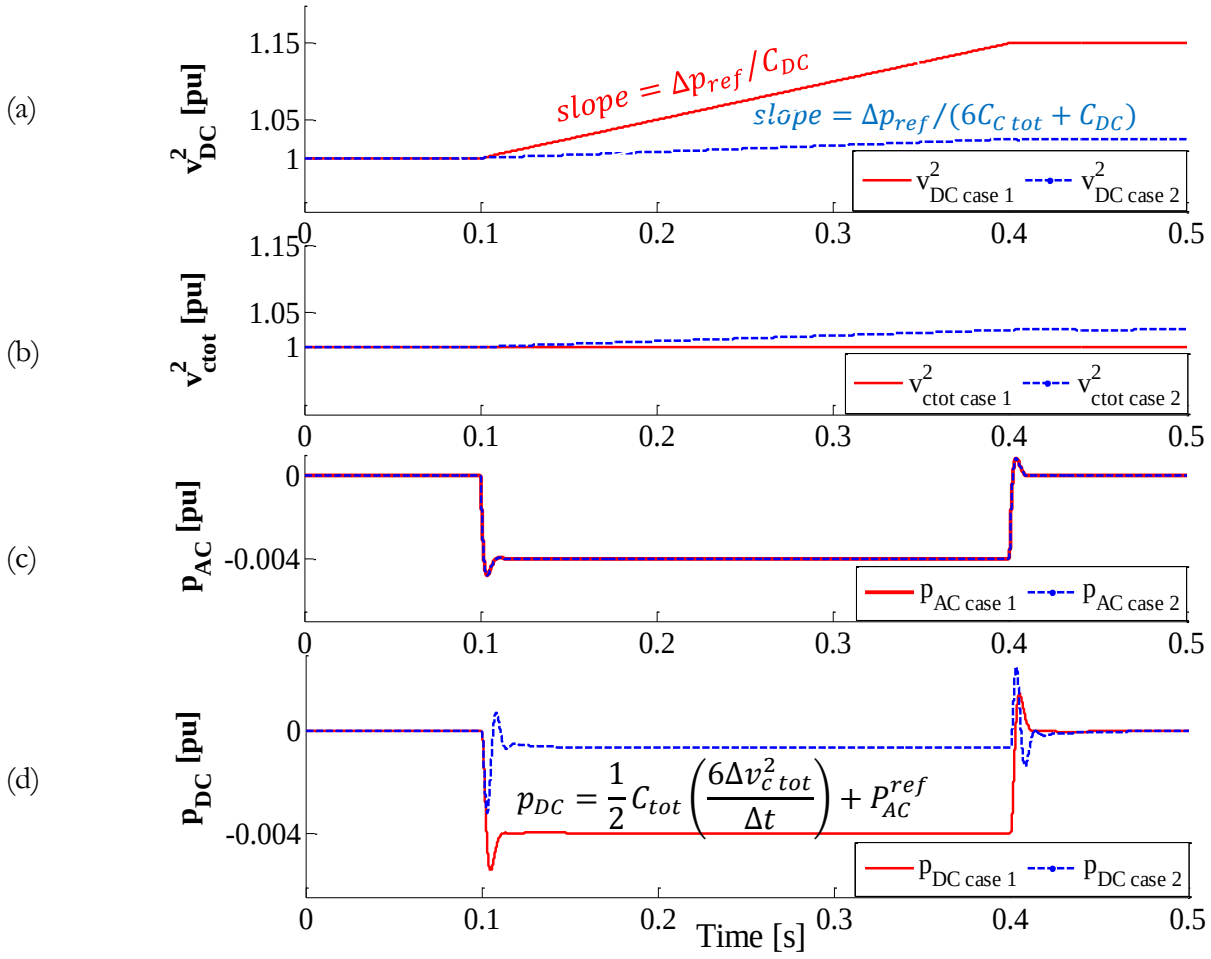

Figure 4-5: Energy controlled by the DC power in two cases:
Case 1: $V^{ref}_{C\,i\,tot} = v_{DC}$ and case 2: $V^{ref}_{C\,i\,tot} = V^{ref}_{DC}$

4.3.1.2. MMC and DC bus model when the MMC energy is controlled by the AC power

In this subsection, the energy is controlled by the AC power, as depicted in Figure 4-6, which means that the DC voltage may be controlled by the DC power reference. Assuming that $p_{DC} \approx p^{ref}_{DC}$ equation (4.2) becomes:

$$\frac{1}{2}C_{DC}\frac{dv^2_{DC}}{dt} = -p^{ref}_{DC} + p_l \qquad \textbf{(4.10)}$$

A direct link is established between v_{DC} and p_{DC}^{ref} with no assumption required on the management of the energy.

From equation (4.4), it is possible to deduce the AC power from the DC power and the total energy.

$$p_{AC} = -\langle \frac{1}{2} C_{tot} \left(6 \frac{dv_{c\,tot}^2}{dt} \right) \rangle_T + p_{DC} \tag{4.11}$$

With the same assumptions as previously, the equation can be written:

$$p_{AC} = -\langle \frac{1}{2} C_{tot} \left(6 \frac{dv_{c\,tot}^{2\,ref}}{dt} \right) \rangle_T + p_{DC}^{ref} \tag{4.12}$$

Depending on the way $v_{c\,tot\,ref}^2$ is managed, the evolution of p_{AC} will be modified.

When $v_{c\,tot\,ref}^2 = constant (W_{tot\,ref}^{\Sigma} = constant)$ equation (4.12) becomes:

$$p_{AC} = -p_{DC}^{ref} \tag{4.13}$$

And when $v_{c\,tot\,ref}^2 = v_{DC}^2$ $(w_{tot\,ref}^{\Sigma} = w_{DC})$ equation (4.12) becomes:

$$p_{AC} = P_{DC}^{ref} - \frac{1}{2} C_{tot} \left(6 \frac{dv_{DC}^2}{dt} \right) \tag{4.14}$$

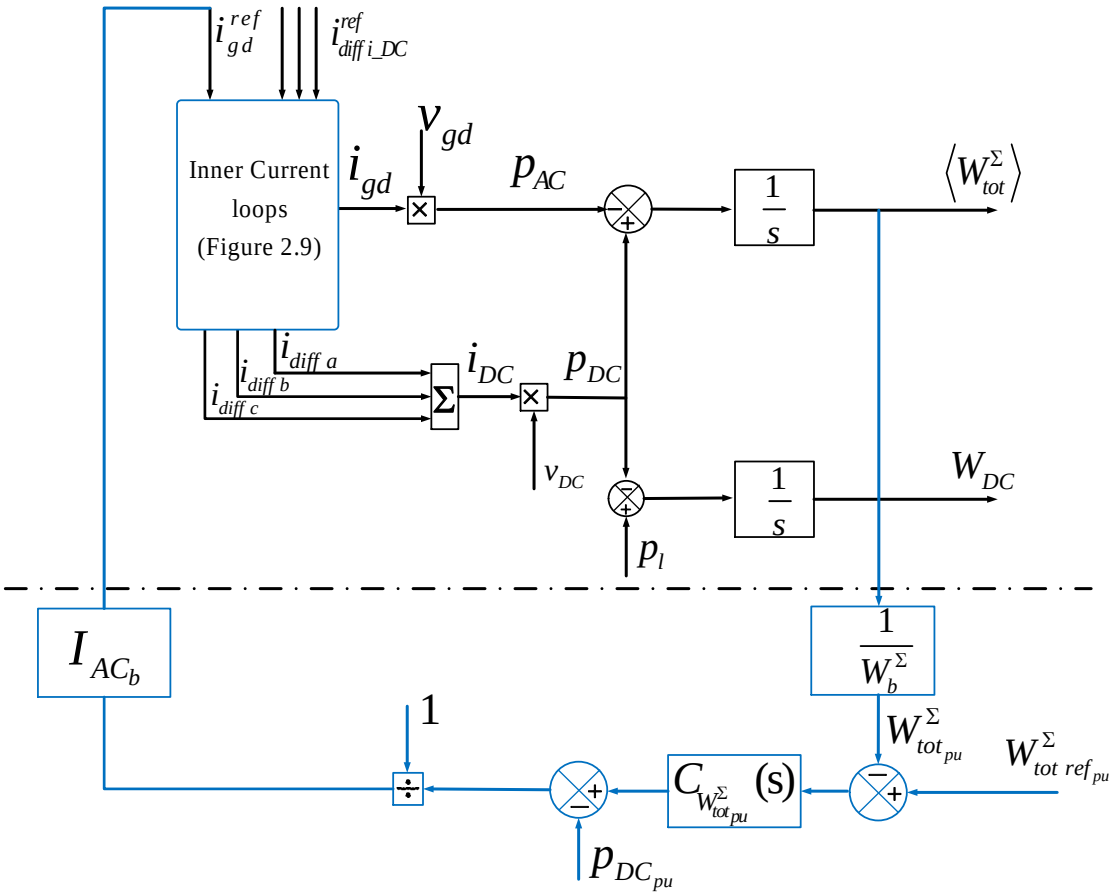

Figure 4-6: MMC connected to a variable DC link when the energy is controlled by the AC power

Like in the previous section, this solution is studied with the two cases and the simulation results are compared in Figure 4-7.

At t = 0.1s, a step of -0.004 pu on p_{DC}^{ref} is applied during 300ms

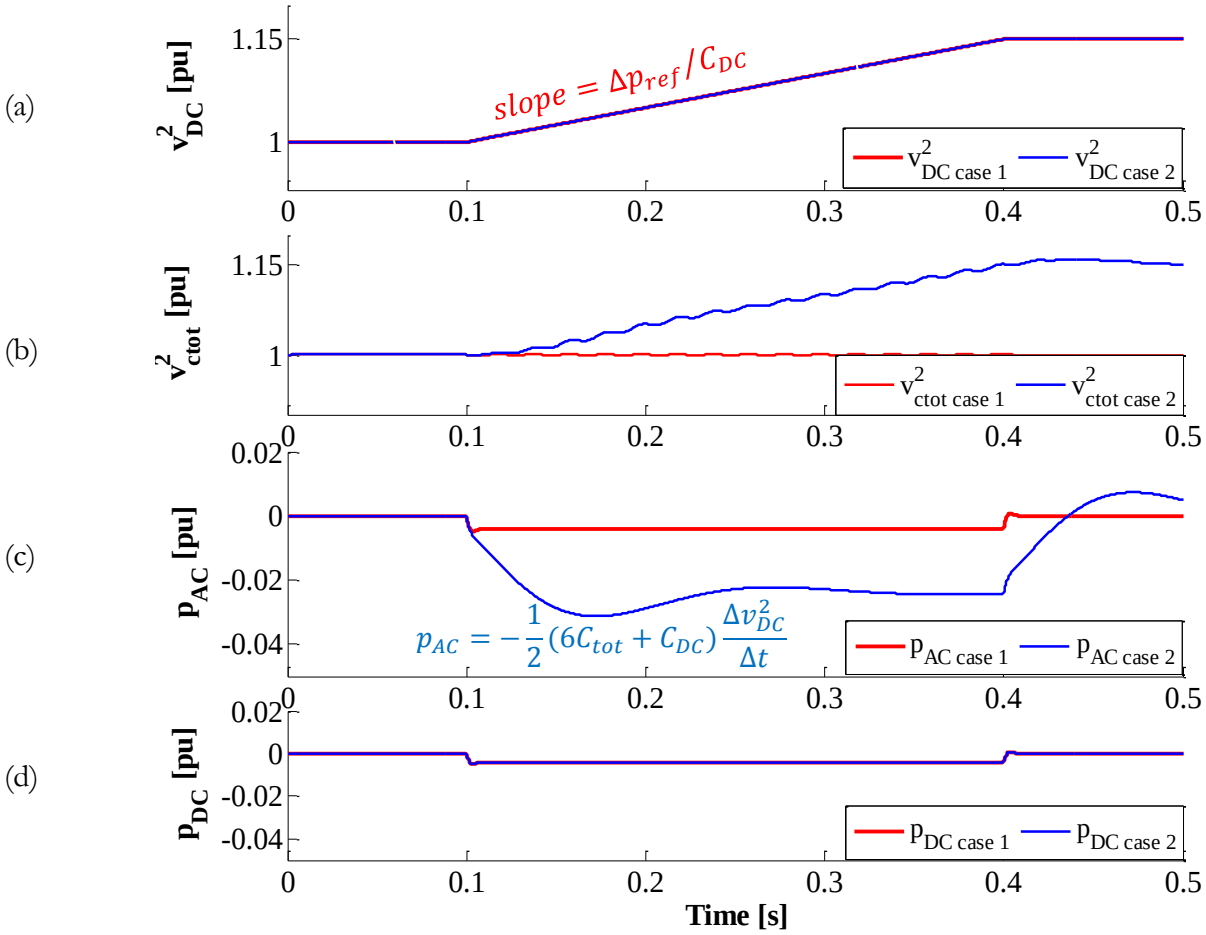

Figure 4-7: Energy controlled by the AC power in two cases:
Case 1: $V_{C\,i\,tot}^{ref} = v_{DC}$ and case 2: $V_{C\,i\,tot}^{ref} = V_{DC}^{ref}$

As depicted in Figure 4-7 and contrary to the first control solution, the dynamic of DC-bus voltage in both cases is the same and it only depends on C_{DC}. The only difference is noticed on p_{AC}. In case1, $p_{AC}$is constant, in case 2, it is depending on the slope of the DC-bus voltage.

4.3.2. DC bus voltage control

As explained in the previous subsection, the dynamic of the DC voltage depends on the MMC energy control scheme. In this part, the DC bus voltage control solutions including the MMC energy control are studied.

4.3.2.1. Control by active power

As shown previously, the DC bus voltage dynamic highly depends on the way the energy us managed in the MMC. Depending on this choice, the DC bus voltage controller has to be adjusted.

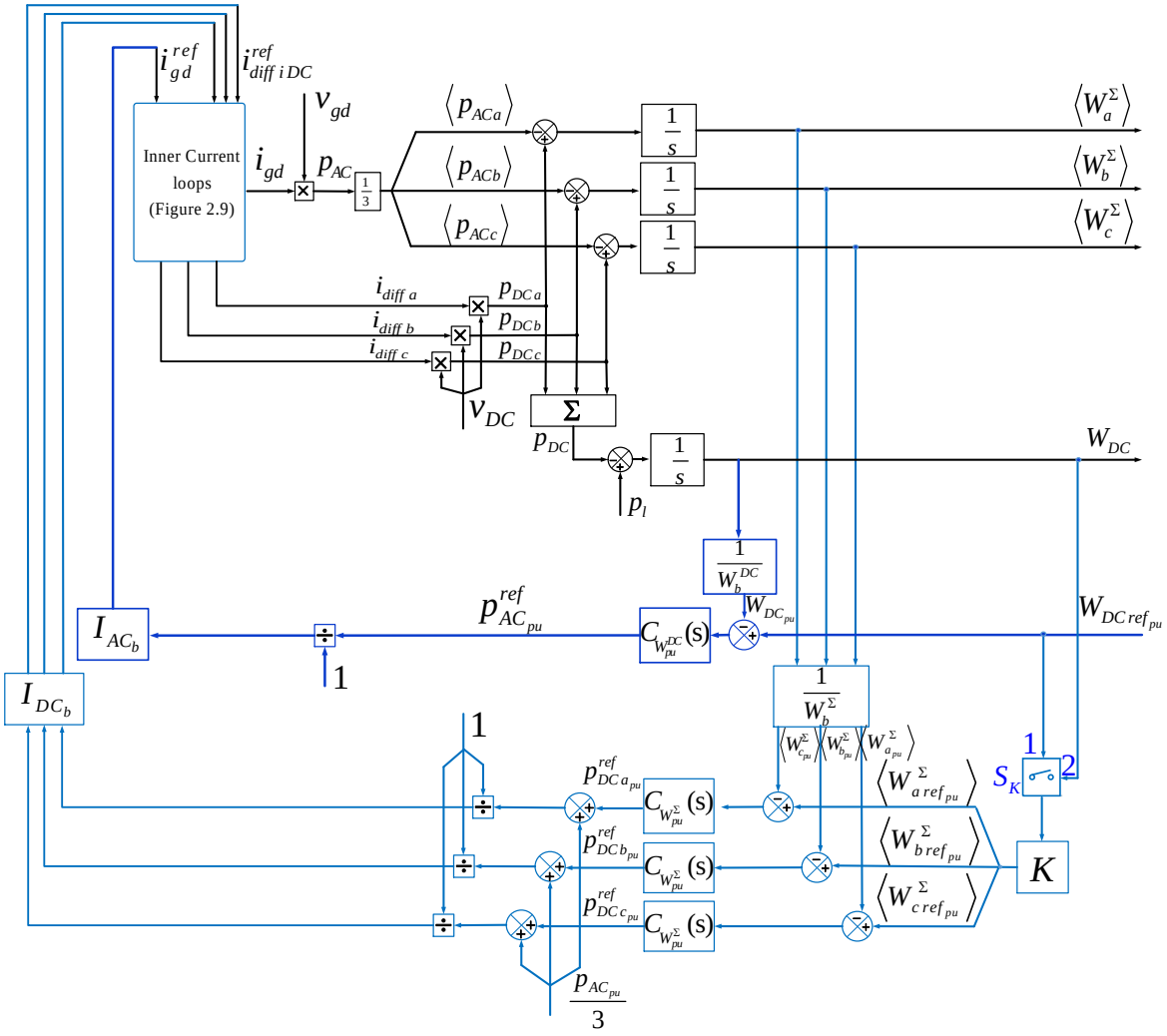

Figure 4-8: Block diagram of an MMC with DC voltage control by active power

In case the switch S_k (see Figure 4-8) is in position 1, the energy reference is constant, the DC bus controller is designed taking into account the model described in equation (4.9). In both cases, the dynamics has to be limited due to the strong assumption needed to obtain a simple equation. (i.e. $W_{tot}^{\Sigma} = W_{tot\,ref}^{\Sigma}$).

The response time of the current and energy loops are 5 ms and 50 ms respectively. The DC voltage response time is set to 100ms.

Three control solutions are now simulated and a comparison of the simulation results is provided. The three control schemes are as follow:

- CCSC, mentioned in chapter2,
- Energy based control with a constant energy reference,
- Energy based control with a variable energy reference

The simulation results are observed after the following event:

Step of -0.1 pu at t = 0.1s on p_l

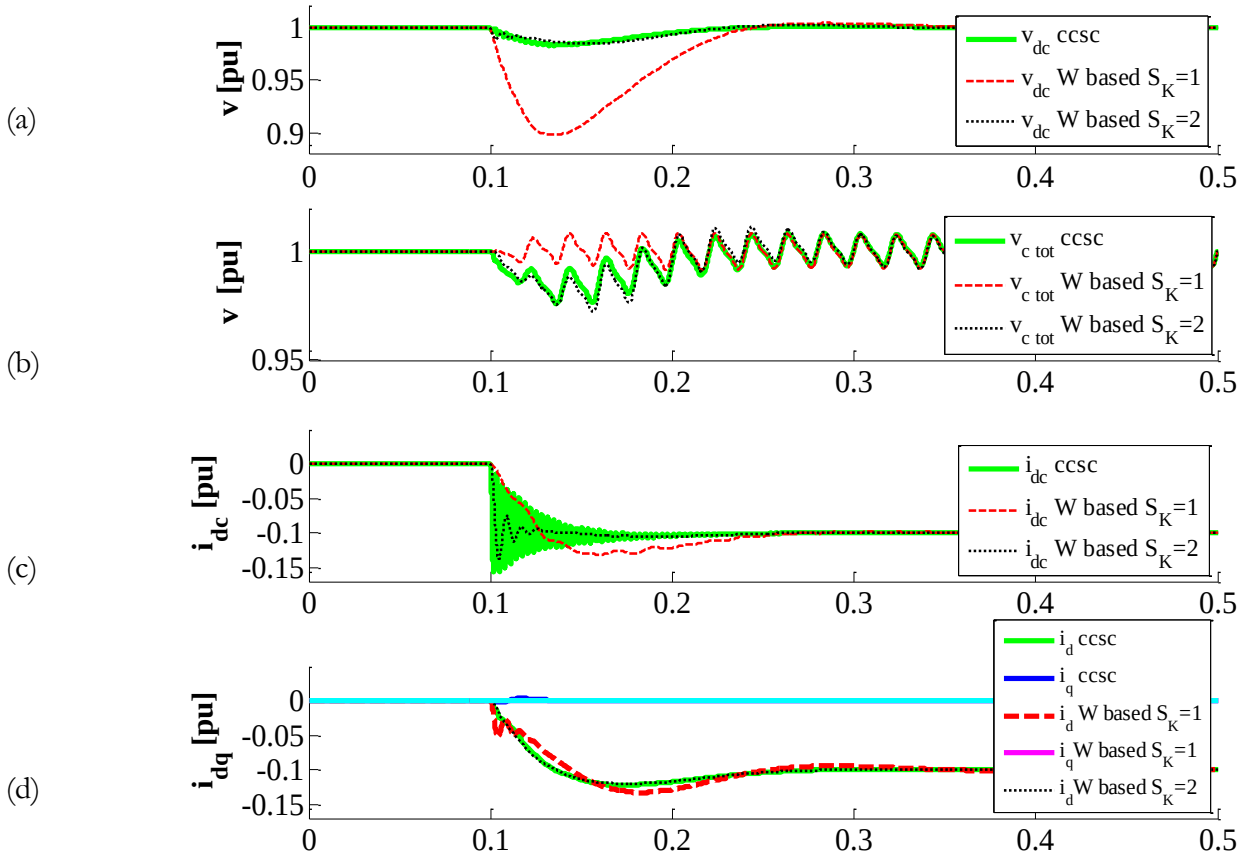

Figure 4-9: Comparison results between CCSC and energy-based control with variable DC bus voltage in two cases if DC voltage controlled by AC power

Figure 4-9(a) shows that the average value of $v_{cu\,tot}$ follows the DC bus voltage variation in the non-energy based control scheme, whereas it depends on S_K in the energy-based control scheme.

Figure 4-9(b) verified that in the energy-based control scenario, v_{dc} variation is more significant when $S_K = 1$ than when $S_K = 2$. Indeed, when $S_K = 1$, this variation depends only on the capacitor of the DC cable.

When $S_K = 2$, the equivalent capacitor is equal to $6C_{tot} + C_{dc}$, the voltage variation is largely decreasing. In CCSC, the DC voltage behavior is nearly the same as in the energy-based control with $S_K = 2$. However, the energy is not controlled, and many oscillations are observed on the

DC current. On the contrary, the DC current is well damped in the energy-based control (Figure 4-9(c)).

These simulation results clearly show that the proposed control merges two main properties: increased equivalent DC bus capacitor and full control of the DC current.

4.3.2.2. Control by DC Power

In case, the energy is controlled by the AC power, the DC voltage level is controlled by the DC power (p_{DC}^{ref}).

As already explained in 4.3.1.2, in this control strategy there is no exchange between MMC stored energy ($W_{i\,ref}^{\Sigma}$) and the energy stored in C_{DC} (W_{DC}).

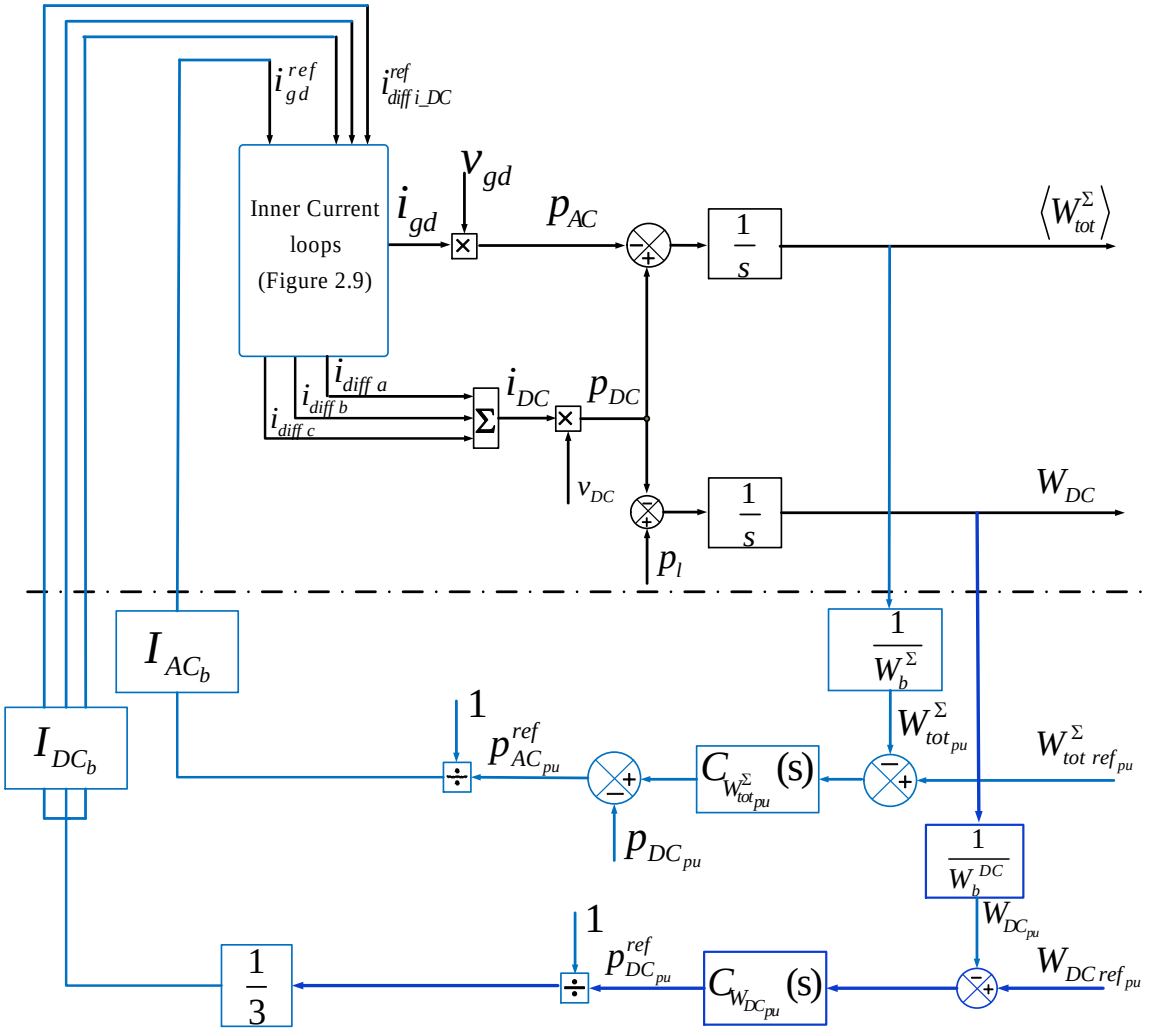

Figure 4-10: Block diagram of an MMC with DC voltage control by DC power

As also explained before, no assumption is needed on the energy loop. It is possible to increase the DC voltage dynamic compare to the previous case. The simulation results are observed after the following event:

Step of -0.1 pu at t = 0.1s on p_l The response time of the current and energy loops are 5 ms and 50 ms respectively. The DC voltage response time is set to 20 ms.

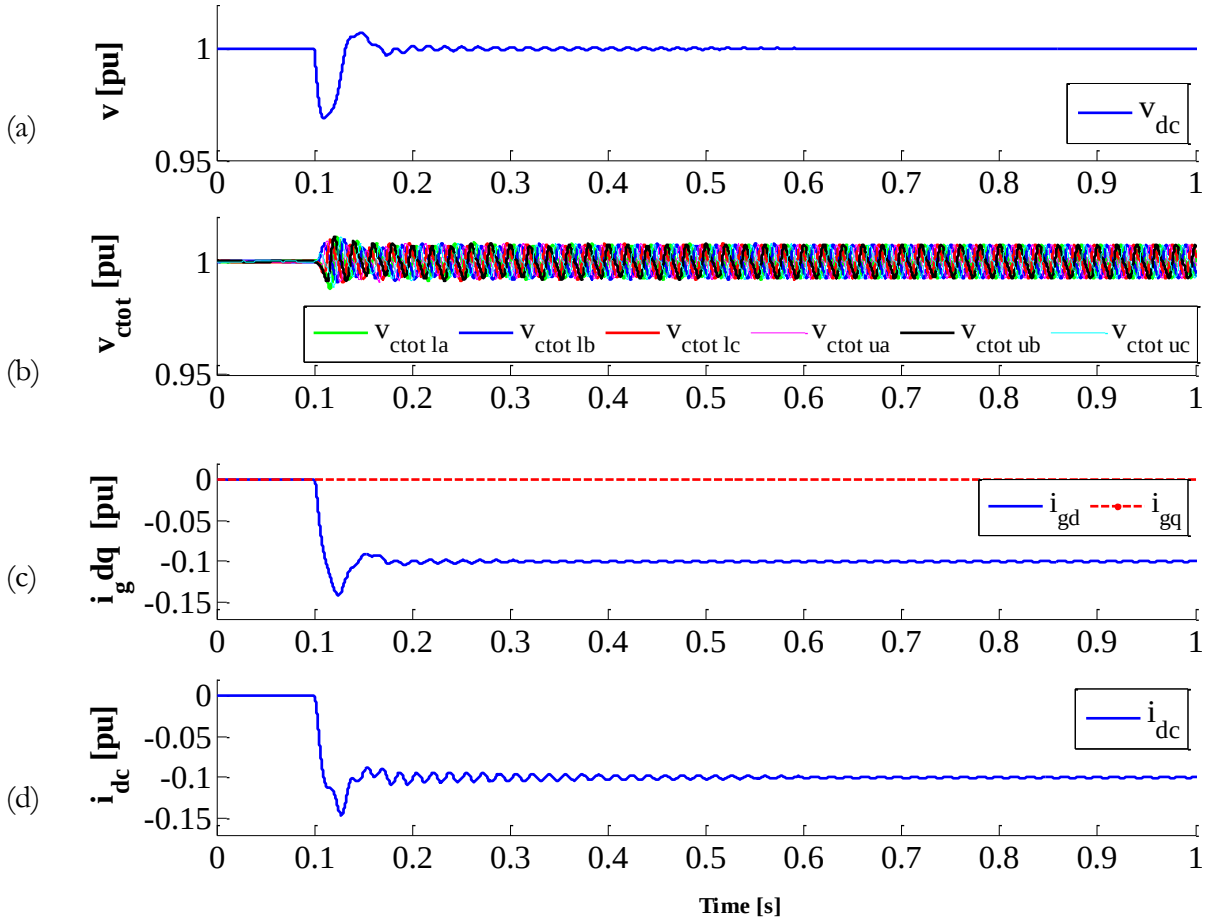

Figure 4-11: Simulation results when DC voltage is controlled by DC Power

Figure 4-11(a) shows that the DC voltage v_{DC} is well controlled at 1 pu. The DC drop

Voltage is as the same as previous control strategy when $S_K = 2$ as shown in Figure 4-9(a). The transient oscillations are related to adjustment of equivalent capacitor voltage per phase since this control strategy is based on control of the total energy stored in the MMC.

Figure 4-11(b), verified that in this control scenario, all equivalent capacitor voltage per arm $(v_{c\,ul\,i\,tot})$ are well controlled around 1 pu

Figure 4-11(c) and (d) show that the grid currents and DC current are well controlled following the step of 0.1 pu on the power.

These simulation results clearly show that when DC voltage is controlled by DC link, it is possible to have a fast dynamic for DC voltage. The DC voltage drop is limited and all MMC state variables are well controlled.

4.4 CONTROL OF AN HVDC LINK

Most of the publications have been focused on the MMC control strategies and in some publications, the proposed control is applied in an HVDC link [81] but they do not explicitly address the two different roles that are held by this converter in an HVDC link: controlling the power or controlling the DC voltage level as discussed in [80].

In addition, the exchange of MMC stored energy and the stored energy in DC-bus is not studied properly yet. The proposed relation between the energy and DC bus voltage has a great role for improving the dynamic behavior of the HVDC link.

It has been observed in this chapter that converter energy control strategy has a great impact on the DC voltage dynamics. The main objective of this section is to obtain a control strategy that can be assumed the stability of DC bus voltage in an HVDC system based on the MMC stations. A simple solution, called CCSC (Circulating Current Suppression Control) [55], already exists but it leads to unwanted oscillations during the transient.

The proposed control before in this chapter is now applied in a two-terminal HVDC system. The studied HVDC link is shown in Figure 4-12. The characteristics of the MMC stations are the same and the characteristics of the cable technology is provided in Table 4-1 (for more details see appendix C)

Table 4-1: The electrical circuit parameters considered for the DC cable[35]

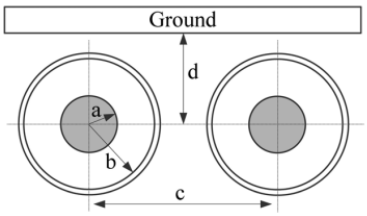

Parameter	Value
Cable length	70 km
Outer radius of sheath	5.82 cm
Outer radius of insulation	6.39 cm
Resistivity of core	$1.72e-8\ \Omega m$
Resistivity of sheath	$2.83e-8\ \Omega mm$
Insulator relative permittivity	2.5
Insulator loss factor	0,0004

As presented in Figure 4-12, the MMC stations have two different roles: Station 1 controls the power flowing into this HVDC link thanks to the reference signal $P_{ac\,1\,ref}$ and station 2 controls the DC voltage level $v_{dc\,2}$. The design of the voltage controller depends on the equivalent capacitor on the DC bus, which is related to the control applied on both stations

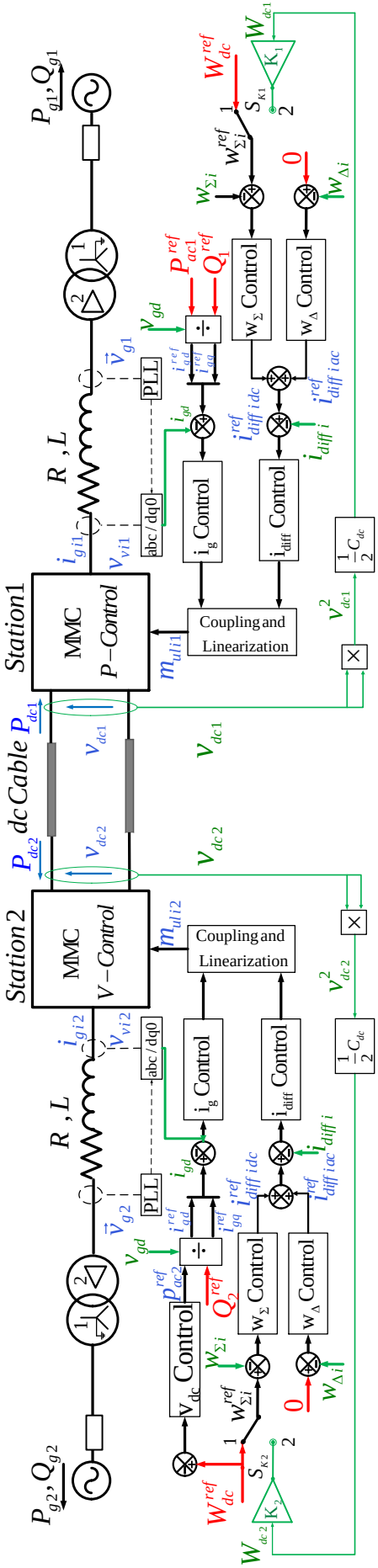

Figure 4-12: Two terminals HVDC studied case based on MMC stations

For both stations, the energy is supposed to be controlled by the DC power. Referring to equation (4.7), two equations may be associated to the converters:

$$\frac{1}{2}C_{DC}\frac{dv_{DC1}^2}{dt}+\langle\frac{1}{2}C_{tot}\left(6\frac{dv_{c1\,tot}^{2\,ref}}{dt}\right)\rangle_T=-p_{AC1}^{ref}+p_{DC2} \tag{4.15}$$

$$\frac{1}{2}C_{DC}\frac{dv_{DC2}^2}{dt}+\langle\frac{1}{2}C_{tot}\left(6\frac{dv_{c2\,tot}^{2\,ref}}{dt}\right)\rangle_T=-p_{AC2}^{ref}+p_{DC1} \tag{4.16}$$

Wherep_{DC1} and p_{DC2} have been substituted to p_l in (4.15) and (4.16) respectively.

Some assumptions are required:

- $v_{DC1}\approx v_{DC2}=v_{DC}$
- $p_{DC2}\approx -p_{DC1}$

Adding (4.15) and (4.16) yields to:

$$C_{DC}\frac{dv_{DC}^2}{dt}+\langle\frac{1}{2}C_{tot}\left(6\frac{dv_{c2\,tot}^{2\,ref}}{dt}\right)\rangle_T+\langle\frac{1}{2}C_{tot}\left(6\frac{dv_{c1\,tot}^{2\,ref}}{dt}\right)\rangle_T=-p_{AC2}^{ref}-p_{AC1}^{ref} \tag{4.17}$$

Depending on the way the energy is managed, this equation may be modified. In the sequel, different solutions are proposed.

- **Case A: Station 1 with ($\mathbf{S_{K1}=1}$) and station 2 with ($\mathbf{S_{K2}=2}$)**

In this case, the $W_{i\,ref}^{\Sigma}$ on the MMC station2 is connected to the DC bus energy W_{DC}.

Hence, only the SM capacitors of station 2 participate in the DC voltage control. Equation (4.17) is adjusted:

$$\frac{1}{2}(6C_{tot\,MMC2}+2C_{DC})\frac{dv_{DC}^2}{dt}=-p_{AC\,2}^{ref}-p_{DC\,1}^{ref} \tag{4.18}$$

Since $W_{tot\,1}^{\Sigma}$ is constant $p_{AC\,1}^{ref}\cong p_{DC\,1}$.

The variation of the DC voltage is considered following a step of 0.1 pu on the active power reference of station 1 $p_{AC\,1}^{ref}$ at t=0.1 s.

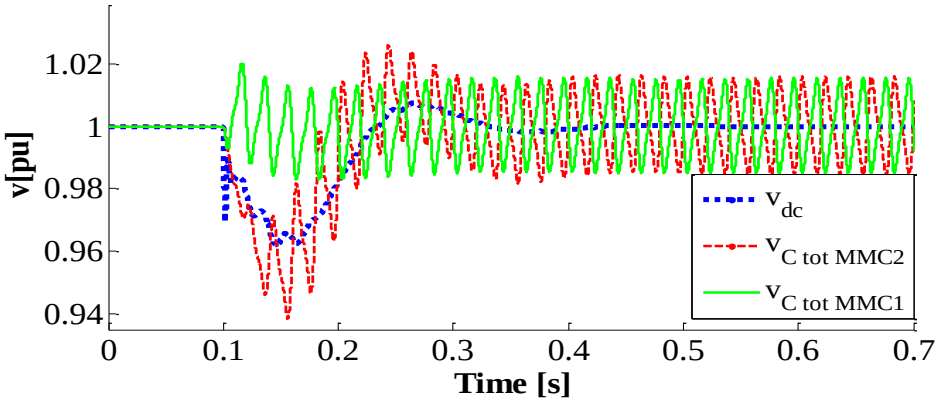

Figure 4-13: Simulation results for Case A: ($\boldsymbol{S_{K1} = 1}, \boldsymbol{S_{K2} = 2}$ with $\boldsymbol{K = 1}$)

Figure 4-13 shows that the v_{ctot_MMC1} is nearly constant, contrary to v_{ctot_MMC2}, which depends on v_{dc} variations.

- **Case B: Station 1 and 2 with ($\mathbf{S_{K1} = S_{K2} = 2}$)and $\mathbf{K = 1}$**

In this case, $W_{i\,ref}^{\Sigma}$ for both stations is connected to the DC bus energy W_{dc} and the SM capacitors of the two MMCs participate in the DC bus control. In this case, application of (4.17)to MMC stations results in:

$$\frac{1}{2}(6C_{tot\,MMC1} + 6C_{tot\,MMC2} + 2\,C_{DC})\frac{dv_{DC}^2}{dt} = -p_{AC\,2}^{ref} - p_{AC\,1}^{ref} \qquad \textbf{(4.19)}$$

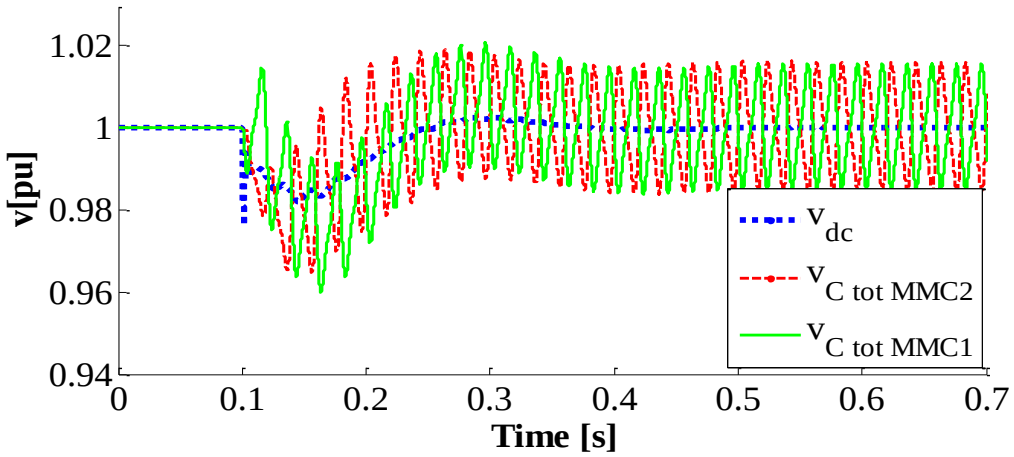

Figure 4-14: Simulation results for Case B: ($\boldsymbol{S_{K1} = 2}, \boldsymbol{S_{K2} = 2}$ with $\boldsymbol{K = 1}$)

Figure 4-14 shows that $v_{ctot\,MMC1}$ and $v_{ctot\,MMC2}$ depend on v_{DC} variations and the stored energy of both converters participate in DC bus voltage regulation. It can be observed that the DC bus voltage drop in this case has been greatly reduced compared with the previous case studied.

- **Case C: Station 1 and 2 with ($S_{K1} = S_{K2} = 2$) and K=1.21**

The idea of providing an exchange of energy between MMC and DC bus can be extended by increasing the MMC stored energy using a larger gain K. The value of the gain is limited to avoid an overvoltage on the SMs. For example, if $K = 1.21$ the steady state voltage is $v_{c\,tot} = 1.1\ pu$ which may be considered as acceptable. DC bus voltage variation in this case is obtained by considering the gain K in (4.20) as:

$$\frac{1}{2}(6KC_{tot\,MMC1} + 6KC_{tot\,MMC2} + 2\,C_{DC})\frac{dv_{DC}^2}{dt} = -p_{AC\,2}^{ref} - p_{AC\,1}^{ref} \quad \textbf{(4.20)}$$

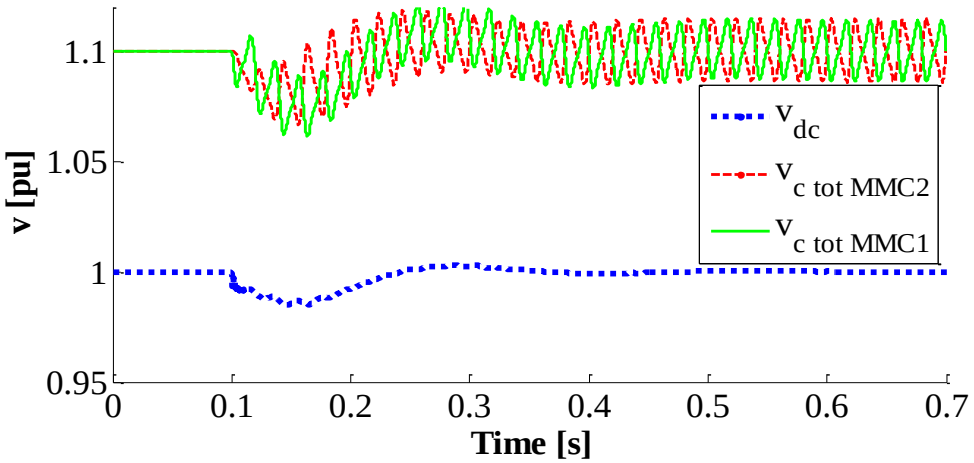

Figure 4-15: Simulation results for Case B: ($S_{K1} = 2, S_{K2} = 2$ with $K = 1.21$)

Figure 4-15, shows that there is more stored energy in MMC as $v_{c\,tot} = 1.1\,pu$, in comparison with the two previous cases. Moreover, a slightly reduced voltage drop can be noticed by increasing the participation of the MMC energy to the voltage regulation.

A comparison between the three studied cases is provided in Figure 4-16.

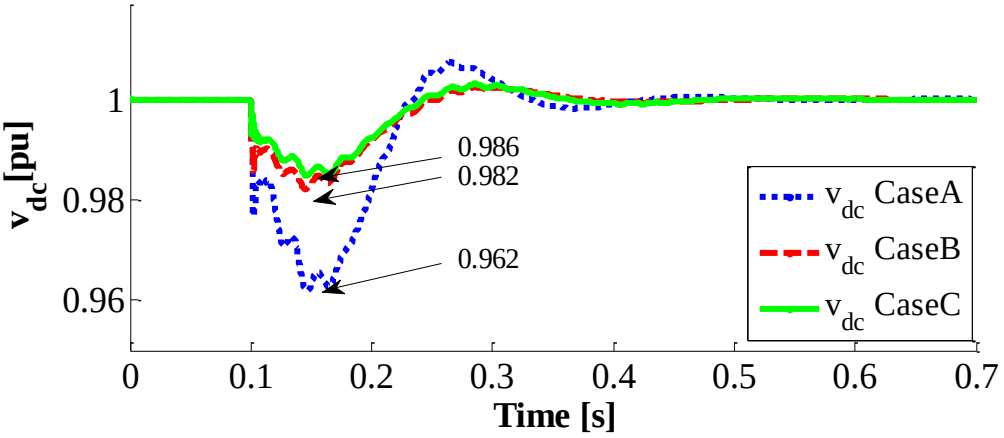

Figure 4-16: Simulation results for comparison of the three cases

In Figure 4-16, it can be seen that the response time is nearly the same since the DC voltage controller has been adjusted based on the DC equivalent capacitor value defined in (4.18), (4.19)and (4.20). Comparing Case A and case B, the DC voltage drop decreased significantly in Case B. As depicted in Fig.14, in case B the DC voltage drop is about 1.8% whereas in case A it is about 3.8%.

Moreover, an additional decrease of DC bus voltage drop can be considered, as shown in case C in Figure 4-16. In case C, when $K = 1.21$ the MMC stored energy increases by 20%, which leads to a DC voltage drop of 1.6%. When comparing Case B and Case C, the DC voltage drop in case C decreases by 20%.

4.5 CONCLUSION

This chapter has presented the modeling of a point-to point HVDC link based on the MMC where the two AC/DC substations have different roles: one station controls the active power flow, the other one provides the DC voltage. The mathematical model for the substation that provides the DC voltage is investigated. The in-depth analysis of the MMC energy based control strategies reveals that the exchange of energy between MMC and DC-bus capacitor depends on the MMC stored control strategy. Regarding to the two main MMC energy based control strategies, the possible control strategy for DC-bus voltage is discussed. The control methods are proposed to assume the stability of the DC bus voltage in an HVDC system based on the MMC stations.

Comparison of an HVDC link based on a classical VSC and an HVDC link based on MMCs, reveals a fundamental difference. Since in case of a classical VSC, the capacitors are directly connected on the DC bus, these storage elements naturally participate in the DC bus voltage stability. Regarding VSC-MMC topology, the storage elements are inside the converter and no direct link exists with the DC bus. In this chapter a control strategy has been proposed to establish a link between the energy stored in the MMC and the DC bus voltage. Then it is compared with the well-known CCSC strategy.

To sum up with the proposed control method the DC bus voltage drop is limited and the transient oscillations are well damped contrary to the CCSC scheme where many oscillations are observed on the DC current due to the uncontrolled energy.

In addition, another control strategy for DC-bus voltage is proposed that enables the application of a fast DC-bus loop. The simulation results demonstrate that the DC-bus voltage with the proposed control is also well controlled.

As conclusion, the matter of this chapter was to bring in the methodological principles on control of the DC-bus voltage in an MMC, in order to improve the dynamic behavior of the MMC-HVDC link.

.

Conclusion

This work aims to assess the "high level" control strategies that provide the desired dynamics of an HVDC transmission. In fact, in this study, the MMC "low level" control is supposed to be ideal. Consequently an equivalent model for the MMC, based on the energy stored in one arm, may be developed. The presented control schemes focus on the MMC power and DC bus voltage control. Their associated control loops are designed and validated for the nominal operating points and the simulations are performed in EMTP^{RV} environment.

Chapter 1 recalls the global principles of the MMC: different MMC topologies and SMs structures, some methodologies for SMs balancing voltage algorithms have been explained. As a step before the "high level control", an equivalent MMC model by considering the average model of each arm is presented. In the last part of chapter 1 different types of high level control strategies studied in the literature are explained briefly.

MMC controls are based on fast inner current loops and outer power or voltage loops. Several methods for the control of the MMC currents: grid currents and differential currents are presented in Chapter 2. The basic control method, which includes the control of the grid currents by a classical dq frame, presents good dynamics performance only for the grid currents and oscillations on the other variables. Then, the well-known CCSC control scheme highlighted a better performance for MMC in steady state values but the transient oscillations on the differential currents shows clearly the lack of control on this currents. From a general point of view, to have a full control of the system, the number of controllers must be equal to the number of independent state variables of the system, it is the reason why other control loops have to be added to this basic propositions. An active control of the differential currents is proposed that shows a good performance for controlling the both MMC inner currents. In addition, the influence of the MMC insert index calculating on the differential currents oscillations is investigated.

In Chapter 3, the principles of MMC energy based control are provided. In the first part of this chapter, different topologies for the MMC energy based model are developed: the sum of energy (W^{Σ}) and difference of energy (W^{Δ}) are defined to facilitate the energy control. This model reveals that the average values of sum of the energy can be controlled either by the DC or grid power. The comparison of both control methodologies demonstrates the exchange of the MMC currents roles in each control has important influence on the MMC dynamics. Several control methods for MMC stored energy are proposed. Comparison of the simulation results highlights that the chosen control may have large influence on the MMC losses.

In Chapter 4, the control of a point-to-point MMC-HVDC link by considering a simple model of a DC cable is investigated. In this topology, contrary to the conventional two or three level VSC-HVDC links, no capacitors are connected directly on the DC bus. Therefore, in such an HVDC link, the DC bus voltage may be much more volatile than in a conventional VSC-HVDC. A solution of an exchange of energy between the stored energy and the DC voltage has been proposed to improve the DC bus voltage stability.

Future works may focus on the following list:

- Study of a MTDC (Multi Terminal DC) grid instead of an HVDC point to point link, since DC bus voltage dynamic and power excursion may be different.
- Assessment of the robustness of control strategies following the AC side balanced or unbalanced faults.
- Improvement of the classical PI controllers. Development of the proposed control strategy by considering advanced controllers for the studied MMC
- Development of the proposed methodology for the design of the control for the MMC based on the Full Bridge SMs.

REFERENCES

[1] Commission of the European Communities, 20 20 by 2020: Europe's Climate Change Opportunity: Communication from the Commission to the European Parliament, the Council, the Economic and Social Committee and the Committee of the Regions. Bruxelles: Official Publications of the European Communities, 2008[Online]. http://eurlex.europa.eu/LexUriServ/LexUriServ.do?uri=CELEX:52008DC0030:EN:HTML:NOT Std.

[2] F. V. H. N. Fichaux, J. Wilkes and C. A., "Oceans of opportunity," *EWEA (European Wind Energy Association), Tech. rep.,*, 2009.

[3] http://en.wikipedia.org/wiki/List_of_HVDC_projects.

[4] W. F. Long, J. Reeve, J. R. McNichol, M. S. Holland, J. P. Taisne, J. LeMay, and D. J. Lorden, "Application aspects of multiterminal dc power transmission," *IEEE Transactions on Power Delivery*, vol. 5, no. 4, pp. 2084–2098, Oct 1990.

[5] R. Adapa, "High-wire act: Hvdc technology: The state of the art," *IEEE Power and Energy Magazine*, vol. 10, no. 6, pp. 18–29, Nov 2012.

[6] S. Cole and R. Belmans, "Transmission of bulk power," *IEEE Industrial Electronics Magazine*, vol. 3, no. 3, pp. 19–24, Sept 2009.

[7] M. Barnes and A. Beddard, ""voltage source converter HVDC links the state of the art and issues going forward," energy procedia, vol. 24, no. 0, pp. 108 – 122, 2012, selected papers from deep sea offshore wind;d conference, trondheim, norway, 19-20 january 2012. [online]. available: http://www.sciencedirect.com/science/article/pii/s1876610212011320."

[8] A. Lesnicar and R. Marquardt, "An innovative modular multilevel converter topology suitable for a wide power range," in *Power Tech Conference Proceedings*, vol. 3, 2003, p. 6.

[9] L. G. Franquelo, J. Rodriguez, J. I. Leon, S. Kouro, R. Portillo, and M. A. M. Prats, "The age of multilevel converters arrives," *IEEE Industrial Electronics Magazine*, vol. 2, no. 2, pp. 28–39, June 2008.

[10] Siemens, HVDC plus – Basics and Principle of Operation,online: http://www.energy.siemens.com/br/pool/br/transmissao-de-energia/transformadores/hvdc-plus-basics-and-principle-of-operation.pdf.

[11] C. W. N. Mahimkar, G. Persson, "Hvdc technology for large scale offshore wind connections," *Smartelec, Vadodara 2013*.

[12] lstom, HVDC-VSC: transmission technology of the future, online:http://www.tresamigasllc.com/docs/ThinkGrid08-06-Chapter1-Art1%20VSC_EN.pdf.

[13] S. N. H.-P. A. H. D. V. H. L. Z. H. L. A., Noman; N., "Hvdc supergrids with modular multilevel converters — the power transmission backbone of the future," *Systems, Signals and Devices (SSD), 2012 9th International Multi-Conference on*, March 2012.

[14] L. Vasiladiotis, M.Angquist, A. Antonopoulos, D. Siemaszko, K. Ilves, and H.-P. Nee, "Inner control of modular multilevel converters-an approach using open-loop estimation of stored energy," in *Power Electronics Conference (IPEC), 2010 International*. IEEE, 2010, pp. 1579–1585. [Online]. Available: http://ieeexplore.ieee.org/xpls/abs_all.jsp?arnumber=5544607

[15] L. Angquist, A. Antonopoulos, D. Siemaszko, K. Ilves, M. Vasiladiotis, and H.-P. Nee, "Open-loop control of modular multilevel converters using estimation of stored energy," *Industry Applications, IEEE Transactions on*, vol. 47, no. 6, pp. 2516–2524, 2011. [Online]. Available: http://ieeexplore.ieee.org/xpls/abs_all.jsp?arnumber=6022768

[16] J. R. S. K. R. L. M. A. Perez, S. Bernet, "Circuit topologies, modeling, control schemes, and applications of modular multilevel converters," vol. 30, no. 1, pp. 4–17, 2015. [Online]. Available: http://ieeexplore.ieee.org/stamp/stamp.jsp?arnumber=6757004

[17] A. Delavari, I. Kamwa, and A. Zabihinejad, "A comparative study of different multilevel converter topologies for high power photovoltaic applications," in *2016 7th Power Electronics and Drive Systems Technologies Conference (PEDSTC)*, Feb 2016, pp. 415–420.

[18] N. Ahmed, A. Haider, D. V. Hertem, L. Zhang, and H. P. Nee, "Prospects and challenges of future hvdc supergrids with modular multilevel converters," in *Power Electronics and Applications (EPE 2011), Proceedings of the 2011-14th European Conference on*, Aug 2011, pp. 1–10.

[19] S. Allebrod, R. Hamerski, and R. Marquardt, "New transformerless, scalable modular multilevel converters for hvdc-transmission," in *Power Electronics Specialists Conference, 2008. PESC 2008. IEEE*. IEEE, 2008, pp. 174–179.

[20] M. Winkelnkemper, A. Korn, and P. Steimer, "A modular direct converter for transformerless rail interties," in *Industrial Electronics (ISIE), 2010 IEEE International Symposium on*. IEEE, 2010, pp. 562–567.

[21] R. Marquardt, "Modular multilevel converter: An universal concept for hvdc-networks and extended dc-bus-applications," in *Power Electronics Conference (IPEC), 2010 International*. IEEE, 2010, pp. 502–507.

[22] F. Z. Peng, J.-S. Lai, J. W. McKeever, and J. VanCoevering, "A multilevel voltage-source inverter with separate dc sources for static var generation," *Industry Applications, IEEE Transactions on*, vol. 32, no. 5, pp. 1130–1138, 1996.

[23] A. S.-S. A. M. for a Modular Multilevel Converter, "A steady-state analysis method for a modular multilevel converter," vol. 28, no. 8, pp. 3702–3713, 2013. [Online]. Available: http://-ieeexplore.ieee.org/stamp/stamp.jsp?arnumber=6353957

[24] S. Kouro, R. Bernal, H. Miranda, C. Silva, and J. Rodriguez, "High-performance torque and flux control for multilevel inverter fed induction motors," *Power Electronics, IEEE Transactions on*, vol. 22, no. 6, pp. 2116–2123, Nov 2007.

[25] L. Baruschka and A. Mertens, "A new three-phase ac/ac modular multilevel converter with six branches in hexagonal configuration," *Industry Applications, IEEE Transactions on*, vol. 49, no. 3, pp. 1400–1410, 2013.

[26] F. Kammerer, J. Kolb, and M. Braun, "Fully decoupled current control and energy balancing of the modular multilevel matrix converter," in *Power Electronics and Motion Control Conference (EPE/PEMC), 2012 15th International*, Sept 2012, pp. LS2a.3–1–LS2a.3–8.

[27] C. Gao, J. Jiang, X. Yang, L. Xie, and K. Cao, "A novel topology and control strategy of modular multilevel converter (mmc)," in *Proc. Int Electrical and Control Engineering (ICECE) Conf*, 2011, pp. 967–971. [Online]. Available: http://ieeexplore.ieee.org/stamp/-stamp.jsp?arnumber=6057270

[28] M. Merlin, T. C. Green, P. D. Mitcheson, D. R. Trainer, R. Critchley, W. Crookes, and F. Hassan, "The alternate arm converter: A new hybrid multilevel converter with dc-fault blocking capability," *Power Delivery, IEEE Transactions on*, vol. 29, no. 1, pp. 310–317, 2014.

[29] Y. Kui Wang, "Voltage balancing and fluctuation-suppression methods of floating capacitors in a new modular multilevel converter," vol. 60, no. 5, pp. 1943–1954, 2013. [Online]. Available: http://ieeexplore.ieee.org/stamp/stamp.jsp?arnumber=6208867

[30] N. Thitichaiworakorn, M. Hagiwara, and H. Akagi, "Experimental verification of a modular multilevel cascade inverter based on double-star bridge cells," *IEEE Transactions on Industry Applications*, vol. 50, no. 1, pp. 509–519, Jan 2014.

[31] P. S. Jones and C. C. Davidson, "Calculation of power losses for mmc-based vsc hvdc stations," in *Power Electronics and Applications (EPE), 2013 15th European Conference on*, Sept 2013, pp. 1–10.

[32] M. Glinka and R. Marquardt, "A new ac/ac multilevel converter family," *IEEE Transactions on Industrial Electronics*, vol. 52, no. 3, pp. 662–669, June 2005.

[33] A. Nami, L. Wang, F. Dijkhuizen, and A. Shukla, "Five level cross connected cell for cascaded converters," in *European Power Electronics and Applications Conference (EPE), Lille, France*, 2013.

[34] www.siemens.com/press/...ultranet/presentation-ultranet-e.pdf.

[35] H. Saad, S. Dennetière, J. Mahseredjian, P. Delarue, X. Guillaud, J. Peralta, and S. Nguefeu, "Modular multilevel converter models for electromagnetic transients," *Power Delivery, IEEE Transactions on*, vol. 29, no. 3, pp. 1481–1489, 2014.

[36] J. Peralta, H. Saad, S. Dennetière, J. Mahseredjian, and S. Nguefeu, "Detailed and averaged models for a 401-level mmc–hvdc system," *Power Delivery, IEEE Transactions on*, vol. 27, no. 3, pp. 1501–1508, 2012. [Online]. Available: http://ieeexplore.ieee.org/xpls/-abs_all.jsp?arnumber=6178298

[37] U. Gnanarathna, A. Gole, and R. Jayasinghe, "Efficient modeling of modular multilevel hvdc converters (mmc) on electromagnetic transient simulation programs," *Power Delivery, IEEE Transactions on*, vol. 26, no. 1, pp. 316–324, Jan 2011.

[38] H. Saad, S. Dennetière, and J. Mahseredjian, "On modelling of mmc in emt-type program," in *2016 IEEE 17th Workshop on Control and Modeling for Power Electronics (COMPEL)*, June 2016, pp. 1–7.

[39] J. G. Slootweg, H. Polinder, and W. L. Kling, "Representing wind turbine electrical generating systems in fundamental frequency simulations," *IEEE Transactions on Energy Conversion*, vol. 18, no. 4, pp. 516–524, Dec 2003.

[40] S. P. Teeuwsen, "Simplified dynamic model of a voltage-sourced converter with modular multilevel converter design," in *Power Systems Conference and Exposition, 2009. PSCE '09. IEEE/PES*, March 2009, pp. 1–6.

[41] M. Hagiwara, R. Maeda, and H. Akagi, "Control and analysis of the modular multilevel cascade converter based on double-star chopper-cells (mmcc-dscc)," *IEEE Transactions on Power Electronics*, vol. 26, no. 6, pp. 1649–1658, June 2011.

[42] X. Li, Q. Song, J. Li, and W. Liu, "Capacitor voltage balancing control based on cps-pwm of modular multilevel converter," in *2011 IEEE Energy Conversion Congress and Exposition*, Sept 2011, pp. 4029–4034.

[43] L. G. Franquelo, J. Rodriguez, J. I. Leon, S. Kouro, R. Portillo, and M. A. M. Prats, "The age of multilevel converters arrives," *IEEE Industrial Electronics Magazine*, vol. 2, no. 2, pp. 28–39, June 2008.

[44] A. Lesnicar and R. Marquardt, "An innovative modular multilevel converter topology suitable for a wide power range," in *Power Tech Conference Proceedings, 2003 IEEE Bologna*, vol. 3, June 2003, pp. 6 pp. Vol.3–.

[45] A. Hassanpoor, L. Ängquist, S. Norrga, K. Ilves, and H. P. Nee, "Tolerance band modulation methods for modular multilevel converters," *IEEE Transactions on Power Electronics*, vol. 30, no. 1, pp. 311–326, Jan 2015.

[46] H. Saad, X. Guillaud, J. Mahseredjian, S. Dennetière, and S. Nguefeu, "Mmc capacitor voltage decoupling and balancing controls," in *2015 IEEE Power Energy Society General Meeting*, July 2015, pp. 1–1.

[47] Q. Tu and Z. Xu, "Impact of sampling frequency on harmonic distortion for modular multilevel converter," *IEEE Transactions on Power Delivery*, vol. 26, no. 1, pp. 298–306, Jan 2011.

[48] A. Antonopoulos, L. Angquist, and H.-P. Nee, "On dynamics and voltage control of the modular multilevel converter," in *Proc. 13th European Conf. Power Electronics and Applications EPE '09*, 2009, pp. 1–10. [Online]. Available: http://ieeexplore.ieee.org/stamp/-stamp.jsp?arnumber=5278794

[49] K. Ilves, A. Antonopoulos, S. Norrga, and H.-P. Nee, "Steady-state analysis of interaction between harmonic components of arm and line quantities of modular multilevel converters," *Power Electronics, IEEE Transactions on*, vol. 27, no. 1, pp. 57–68, Jan 2012.

[50] Y. Zhang, Q. Ge, R. Zhang, Y. Du, , . K. L. of Power ElectronicsElectric Drive, I. of Electrical Engineering, and C. A. of Sciences, "The control of arm currents and the parameters for modular multilevel converters."

[51] J. Qin and M. Saeedifard, "Predictive control of a modular multilevel converter for a back-to-back HVDC system," vol. 27, no. 3, pp. 1538–1547, 2012. [Online]. Available: http://-ieeexplore.ieee.org/stamp/stamp.jsp?arnumber=6192340

[52] M. H. M. I. Hirofumi Akagi, Fellow IEEE, "Control and experiment of pulsewidth-modulated modular multilevel converters," 2009.

[53] Q. Tu, Z. Xu, and J. Zhang, "Circulating current suppressing controller in modular multilevel converter," in *IECON 2010 - 36th Annual Conference on IEEE Industrial Electronics Society*, Nov 2010, pp. 3198–3202.

[54] Q. Tu, Z. Xu, and L. Xu, "Reduced switching-frequency modulation and circulating current suppression for modular multilevel converters," *Power Delivery, IEEE Transactions on*, vol. 26, no. 3, pp. 2009–2017, 2011. [Online]. Available: http://ieeexplore.ieee.org/xpls/-abs_all.jsp?arnumber=5740974

[55] L. Harnefors, A. Antonopoulos, S. Norrga, L. Angquist, and H. Nee, "Dynamic analysis of modular multilevel converters," 2012. [Online]. Available: http://ieeexplore.ieee.org/xpls/-abs_all.jsp?arnumber=6185665

[56] M. Akaji, Hagiwara and H. Maeda, Ryo, "Control and analysis of the modular multilevel cascade converter based on double-star chopper-cells (mmcc-dscc)," *Power Electronics, IEEE Transactions on*, vol. 26, no. 6, pp. 1649–1658, 2011. [Online]. Available: http://-ieeexplore.ieee.org/xpls/abs_all.jsp?arnumber=5605667

[57] Q. Tu, Z. Xu, Y. Chang, and L. Guan, "Suppressing dc voltage ripples of mmc-hvdc under unbalanced grid conditions," *IEEE Transactions on Power Delivery*, vol. 27, no. 3, pp. 1332–1338, July 2012.

[58] J. W. Moon, C. S. Kim, J. W. Park, D. W. Kang, and J. M. Kim, "Circulating current control in mmc under the unbalanced voltage," *IEEE Transactions on Power Delivery*, vol. 28, no. 3, pp. 1952–1959, July 2013.

[59] P. Delarue, F. Gruson, and X. Guillaud, "Energetic macroscopic representation and inversion based control of a modular multilevel converter," in *Power Electronics and Applications (EPE), 2013 15th European Conference on*. IEEE, 2013, pp. 1–10.

[60] G. Bergna, A. Garces, E. Berne, P. Egrot, A. Arzandé, J.-C. Vannier, and M. Molinas, "A generalized power control approach in abc frame for modular multilevel converter hvdc links based on mathematical optimization," *Power Delivery, IEEE Transactions on*, vol. 29, no. 1, pp. 386–394, 2014.

[61] G. B. Egrot, Diaz, Berne, P. Lefranc, A. Arzandé, J.-C. Vannier, M. Molinas *et al.*, "An energy-based controller for hvdc modular multilevel converter in decoupled double synchronous reference frame for voltage oscillations reduction," no. 99, 2012. [Online]. Available: http://-hal.archives-ouvertes.fr/hal-00764809/

[62] S. Samimi, P. Delarue, F. Gruson, and X. Guillaud, "Control of dc bus voltage with a modular multilevel converter," in *PowerTech., 2015 IEEE Eindhoven*. IEEE, 2015.

[63] B. S. Riar, T. Geyer, and U. K. Madawala, "Model predictive direct current control of modular multi-level converters," in *Industrial Technology (ICIT), 2013 IEEE International Conference on*, Feb 2013, pp. 582–587.

[64] M. Vatani, B. Bahrani, M. Saeedifard, and M. Hovd, "Indirect finite control set model predictive control of modular multilevel converters," *IEEE Transactions on Smart Grid*, vol. 6, no. 3, pp. 1520–1529, May 2015.

[65] G. Bergna, J. A. Suul, A. Garcés, E. Berne, P. Egrot, A. Arzandé, J. C. Vannier, and M. Molinas, "Improving the dynamics of lagrange-based mmc controllers by means of adaptive filters for single-phase voltage, power and energy estimation," in *Industrial Electronics Society, IECON 2013 - 39th Annual Conference of the IEEE*, Nov 2013, pp. 6239–6244.

[66] E. Rakhshani, A. M. Cantarellas, D. Remon, P. Rodriguez, and I. Candela, "Modeling and control of multi modular converters using optimal lqr controller with integral action," in *2013 IEEE Energy Conversion Congress and Exposition*, Sept 2013, pp. 3965–3970.

[67] A. G. Hans Barnklau and J. Rudolph, "A model-based control scheme for modular multilevel converters," vol. 60, no. 12, pp. 5359–5375, 2013. [Online]. Available: http://-ieeexplore.ieee.org/stamp/stamp.jsp?arnumber=6399588

[68] R. Cisneros, R. Ortega, M. Pirro, G. Ippoliti, G. Bergna, and M. M. Cabrera, "Global tracking passivity-based pi control for power converters: An application to the boost and modular multilevel converters," in *2014 IEEE 23rd International Symposium on Industrial Electronics (ISIE)*, June 2014, pp. 1359–1365.

[69] P. Münch, D. Görges, M. Izák, and S. Liu, "Integrated current control, energy control and energy balancing of modular multilevel converters," in *IECON 2010 - 36th Annual Conference on IEEE Industrial Electronics Society*, Nov 2010, pp. 150–155.

[70] L. Harnefors, A. Antonopoulos, K. Ilves, and H. P. Nee, "Global asymptotic stability of current-controlled modular multilevel converters," *IEEE Transactions on Power Electronics*, vol. 30, no. 1, pp. 249–258, Jan 2015.

[71] *Global asymptotic stability of modular multilevel converters with measurement lag and circulating-current control*, 2013. [Online]. Available: http://ieeexplore.ieee.org/stamp/stamp.jsp?arnumber=6634453

[72] G. B. Diaz, "Modoular multilevel converter control for hvdc operation," Ph.D. dissertation, Centrale Supélec & Norwegian Unversity of Science and Technology, 2015.

[73] M. Vatani, M. Hovd, and M. Saeedifard, "Control of the modular multilevel converter based on a discrete-time bilinear model using the sum of squares decomposition method," *IEEE Transactions on Power Delivery*, vol. 30, no. 5, pp. 2179–2188, Oct 2015.

[74] J. Mahseredjian, S. Dennetière, L. Dubé, B. Khodabakhchian, and L. Gérin-Lajoie, "On a new approach for the simulation of transients in power systems," *Electric Power Systems Research*, vol. 77, no. 11, pp. 1514–1520, 2007.

[75] H. Saad, "Modelisation et simulation d'un liason hvdc de type vsc-mmc," Ph.D. dissertation, Ecole Polytechnique de Motreal, 2015.

[76] S. Rohner, S. Bernet, M. Hiller, and R. Sommer, "Modelling, simulation and analysis of a modular multilevel converter for medium voltage applications," in *Industrial Technology (ICIT), 2010 IEEE International Conference on*, March 2010, pp. 775–782.

[77] S. Li, X. Wang, Z. Yao, T. Li, and Z. Peng, "Circulating current suppressing strategy for mmc-hvdc based on nonideal proportional resonant controllers under unbalanced grid conditions," *IEEE Transactions on Power Electronics*, vol. 30, no. 1, pp. 387–397, Jan 2015.

[78] Y. Li, "Arm inductance and sub-module capacitance selection in modular multilevel converter," Master's thesis, University of Tennessee, 2013.

[79] M. M. Belhaouane, H. Saad, and X. Guillaud, "Control and performance of modular multilevel converters currents using resonant controller," in *IECON 2014 - 40th Annual Conference of the IEEE Industrial Electronics Society*, Oct 2014, pp. 4575–4581.

[80] G. Bergna, M. Boyra, and J. Vivas, "Evaluation and proposal of mmc-hvdc control strategies under transient and steady state conditions," in *Power Electronics and Applications (EPE 2011), Proceedings of the 2011-14th European Conference on*, vol. 30. IEEE, 2011, pp. 1–10.

[81] F. Xu, Z. Xu, H. Zheng, G. Tang, and Y. Xue, "A tripole hvdc system based on modular multilevel converters," *Power Delivery, IEEE Transactions on*, vol. 29, no. 4, pp. 1683–1691, 2014.

APPENDICES

A. CONTROLLER TUNING

A.1. Current controller tuning

The PI current controller has following form:

$$C_i(s) = k_{p_i} + \frac{k_{i_i}}{s} \tag{A.1}$$

The current controller in the dq frame, presented in Chapter 1 part 1.3.1 is arranged as the d-axis and q-axis are fully decoupled. The transfer function of the current control is the same for both axes, the d-axis current control loop transfer function is given:

$$\frac{i_{s_d}}{i_{s_d}^*}(s) = \frac{1 + \frac{k_{p_i}}{k_{i_i}} s}{1 + \frac{k_{p_i} + R_s}{k_{i_i}} s + \frac{L_s}{k_{i_i}} s^2} \tag{A.2}$$

PI controllers are tuned considering the pole placement method, the denominator of this transfer function is compared to a desired characteristic equation whose the dynamics are known:

$$P(s) = 1 + \frac{2\zeta}{\omega_n} s + \frac{1}{\omega_n^2} s^2 \tag{A.3}$$

Where:

ζ Is the damping ratio

ω_n Is the natural frequency [rad/s]

A step response of this second order polynomial is presented in Figure A-1 for two damping values and for desired response time at 5 % of 1 s, i.e. the system output must enter between bounds of ±5 % of the final value one second after the input step. The damping ratio defines the overshoot while the natural frequency is about dynamics. There is second order abacus which enables to find the natural frequency as function to the desired response time at 5% and a damping ratio. Typically, the value of damping ratio is set at 0.7 to achieve a 5% overshoot and at 1 to have no overshoot. For these values, the natural frequency is obtained by:

$$\begin{aligned} \omega_n &= \frac{3}{t_{r_i 5\%}} \quad if\ \zeta = 0.7 \\ \omega_n &= \frac{5}{t_{r_i 5\%}} \quad if\ \zeta = 1 \end{aligned} \tag{A.4}$$

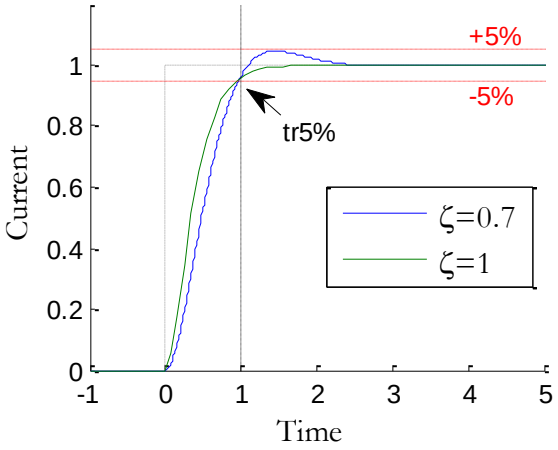

Figure A-1 : Step response for different damping values and same response time

The controller parameters are tuned for the current transfer function characteristic polynomial to fit the desired polynomial:

$$k_{i_i} = L_s \omega_n^2 \tag{A.5}$$

$$k_{p_i} = 2\zeta\omega_n L_s - R \tag{A.6}$$

A.2. Power controller tuning

The PI power controller has following form:

$$C_p(s) = k_{p_p} + \frac{k_{i_p}}{s} \tag{A.7}$$

To tune the power controller, it is considered that the response time of the power control loops is set at least ten times slower than those of current control loops, so current control loops dynamics can be neglected and replaced by a simple unitary gain. In these conditions, the power control loop presented in Chapter 1 part 1.3.2 can be defined by the following transfer function:

$$\frac{p_g}{p_g^*}(s) = \frac{1 + \frac{k_{p_p}}{k_{i_p}} s}{1 + \frac{1 + k_{p_p}}{k_{i_p}} s} \tag{A.8}$$

This transfer function can be assimilated at a first order transfer function of time constant τ_p. Controller parameters are tuned to achieve a desired response time:

$$k_{i_p} = \frac{1}{\tau_p} \tag{A.9}$$

$$k_{p_p} = 0 \tag{A.10}$$

A.3. Voltage controller tuning

The PI DC voltage controller has following form:

$$C_v(s) = k_{p_v} + \frac{k_{i_v}}{s} \tag{A.11}$$

Similarly to the power control, the dynamics of the DC voltage control loop must be at least ten times slower than current control loop dynamics to avoid interactions between both control loops. Once the dynamics of current control loop is neglected, the voltage control loop presented in Chapter 1 part 1.3.3 and considering an IP controller (see Figure 2–7b in Chapter 2 part 2.2.3) can be defined by the following transfer function:

$$\frac{u_s}{u_s^*}(s) = \frac{1}{1 + \frac{k_{p_v}}{k_{i_v}} s + \frac{C_s}{k_{i_v}} s^2} \tag{A.12}$$

The controller parameters are tuned for the voltage transfer function characteristic polynomial to fit the desired second order polynomial:

$$k_{i_v} = C_s \omega_n^2 \tag{A.13}$$

$$k_{p_v} = 2\zeta \omega_n C_s \tag{A.14}$$

A.4. PLL tuning

The rotating frame is synchronized with the AC voltage phasor at the point of common coupling. At this node, the three phase voltages may be written as:

$$\begin{aligned} v_{g_a}(t) &= V_g\sqrt{2}\, sin(\delta_g) \\ v_{g_b}(t) &= V_g\sqrt{2}\, sin(\delta_g - {}^{2\pi}/_{3}) \\ v_{g_c}(t) &= V_g\sqrt{2}\, \sin(\delta_g - {}^{4\pi}/_{3}) \\ \delta_g &= \omega t \end{aligned} \tag{A.15}$$

The Phase Lock Loop (PLL) enables retrieving the voltage phase angle (δ_g). To this purpose, Figure A-2 recalls the classical arrangement of a synchronous reference frame PLL, where the q component is controlled at zero.

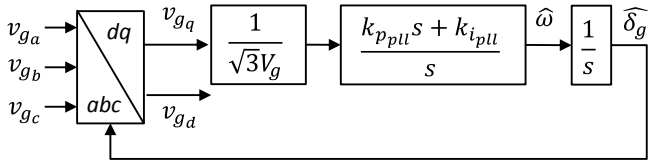

Figure A-2 : Synchronous reference frame PLL scheme

The PLL response time can be obtained by linearizing the relationship between the estimated angle ($\widehat{\delta_g}$) and the exact voltage angle (δ_g). The following transfer function is easily found:

$$\frac{\Delta\widehat{\delta_g}}{\Delta\delta_g} = \frac{1 + \frac{k_{p_{pll}}}{k_{i_{pll}}} s}{1 + \frac{k_{p_{pll}}}{k_{i_{pll}}} s + \frac{1}{k_{i_{pll}}} s^2} \tag{A.16}$$

The controller parameters are tuned for the PLL transfer function characteristic polynomial to fit the desired second order polynomial:

$$k_{i_{pll}} = \omega_n^2 \quad \textbf{(A.17)}$$

$$k_{p_{pll}} = 2\zeta\omega_n \quad \textbf{(A.18)}$$

B. HVDC PERUNIT SYSTEM

In the power system analysis field of electrical engineering, a per-unit system is the expression of system quantities as fractions of a defined base unit quantity. Per unit in AC domain is quite familiar. Since MMC is a mixed of AC and DC variables the per unit definitions are complex as there are different approaches. This paragraph is provided to clear the difference between different per unit notions in an MMC.

HVDC Parameters – BASE VALUES

$$S_b = 1\times10^9[\text{VA}]$$
$$\text{power factor} = \cos(\phi_n) = 1$$
$$P_b = S_b\cos(\phi_n) = 1\times10^9[W]$$
$$U_{1n} = 320\times10^3[kV]$$
$$V_b = V_{1n} = \frac{U_{1n}}{\sqrt{3}}[V]$$
$$f_b = 50[\text{Hz}]$$
$$\omega_b = 2\pi f_b[{}^{rad}/_{s}]$$
$$V_{dcb} = 640\times10^3[V]$$

AC Side Values

$$I_b = \frac{S_b}{3V_b} = \frac{S_b}{\sqrt{3}U_{1n}}[\text{A}]$$
$$Z_b = \frac{V_b}{I_b} = \frac{3V_b{}^2}{S_b}[\Omega]$$
$$L_b = \frac{Z_b}{\omega_b}[\text{H}]$$
$$C_b = \frac{1}{Z_b\omega_b}[\text{F}]$$

DC Side Values

$$I_{dcb} = \frac{P_b}{V_{dcb}}[\mathrm{A}]$$

$$R_{dcb} = \frac{V_{dcb}}{I_{dcb}}[\Omega]$$

$$\rightarrow H_{C^*} = \frac{1}{2} C^* \frac{{V_{dcb}}^2}{P_n}[s]$$

$$\rightarrow H_{L^*} = \frac{1}{2} L^* \frac{{I_{dcb}}^2}{P_n}[s]$$

DQ Values :

$$v_{sd\ nom} = \sqrt{3} V_{sn}$$

$$i_{sd\ nom} = \sqrt{3} I_{sn}$$

$$V_{b\,dq} = \sqrt{3} V_{sn} = \sqrt{3} V_b$$

$$I_{b\,dq} = \sqrt{3} I_{sn} = \sqrt{3} I_b$$

$$V_{b\,dq} I_{b\,dq} = 3\, V_{sn}\ I_{sn} = S_b$$

$$p = v_{gd} i_{gd} + v_{gq} i_{gq}$$

$$p_{pu} S_b = v_{gd\ pu} V_{b\,dq} i_{gd\ pu} I_{b\,dq} + v_{gq} V$$

If considered: $\boldsymbol{V_{dcb} = 2U_{1n} = 2\sqrt{3}V_b}$ **:**

$$I_{dcb} = \frac{P_b}{V_{dcb}} = \frac{S_b \cos(\phi)}{2U_{1n}} = \frac{S_b \cos(\phi)}{V_b 2\sqrt{3}} = \frac{3 I_b \cos(\phi)}{2\sqrt{3}} = \frac{\sqrt{3} I_b \cos(\phi)}{2}[\mathrm{A}]$$

$$R_{dcb} = \frac{2\sqrt{3} V_b}{\frac{\sqrt{3} I_b \cos(\phi)}{2}} = \frac{4 V_b}{I_b \cos(\phi)} = \frac{4 Z_b}{\cos(\phi)}[\Omega]$$

If $\cos(\phi) = 1$,

$$I_{dcb} = \frac{\sqrt{3} I_b}{2}[\mathrm{A}]$$

$$R_{dcb} = 4 Z_b[\Omega]$$

EXEMPLE of a RLC

The above equations can be applied in a RLC circuit**:**

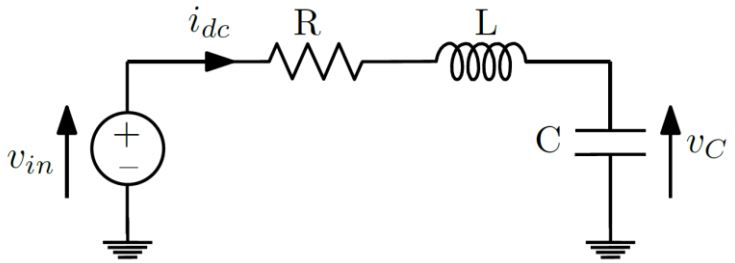

State Space representation in SI:

$$L\frac{di_{dc}}{dt} = v_{in} - Ri_{dc} - v_C$$

$$C\frac{dv_C}{dt} = i_{dc}$$

$$\begin{bmatrix} \dot{v}_C \\ \dot{i}_{dc} \end{bmatrix} = \begin{bmatrix} 0 & \frac{1}{C} \\ -\frac{1}{L} & -\frac{R}{L} \end{bmatrix} \begin{bmatrix} v_C \\ i_{dc} \end{bmatrix} + \begin{bmatrix} 0 \\ -\frac{1}{L} \end{bmatrix} v_{in}$$

$$\begin{bmatrix} v_C \\ i_{dc} \end{bmatrix} = \begin{bmatrix} 1 & 0 \\ 0 & 1 \end{bmatrix} \begin{bmatrix} v_C \\ i_{dc} \end{bmatrix} + \begin{bmatrix} 0 \\ 0 \end{bmatrix} v_{in}$$

Per unit :

$$C_{pu}C_bV_{dcb}\frac{dv_{C,pu}}{dt} = i_{dc,pu}I_{dcb}$$

$$\rightarrow C_b = \frac{1}{Z_b\omega_b}[\mathrm{F}]; R_{dcb} = \frac{V_{dcb}}{I_{dcb}} = 4Z_b[\Omega]$$

$$C_{pu}\frac{1}{Z_b\omega_b}\frac{V_{dcb}}{I_{dcb}}\frac{dv_{C,pu}}{dt} = i_{dc,pu}$$

$$C_{pu}\frac{4}{\omega_b}\frac{dv_{C,pu}}{dt} = i_{dc,pu}$$

So,

$$\frac{L_{pu}}{4\omega_b}\frac{di_{dc,pu}}{dt} = v_{in,pu} - R_{pu}i_{dc,pu} - v_{C,pu}$$

$$\frac{4C_{pu}}{\omega_b}\frac{dv_{C,pu}}{dt} = i_{dc,pu}$$

$$LI_{dcb}\frac{di_{dc,pu}}{dt} = v_{in,pu}V_{dcb} - R_{pu}R_{dcb}I_{dcb}i_{dc,pu} - v_{C,pu}V_{dcb}$$

$$2H_L\frac{P_{dcb}}{I_{dcb}I_{dcb}}\frac{I_{dcb}}{V_{dcb}}\frac{di_{dc,pu}}{dt} = v_{in,pu} - R_{pu}i_{dc,pu} - v_{C,pu}$$

$$2H_L\frac{di_{dc,pu}}{dt} = v_{in,pu} - R_{pu}i_{dc,pu} - v_{C,pu}$$

$$2H_C\frac{P_{dcb}}{V_{dcb}V_{dcb}}\frac{V_{dcb}}{I_{dcb}}\frac{dv_{C,pu}}{dt} = i_{dc,pu}$$

$$2H_C\frac{dv_{C,pu}}{dt} = i_{dc,pu}$$

So,

$$2H_L\frac{di_{dc,pu}}{dt} = v_{in,pu} - R_{pu}i_{dc,pu} - v_{C,pu}$$

$$2H_C\frac{dv_{C,pu}}{dt} = i_{dc,pu}$$

$$\begin{bmatrix}\dot{v}_{C,pu}\\ \dot{i}_{dc,pu}\end{bmatrix} = \begin{bmatrix}0 & \frac{1}{2H_C}\\ -\frac{1}{2H_L} & -\frac{R_{pu}}{2H_L}\end{bmatrix}\begin{bmatrix}v_{C,pu}\\ i_{dc,pu}\end{bmatrix} + \begin{bmatrix}0\\ -\frac{1}{2H_L}\end{bmatrix}v_{in,pu}$$

$$\begin{bmatrix}v_{C,pu}\\ i_{dc,pu}\end{bmatrix} = \begin{bmatrix}1 & 0\\ 0 & 1\end{bmatrix}\begin{bmatrix}v_{C,pu}\\ i_{dc,pu}\end{bmatrix} + \begin{bmatrix}0\\ 0\end{bmatrix}v_{in,pu}$$

Per unit – in case of $V_{dcb} = 2U_{1n} = 2\sqrt{3}V_b$:

$$L_{pu}L_bI_{dcb}\frac{di_{dc,pu}}{dt} = v_{in,pu}V_{dcb} - R_{pu}R_{dcb}I_{dcb}i_{dc,pu} - v_{C,pu}V_{dcb}$$

$$L_{pu}L_b\frac{I_{dcb}}{V_{dcb}}\frac{di_{dc,pu}}{dt} = v_{in,pu} - R_{pu}i_{dc,pu} - v_{C,pu}$$

$$\rightarrow L_b = \frac{Z_b}{\omega_b} = \frac{Z_b}{\omega_b}[\mathrm{H}]; R_{dcb} = \frac{V_{dcb}}{I_{dcb}} = 4Z_b[\Omega]$$

$$L_{pu}\frac{1}{4\omega_b}\frac{di_{dc,pu}}{dt} = v_{in,pu} - R_{pu}i_{dc,pu} - v_{C,pu}$$

$$\begin{bmatrix} \dot{v}_{C,pu} \\ \dot{i}_{dc,pu} \end{bmatrix} = \begin{bmatrix} 0 & \dfrac{1}{\dfrac{4C_{pu}}{\omega_b}} \\ -\dfrac{1}{\dfrac{L_{pu}}{4\omega_b}} & -\dfrac{R_{pu}}{\dfrac{L_{pu}}{4\omega_b}} \end{bmatrix} \begin{bmatrix} v_{C,pu} \\ i_{dc,pu} \end{bmatrix} + \begin{bmatrix} 0 \\ -\dfrac{1}{\dfrac{L_{pu}}{4\omega_b}} \end{bmatrix} v_{in,pu}$$

$$\begin{bmatrix} v_{C,pu} \\ i_{dc,pu} \end{bmatrix} = \begin{bmatrix} 1 & 0 \\ 0 & 1 \end{bmatrix} \begin{bmatrix} v_{C,pu} \\ i_{dc,pu} \end{bmatrix} + \begin{bmatrix} 0 \\ 0 \end{bmatrix} v_{in,pu}$$

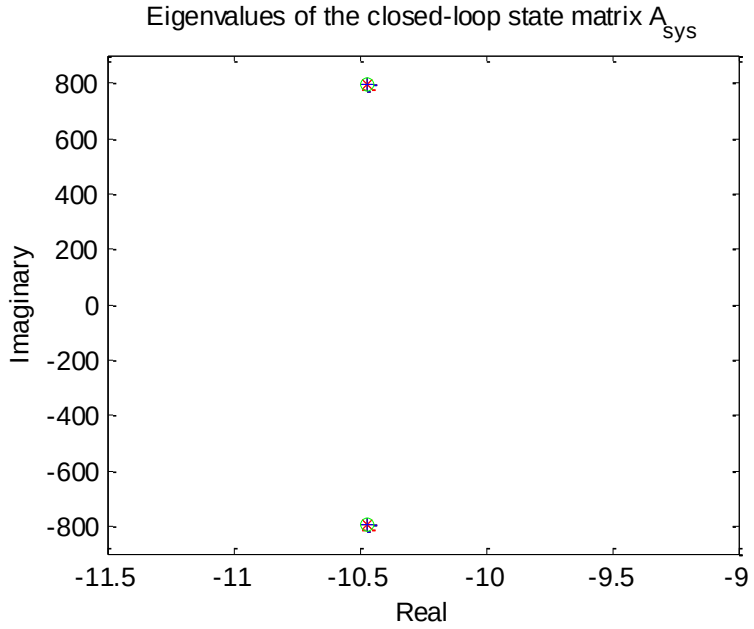

Comparison of both per unit definition shows that there is no difference between them.

C. CABLE

C.1. Cable data

Each DC transmission is associated with two cables, one for the positive pole and one for the negative pole. They are buried beneath the ground. Electrical data are calculated thanks to the EMTP-RV® routine, main parameters are summarized in Table C-1.

Table C-1 : Cable parameters (calculated at 10 μHz)

	Cable 320 kV 2500 mm²	Cable 320 kV 500 mm²
Cable section [mm²]	2500	500
Nominal current [A]	1800 – 2700	700 – 1100
Core resistance [mΩ/km]	5.3	3.1
Screen resistance [mΩ/km]	60.2	88.2
Core inductance [mH/km]	3.6	3.8
Screen inductance [mH/km]	3.5	3.6
Core-screen mutual inductance [mH/km]	3.5	3.6
Core-to-ground conductance [μS/km]	0.06	0.04
Core-to-ground capacitance [μF/km]	0.24	0.15

Modular Multilevel Converter Model and Control for the integration to the grid system

ABSTRACT

In future, the capability of the electric power transmission continues to grow due to renewable energy production and the needs of electrical market. Consequently many HVDC transmission systems are developed. Definitely the power electronic interfaces will play a key role to provide high reliability, good efficiency and cost effectiveness for this AC/DC conversion. Recently, the Modular Multilevel Converter (MMC) has taken the advantage over the more classical converter as three-level VSC. Since MMC topology is complex, two different control levels may be distinguished: the control of the switches mainly orientated on the balance of hundreds of voltage on the elementary submodules, the higher level control whose aim is to control the currents, power and energy in the system. This thesis is oriented mainly on the latter. It discusses a hierarchical and formal approach for the MMC to control the energy in all the storage elements. At first it is shown that an energy control is required mandatory. Secondly, it supposes to develop an energetic model which is inverted to design the energy control. Then different solutions of control have been developed and discussed. In the majority of applications, MMC is integrated in an HVDC point to point link where the two AC/DC substations have different roles. A specific attention has to be paid on the station which controls the voltage since the way to manage the energy in the MMC has a critical role in the DC voltage stability. Finally, all these types of control have been tested and discussed on an HVDC. It is shown that the exchange between the DC bus and the MMC placed on both sides play a key role in the DC bus voltage regulation

KEYWORDS: Modular Multilevel Converters, energy and Power Control, Modeling, High Voltage Direct Current (HVDC),

Modélisation et Commande des Convertisseurs MMC en vue de leur Intégration dans le Réseau Electrique

RESUME:

Le système de transport d'électricité doit évoluer pour satisfaire les besoins du marché de l'électricité et de l'insertion de la production renouvelable. Les systèmes de transport dits HVDC se développent. Les interfaces d'électroniques de puissance vont jouer un rôle majeur et doivent faire preuve d'une extrême fiabilité, d'une grande efficacité et rester économiquement abordables. La technologie MMC (Convertisseur Modulaire Multi-niveaux) connaît un essor par rapport à des technologies classiques, comme le convertisseur trois-niveaux. Sa topologie étant complexe, deux niveaux de contrôle peuvent être définis. Le premier niveau porte sur le contrôle des interrupteurs pour équilibrer les tensions des sous-modules. Le second niveau contrôle les courants, la puissance et l'énergie dans le système. Cette thèse est axée sur ce deuxième niveau de contrôle. Une approche hiérarchisée et formelle, basée sur l'inversion du modèle pour le contrôle de l'énergie du MMC est présentée. Pour ce contrôle, différentes méthodes ont été proposées et comparées. Cela implique de développer une modélisation, mettre en place un contrôle. Différentes modèles et contrôles ont été développés. Le MMC est généralement intégré dans une liaison HVDC où deux stations AC/DC ont un contrôle différent. Un soin particulier doit être apporté à la station dédiée au contrôle de la tension. En effet, la gestion de l'énergie dans le MCC est un point critique pour la stabilité de la tension. Enfin, les différents types de contrôle évoqués ont été étudiés dans le cas d'une liaison HVDC. Il a été montré que les échanges entre le bus DC et les MMC jouent un rôle important pour la régulation de la tension du bus DC.

MOTS CLES : Convertisseur modulaire multiniveau, Contôle de l'enérgie et la puissance, Modélisation, Haute Tension Courant Continu (HVDC)